UNIVERSITÀ DEGLI STUDI DI PADOVA

Dipartimento di Ingegneria Industriale

Corso di Laurea Magistrale in Ingegneria Chimica e dei Processi Industriali

Tesi di Laurea Magistrale in
Ingegneria Chimica e dei Processi Industriali

ALTERNATIVE SUSTAINABLE ROUTES TO METHANOL PRODUCTION: TECHNO-ECONOMIC AND ENVIRONMENTAL ASSESSMENT

Relatore: Prof. Fabrizio Bezzo

Correlatrice: Ing. Elena Barbera

Laureando: MARCO SCOMAZZON

ANNO ACCADEMICO 2021 - 2022

Abstract

Climate change effects are more and more impacting on Earth, since 1800s with many consequences to the environment. The results are represented by an increase in global temperature of 1.1 °C since late 1800s. Several objectives have been set to mitigate those effects by intergovernmental organizations, such as European Union or United Nations. In order to pursuit the objectives set by the signing of Paris Agreement in 2016, fossil fuel production must decline by roughly 6 percent in the next years, and a more rapid switch of energy systems, from fossil fuels to renewables, needs to be applied all over the world. Nowadays, methanol is produced almost exclusively from fossil fuel-based methane, thus the need of studying and developing more sustainable alternative routes is increasing importance over the years. In this thesis, the evaluation of alternative natural feedstocks is considered, taking biomass as raw material either via gasification or through biogas production and subsequent reforming. In addition, an innovative process is considered, which is the methanol production via CO_2 hydrogenation. This has the potential of reducing to zero the carbon emission-related impact, by employing renewable energy for the production of hydrogen via water electrolysis, captured carbon dioxide, and possibly green energy generation for plant operation requirements. Four different routes are considered in addition to the conventional production process of methanol from methane steam reforming, largely employed in industry for almost a century. Technological, economic, and carbon impact analyses have been performed for each process. Biogas reforming is the most promising alternative route from an economic point of view, considering the reduced operating costs, and the possibility of a larger energy integration, with respect to the traditional way to methanol from methane steam reforming. From an environmental point of view, the most performing alternative is represented by the carbon dioxide hydrogenation process, which however, should employ only renewable energy, due to its high-energy intensity, to nullify its carbon impact.

Riassunto esteso

Gli effetti del cambiamento climatico sul pianeta si stanno presentando sempre più pesantemente col passare degli anni, manifestandosi sottoforma di eventi atmosferici violenti, carestie, scarsità d'acqua, incendi pesanti, innalzamento del livello dei mari, scioglimento dei ghiacci perenni. Il trend, iniziato con le rivoluzioni industriali dell'Ottocento, è giunto a determinare un innalzamento della temperatura media globale di circa 1.1 °C. Numerosi obiettivi sono stati fissati da organismi internazionali come le Nazioni Unite o l'Unione Europea, in termini di mitigazione dell'incremento della temperatura globale che deve essere limitato a non più di 1.5 °C per mantenere una certa vivibilità climatica del pianeta. Tuttavia, considerate le attuali politiche, un incremento di 2.8 °C è previsto entro la fine del secolo.

Il metanolo è uno dei composti chimici più prodotti al mondo, raggiungendo un livello produttivo di oltre 157 milioni di tonnellate nell'anno 2020, a fronte di una domanda di circa 85 milioni di tonnellate. Considerato che l'utilizzo del metanolo come combustibile sta prendendo sempre più spazio, la domanda è prevista aumentare fino a 135 milioni di tonnellate al 2030.

Il processo produttivo del metanolo attualmente impiegato in industria, mediante la reazione di reforming con vapore, alimentando metano proveniente da fonti fossili, non è particolarmente sostenibile in termini di impatto ambientale (emissioni di CO_2). Da qui la necessità di valutare delle alternative, economicamente sostenibili, che consentano di abbattere le emissioni di gas serra. Quattro processi alternativi alla via classica sono considerati in questo lavoro: due sono basati sulla generazione verde del syngas, precursore della sintesi del metanolo, gli altri due rappresentano una via innovativa di produzione del metanolo mediante idrogenazione della CO_2. Per generazione verde si intende l'applicazione di processi produttivi caratterizzati dall'impiego di materie prime naturali in sostituzione del gas naturale di estrazione fossile, e dall'uso di energia rinnovabile nell'operazione dei processi stessi. In particolare, sono stati considerati i processi di gasificazione della biomassa e di reforming del biogas ottenuto da digestione anaerobica della stessa.

Mediante l'uso del simulatore di processo Aspen Plus, dopo la scelta ragionevole di un modello termodinamico e di un modello cinetico per la simulazione del reattore del metanolo, i cinque processi sono simulati ed i risultati sono utilizzati per condurre un'analisi tecnico-economica e la valutazione delle emissioni di CO_2 legate ai singoli processi. Per tutti i processi è stata inoltre condotta un'analisi di integrazione energetica per ridurre l'impiego delle *utilities* ed il costo

relativo. Per la valutazione dell'impatto ambientale dei processi sono considerati quattro casi studio, che prendono come riferimento quattro diversi paesi europei, stati membri dell'Unione Europea, in base al diverso mix energetico che li caratterizza: la Francia che è caratterizzata da un largo impiego del nucleare per la generazione di energia elettrica, l'Italia che utilizza per la maggior parte gas naturale per la produzione di elettricità, la Polonia che impiega largamente le vecchie centrali a carbone e la Svezia che è lo stato membro dell'Unione Europea con la maggior quota di rinnovabili impiegate per la generazione di energia. Per le simulazioni si è considerata come riferimento una produttività del metanolo di 100000 tonnellate l'anno, mentre i processi sono progettati e studiati per ottenere una produzione di metanolo ad elevata purezza (> 99.85 % in peso, pari al valore del prodotto commerciale).

Considerando che in letteratura non sono presenti lavori caratterizzati da un'analisi comparativa di vie alternative per la produzione di metanolo, rispetto al processo standard di riferimento, l'obiettivo di questo lavoro di tesi è colmare questa lacuna: in particolare, lo scopo è quello di confrontare i cinque processi considerati, da tre punti di vista differenti: un'analisi tecnologica, economica e di emissioni nette di gas serra è dunque condotta per ognuno di essi.

In base ai risultati ottenuti, i reforming di biogas appare l'alternativa più promettente al processo standard per la produzione di metanolo, dal punto di vista economico, considerato il minore costo operativo a la possibilità di ottenere una migliore integrazione energetica. Dal punto di vista delle emissioni, l'alternativa più interessante è invece rappresentata dall'idrogenazione della CO_2 che, ad ogni modo, deve essere impiegata partendo dal presupposto di utilizzare energia rinnovabile per l'alimentazione dell'intero processo. I processi elettrolitici e di cattura diretta della CO_2 dall'aria, infatti, richiedono l'utilizzo di una notevole quantità di energia elettrica e solo un totale impiego di energia prodotta da fonti rinnovabili consente l'azzeramento dell'impatto ambientale del processo; considerando che il biossido di carbonio è catturato, e quindi rimosso, dall'atmosfera, si può potenzialmente raggiungere un impatto ambientale negativo.

Contents

List of Figures

List of Tables

Introduction

Methanol is one of the most produced commodity chemicals in the world, considering its role as an intermediate in the production of several monomers and solvents; in 2020 global production capacity reached the value of over 157 millions of tonnes, while demand stood at about 85 million tonnes. Since its employment as a fuel in the energy sector is largely increasing recently, a higher demand is expected to arise in the following years, that is forecast to reach over 135 million tonnes up to 2030. Considering the carbon impact of the traditional methanol production process, mainly related to the employment of natural gas as raw material, and the high-energy consumption, more sustainable alternative routes need to be explored and investigated. The objective is to find a different production way that is economically feasible, with the potential of reducing the impact on the environment of methanol production.

Starting from the conventional methanol production route, taken as the reference process, four alternatives are evaluated, based on natural feedstocks and renewable energy generation, in substitution to the fossil-based ones. By means of Aspen Plus process simulator, after the proper choice of reasonable assumptions and models, the five processes are studied and their performances are evaluated in terms of technological, economic profitability, and carbon impact. Heat integration is performed to minimize utilities usage and costs; afterwards, a comparison between the different routes is made, considering the different aspects previously underlined. In order to assess the carbon impact analysis results, four case studies are considered, with reference to four European countries, characterized by very different energetic mixes: France electricity generation mix is dominated by the share of nuclear, Italy employs mainly natural gas to generate electricity, Poland is currently operating old coal-based electricity generation plants, while Sweden represents the European leading country in terms of renewable electricity generation, among European Union member states.

A methanol productivity of 100000 tonnes per year is assumed to be the reference target for the simulation, designed and developed to guarantee a high-purity product ($>$ 99.85 wt.% of methanol).

This thesis is structured as follows:

- in chapter 1 a general overview of the main characteristics and properties of methanol, and raw materials needed to produce it, is presented. Aim and objectives of the work are finally presented, after the illustration of the socio-political context that governs the

climate change mitigation and environment protection measures;

- in chapter 2 Aspen Plus process simulator is presented with the assumptions considered for the simulation purposes. Kinetic and thermodynamic models implemented in the software are presented. Then, the classical route to methanol production is described, along with the four alternatives chosen to make the comparative assessment. Finally, the block flow diagrams of the five processes considered are described;
- in chapter 3 the results of Aspen Plus simulations are presented, starting from the definition and the description of the process flowsheets. Pinch analysis is then carried out to save energy and utilities requirement, with the related operating cost savings.
- in chapter 4 the results of the economic and carbon impact analysis are presented for the five processes. Profitability analysis is then performed, in order to evaluate the possibility, and the economic feasibility, of developing real projects related to the simulated processes;
- conclusions summarize results in terms of comparative assessments for the processes considered, based on techno-economic and carbon impact analysis. Possible improvements to this work are finally outlined, along with future perspectives.

Chapter 1

Sustainable Methanol Production: Background and Context

In this Chapter a general overview of characteristics and properties of methanol, and raw materials needed to produce it, is presented, along with production processes and sources to get them; state-of-the-art is also considered for such processes with a vision to the implementation of sustainable solutions, particularly for methanol production. After considering socio-political context in which Europe and EU member states are inserted, with regard to environment protection and climate change mitigation, aim and objectives of the thesis are finally outlined.

1.1 Methanol

Methanol (CH_3OH) is one of the most produced commodity chemicals in the world, since it represents an important intermediate in the production of several monomers and solvents (figure 1.1): formaldehyde (CH_2O), acetic acid (CH_3COOH) and methyl *tert*-butyl ether ($(CH_3)_3COCH_3$) are the main derivatives, covering about 80% of the global production; its use in the energy sector is increasing, considering that methanol can be employed as a fuel (Research Octane Number, RON=108 and Motor Octane Number, MON=89), pure or as a blend with other hydrocarbons, both for gasoline and in diesel engines. Its main physical-chemical properties are summarized in table 1.1.
Other minor uses for methanol are:

- refrigeration, due to low freezing point and its miscibility with water (used in refrigeration systems or as an antifreeze in heating and cooling);
- protection of natural gas pipelines, it is added to NG and circulated in liquid form against the formation of gas hydrates at low temperature;
- absorption agent, e.g. removal of CO_2 and hydrogen sulfide at low temperature (Rectisol process).

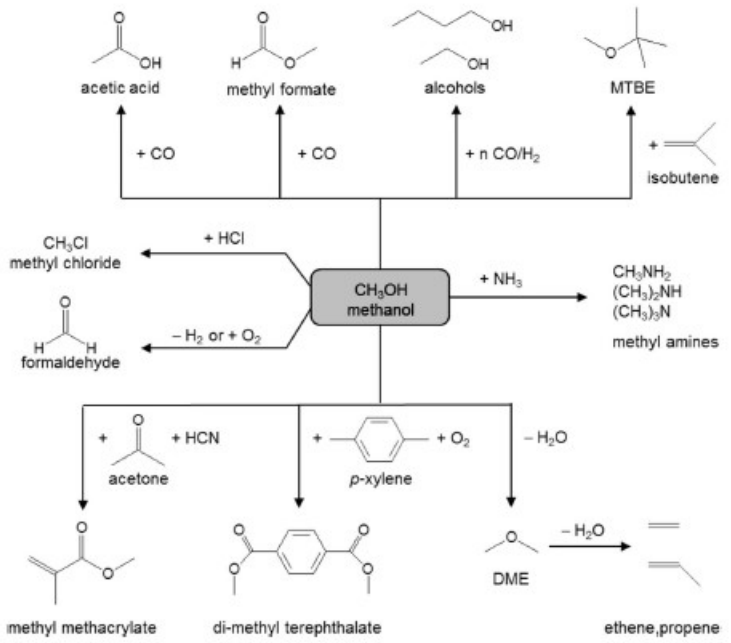

Figure 1.1: Methanol as base chemical (Moulijn *et al.*, 2013)

In 2020, global methanol production capacity reached the value of over 157 millions metric tons, while demand stood at 84.55 million tonnes; anyway it is forecast to reach 135.60 million tonnes in 2030, due to an important increase of demand for use as a fuel.

From a commercial point of view methanol is classified as grade A or grade AA purity (O-M-232L USA federal specification, methanol > 99.85 wt.%), according to American Society for Testing and Materials (ASTM); impurities generally include water, acetone (by-product of the synthesis, very difficult to separate by distillation) and ethanol. Crude methanol can be used for energy, as a fuel itself (fuel methanol) or as a precursor for other synthetic fuels, and for specific chemical or technical purposes, such as Methanol to Olefin (MTO) process.

1.1.1 Methanol synthesis

Methanol is traditionally synthesized from syngas (a mixture of CO and H_2), according to an exothermic reaction that is carried out at a moderately high pressure, as suggested from thermodynamics:

$$CO + 2\,H_2 \rightleftharpoons CH_3OH \qquad (\Delta H_{298\ K} = -90.8\ \text{kJ/mol}) \tag{1.1}$$

Side reactions can occur in presence of CO_2:

$$CO_2 + 3\,H_2 \rightleftharpoons CH_3OH + H_2O \qquad (\Delta H_{298\ K} = -49.6\ \text{kJ/mol}) \tag{1.2}$$

$$CO_2 + H_2 \rightleftharpoons CO + H_2O \qquad (\Delta H_{298\ K} = 41.0\ \text{kJ/mol}) \tag{1.3}$$

Table 1.1: Selection of physical data of methanol (Ott *et al.*, 2012)

Property	Value	Unit	Conditions
Molar mass	32.042	g/mol	
Density	786.68	kg/m^3	298.15 K
Boiling point	337.8	K	ambient
Melting point	175.27	K	ambient
Viscosity	0.5513	$mPa \cdot s$	298 K, liquid
Critical temperature	513	K	
Critical pressure	8.1	MPa	
Critical density	8.51	mol/l	
Critical molar volume	116	cm^3/mol	
Standard enthalpy of formation	-205	kJ/mol	273.15 K, 101.3 kPa
Specific heat capacity	42.59	$J\,mol^{-1}\,K^{-1}$	273.15 K, 1 bar, gas
at constant pressure (C_p)	80.9	$J\,mol^{-1}\,K^{-1}$	298.15 K, 101.3 kPa, liquid
Thermal conductivity	190.16	$mW\,m^{-1}\,K^{-1}$	298.15 K, liquid
Dielectric constant	32.65		298.15 K
Flash point	288.75	K	DIN 51 755
Ignition temperature	743.15	K	DIN 51 794
Explosion limits	6.72-36.50	vol%	
Explosion group	II B, T1		
Heating value	22.693	MJ/kg	298.15 K

Reaction 1.2 is an alternative methanol-forming reaction while endothermic reaction 1.3 is undesired and it is called reverse water gas shift (rWGS).

First methanol synthesis processes operated at quite high temperatures (370-410 °C) due to constraints imposed by old ZnO/Cr_2O_3 catalysts that where not active below that range: single-pass conversion, due to exothermicity of reaction, was very low thus operating pressure had to reach 300 atm, with related high operating processing costs. These processes are no more economically viable, indeed the last high-pressure process plant closed in the mid-1980s.
Catalysts used nowadays in industry for low-pressure synthesis are based on Cu-ZnO-Al_2O_3, where each element has an essential role in performance: activity for Cu-centers, presence of ZnO guarantees stability to Cu(I) and Al_2O_3 (or the alternative Cr_2O_3) stabilizes and prevents sinterization that typically develops when reaching too high temperatures; final result is a very high selectivity towards methanol. Nowadays, industrially, methanol synthesis is carried out through syngas reaction (1.1) at medium or low pressures, ranging from 50 to 100 atm (Ott *et al.*, 2012).
Typical byproducts of the reaction can be higher alcohols (mainly ethanol), ethers (mainly dimethyl ether, DME), esters (e.g. formates), ketones (e.g. acetone or methyl ethyl ketone, MEK) and hydrocarbons:

1. Higher alcohols are formed by:

$$n\,CO + 2n\,H_2 \rightleftharpoons C_nH_{2n+1}OH + (n-1)\,H_2O \tag{1.4}$$

2. DME is formed as:

$$2\,CO + 4\,H_2 \xrightleftharpoons{Al_2O_3} CH_3{-}O{-}CH_3 + H_2O \tag{1.5}$$

3. Esters come from the surface reaction:

$$(CH_2O)_{ads} + (RCHO)_{ads} \rightleftharpoons CH_3COOR \tag{1.6}$$

4. Ketones are obtained by reaction catalysis:

$$RCH_2CH_2OH \rightleftharpoons RCH_2CHO + H_2 \tag{1.7}$$

$$2\,RCH_2CHO \rightleftharpoons RCH_2COCHRCH_3 + O_{ads} \tag{1.8}$$

5. Hydrocarbons are formed by catalysis with traces of iron, cobalt, and nickel (Fischer-Tropsch process):

$$CO + 3\,H_2 \rightleftharpoons CH_4 + H_2O \tag{1.9}$$

$$CO_2 + 4\,H_2 \rightleftharpoons CH_4 + 2\,H_2O \tag{1.10}$$

$$n\,CO + (2n-1)\,H_2 \rightleftharpoons C_nH_{2n+2} + nH_2O \tag{1.11}$$

Methanol production from carbon dioxide, through hydrogenation reaction (1.2), is currently the main investigated alternative route to classical synthesis from syngas, in a sustainability optics. Main limitations are related to low conversion of carbon dioxide and economy of raw materials, at least for what regards *green* generation of them. In this regard, more details on the production and/or purification of H_2 and CO_2 as feedstocks for methanol production will be discussed in the next paragraph.

1.2 Hydrogen

Hydrogen in standard conditions exists in gaseous diatomic molecular form, as a result of the combination between 2 spin isomers that are interconvertible and in equilibrium with each other:

- ortho-hydrogen: both atomic nuclei rotate in the same direction (parallel nuclear spin)
- para-hydrogen: atom nuclei rotate in the opposite direction (anti-parallel nuclear spin)

Normal-Hydrogen ($n - H_2$) is a mixture of equilibrium concentration at ambient temperature (75 mol% ortho-form and 25 mol% para-form), while at low temperatures $p - H_2$ and $o - H_2$ can be present in a virtually pure state. Their properties are summarized in table 1.2.

Hydrogen is not available in its elemental form in nature, and needs to be generated for a lot

Table 1.2: Selection of physical properties of n-hydrogen and p-hydrogen at fixed points. Unless differently specified properties are referred to STP (273.15 K and 101.3 kPa). Adapted from Häussinger *et al.* (2002)

Property	p-Hydrogen	n-Hydrogen	Unit
Molar mass	2.016	2.016	g/mol
Density	0.0899	0.0899	kg/m^3
Boiling point (101.3 kPa)	20.268	20.390	K
Heat of vaporization	898.30	899.10	J/mol
Critical temperature	32.976	33.19	K
Critical pressure	1.290	1.325	MPa
Critical density	31.43	30.12	kg/m^3
Specific heat capacity (c_p)	30.35	28.59	$J\,mol^{-1}\,K^{-1}$
Specific heat capacity (c_v)	21.87	20.30	$J\,mol^{-1}\,K^{-1}$
Thermal conductivity	182.6	173.9	$mW\,m^{-1}\,K^{-1}$
Autoignition temperature		858	K
Flammability limits in air		4.0-75.0	vol%
Detonability limits in air		18.3-59.0	vol%
Lower Heating value		119.93	MJ/kg
Higher Heating value		141.80	MJ/kg

purposes, one of these is the use as a raw material for synthesis of a very large amount of organic compounds: methanol represents one of the main objectives in this sense (figure 1.2). Furthermore, it represents the most promising energy carrier to satisfy global power demand in the future, considering its carbon-free nature: storage and safe handling represent the main limitations, thus employment of substances like methanol or ammonia to store it safely is considered of paramount importance in this historical period.

Since 1785, when Lavoisier demonstrated the splitting of water into hydrogen and oxygen in a heated copper tube, from which the name "hydro-genes" ("born of water"), many alternatives to hydrogen generation route from refining industry have been investigated and discovered: result is that currently several production processes are available and for each of them an environmental impact can be evaluated. In particular, hydrogen can be classified as IEA (2019):

- grey hydrogen: hydrogen generated through reforming reactions. Raw materials can be coal, natural gas, pure methane, biogas/biomethane or other hydrocarbons;

- blue hydrogen: carbon generated through Methane Steam Reforming (MSR) reaction or gasification technologies is captured and stored underground through Carbon Capture and Storage (CCS). Raw materials needed are the same of previous case plus biomass;

- green hydrogen: hydrogen produced from water electrolysis using renewable energy sources.

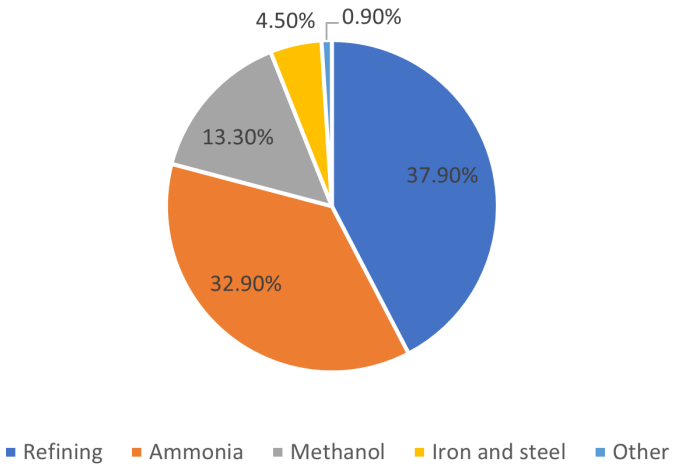

Figure 1.2: Uses of hdyrogen in chemical industry (data from *IEA*)

1.2.1 Hydrogen production

Hydrogen can be produced in several ways and it represents a valuable by-product of many petrochemical processes. In this section a general outline is presented:

1. Catalytic steam reforming of hydrocarbons, they react with steam forming carbon monoxide and hydrogen. Most important feedstock is natural gas, but propane, butane, LPG, naptha fractions, heavy oils and coal can be also used. The general reaction is described below while reaction enthalpies vary depending on feedstock, and are reported in table 1.3:

$$\mathrm{C_nH_m} + n\,\mathrm{H_2O} \rightleftharpoons n\,\mathrm{CO} + \left(n + \frac{m}{2}\right)\mathrm{H_2} \tag{1.12}$$

   Concurrently Water Gas Shift (WGS) reaction occurs, due to steam excess, generating an additional amount of hydrogen through an exothermic reaction:

$$\mathrm{CO} + \mathrm{H_2O} \rightleftharpoons \mathrm{CO_2} + \mathrm{H_2} \qquad (\Delta H_{298\ \mathrm{K}} = -41.16\ \mathrm{kJ/mol}) \tag{1.13}$$

2. Gasification of coal and heavy hydrocarbons: as regards coal gasification, for the production of hydrogen or H_2-rich gases, it is usually performed with oxygen at high temperature and pressure; gasification of other solid fuels is not suitable for hydrogen production, due to low-energy of product gas and to high moisture and oxygen content of raw material, indeed they are generally used for heat or electricity production in the plant. Gasification of liquid and gaseous hydrocarbons occurs through partial oxidation (PO) processes and can be applied to all hydrocarbons, but for hydrogen production the use of heavy residues as feedstock is the only economically viable; gaseous hydrocarbons are occasionally used but only when these gases can not be processed by catalytic steam reforming because of high concentration of impurities.
   Overall general reactions occurring during PO are reported below while reaction enthalpies vary depending on feedstock and are reported in table 1.3:

Table 1.3: Equation and reaction enthalpies for the most frequent reactions occurring during catalytic steam reforming. Adapted from Häussinger *et al.* (2002)

Reforming reactions	ΔH at STP (kJ/mol)
$CH_4 + H_2O \rightleftharpoons CO + 3\,H_2$	206.36
$CH_4 + 2\,H_2O \rightleftharpoons CO_2 + 4\,H_2$	165.13
$C_2H_6 + H_2O \rightleftharpoons CO + CH_4 + 2\,H_2$	141.22
$C_2H_6 + 2\,H_2O \rightleftharpoons 2\,CO + 5\,H_2$	347.50
$C_3H_8 + H_2O \rightleftharpoons C_2H_6 + CO + 2\,H_2$	150.68
$C_3H_8 + 2\,H_2O \rightleftharpoons CH_4 + 2\,CO + 4\,H_2$	291.99
$C_3H_8 + 3\,H_2O \rightleftharpoons 3\,CO + 7\,H_2$	498.36
Oxidation reactions	**ΔH at STP (kJ/mol)**
$C + O_2 \rightleftharpoons CO_2$	-196.89
$_2CO + O_2 \rightleftharpoons 2\,CO_2$	-566.37
$2\,H_2 + O_2 \rightleftharpoons 2\,H_2O$	-484.17
$CH_4 + 2\,O_2 \rightleftharpoons 2\,H_2O + CO_2$	-803.04
$2\,C_2H_6 + 7\,O_2 \rightleftharpoons 6\,H_2O + 4\,CO_2$	-2857.6
$C_3H_8 + 5\,O_2 \rightleftharpoons 4\,H_2O + 3\,CO_2$	-2045.4

$$C_mH_nS_o + \frac{m}{2}\,O_2 \rightleftharpoons m\,CO + \left(\frac{n}{2} - o\right) H_2 + o\,H_2S \tag{1.14}$$

$$2\,C + O_2 \rightleftharpoons 2\,CO \tag{1.15}$$

3. Biomass gasification: biomass represents the sustainable alternative to fossil solid feedstocks, it is available from a wide variety of sources, such as municipal wastes, agricultural wastes, crop residues, sawdust and other wood processing residues. The polymeric structure of biomass is broken through gasification that can use oxygen, steam or a combination of them as oxidizing agents; products are gases, tars, chars and ash but only gases are the desired ones, so that a further purification is required to get syngas. General reaction can be described as from Subramani *et al.* (2015):

$$C_xH_yO_z + H_2O + O_2 \rightleftharpoons CO + CO_2 + H_2 + CH_4 + LHC + Tars + Chars \tag{1.16}$$

where LHC (Light Hydrocarbons) definition includes C_2, C_3 and C_4 species.

4. Catalytic partial oxidation, occurs in autothermal reactors where the heat of reaction necessary to form syngas is generated by combustion of part of the feed with oxygen (Häussinger *et al.*, 2002). Usually PO is almost never performed by itself because of high investment and operating costs: when coupled with steam reforming, the same reactor can be used (refractory-lined pressure vessel) and endothermic reforming duty

is provided by exothermic oxidation reaction; in the production of syngas for ammonia synthesis, autothermal reforming reactor is sometimes installed downstream of steam reformer, giving it the name of secondary reformer (Moulijn *et al.*, 2013).

5. Refinery processes: hydrogen is recovered from hydrogen-rich product gases and off-gases formerly used as heating media (Häussinger *et al.*, 2002):

   (a) Thermal cracking processes: olefins like ethylene and propylene are produced by steam cracking, generating also large amounts of hydrogen as by-product through the following highly endothermic reactions:

$$\mathrm{C_{m+n}H_{2(m+n)+2}} \longrightarrow \mathrm{C_mH_{2m}} + \mathrm{C_nH_{2n+2}} \tag{1.17}$$

$$\mathrm{C_nH_{2n+2}} \rightleftharpoons \mathrm{C_nH_{2n}} + \mathrm{H_2} \tag{1.18}$$

   (b) Catalytic cracking, process used for the production of light products from gas oil, vaccum gas oil and residues. The molecular mass of the main fraction of feed is lowered while the other part is converted into coke that deposits on the hot catalyst which is regenerated through one or two stages where coke is burned with air. Cracking processes that occur can be classified into 3 steps: 1) paraffins and napthenes are cracked to olefins and alkanes, with shorter chain length 2) monoaromatic compounds are dealkylated without ring cleavage 3) diaromatics and polyaromatics are dealkylated and converted to coke. Just the last one produces hydrogen while the other 2 need it.

   (c) Catalytic reforming: naphta fractions are reformed to improve quality of gasoline, most important reactions occurring are dehydrogenation of naphtenes to aromatics. For example in dehydrogenation of cyclohexane hydrogen comes from:

$$\mathrm{C_6H_{12}} \longrightarrow \mathrm{C_6H_6} + 3\,\mathrm{H_2} \qquad (\Delta H_{298\ \mathrm{K}} = 206.20\ \mathrm{kJ/mol}) \tag{1.19}$$

6. Electrolysis has been used for a century for hydrogen productions, considering that first large installations were built up in 1920s. When a potential is applied to electrodes of an electrolysis cell filled with a suitable electrolyte (e.g. alkali solution), following reactions occur at the electrodes (Häussinger *et al.*, 2002):

$$\textit{Cathode}: \qquad 2\,\mathrm{H_2O} + 2\,e^- \longrightarrow \mathrm{H_2} + 2\,\mathrm{OH^-} \tag{1.20}$$

$$\textit{Anode}: \qquad 2\,\mathrm{OH^-} \longrightarrow \frac{1}{2}\,\mathrm{O_2} + \mathrm{H_2O} + 2\,e^- \tag{1.21}$$

$$\textit{Cell reaction}: \qquad \mathrm{H_2O} \longrightarrow \mathrm{H_2} + \frac{1}{2}\,\mathrm{O_2} \tag{1.22}$$

7. Other processes (Häussinger *et al.*, 2002): hydrogen can also be generated by conversion of metals (alkali and alkaline earth) when reacting with water or steam (reaction 1.23), as well as in laboratory when making them react with acids or bases (reactions 1.24 and 1.25). Another hydrogen source is hydrogen sulfide (H_2S), obtained from desulfurizing processes in refineries, by endothermic decomposition reaction (1.26) that is thermodynamically unfavorable with respect to hydrogen formation at temperatures below 1600 °C; the use of a catalyst is thus necessary, for example Pt-Co at 1000 °C, disulfides of Mb or W at 800 °C or other transition metal sulfides supported on Al_2O_3 at 500-800 °C.

$$Me + \mathrm{H_2O} \longrightarrow \frac{1}{2}\,\mathrm{H_2} + Me\mathrm{OH} \qquad (Me: \textit{generic metal}) \tag{1.23}$$

$$\mathrm{Zn} + 2\,\mathrm{HCl} \longrightarrow \mathrm{H_2} + \mathrm{ZnCl_2} \tag{1.24}$$

$$\mathrm{Al} + \mathrm{NaOH} + 2\,\mathrm{H_2O} \longrightarrow \frac{3}{2}\,\mathrm{H_2} + \mathrm{NaAlO(OH)_2} \tag{1.25}$$

$$2\,\mathrm{H_2S} \rightleftharpoons 2\,\mathrm{H_2} + \frac{1}{4}\,\mathrm{S_2} \qquad (\Delta H_{298\ \mathrm{K}} = 84.90\ \mathrm{kJ/mol}) \tag{1.26}$$

From renewable sources, different from aforementioned biomass gasification and water electrolysis, hydrogen can be produced in the following ways that are currently under study (Subramani *et al.*, 2015):

(a) thermochemical splitting of water: one-step thermolysis of water molecule, by use of solar energy, that requires very high temperatures with related problems regarding materials and solar concentration needed;

(b) photocatalytic splitting of water: solar photon energy is used to be converted into chemical energy like in natural photosynthesis through the use of a photocatalyst, limitations are related to costs and efficiency;

(c) plasma reforming: energy and free radicals needed for reforming reaction are provided by plasma generated with electricity or heat, main limitations are related to high-electricity consumption and to electrode erosion due to high-pressure;

(d) microchannel reactors for steam reforming process: deal with intensification of reactor equipment by improving heat and mass transfer thus reducing capital costs, they need to be further developed to better match costs and benefits.

All of these processes are still at an early stage, and are not close to industrial applications

yet.

1.3 Carbon dioxide

Carbon dioxide (CO_2) is a colorless, odorless, nonflammable gas with a slightly sour taste; in table 1.4 the main physical properties are summarized. CO_2 is naturally present in Earth's lithosphere, hydrosphere and atmosphere and a balance exists between processes by which it is produced and consumed, in particular:

- lithosphere is the part of Earth not covered by oceans. An estimated amount of 5.5×10^{16} t of CO_2 is bound in crust in the form of carbonates of calcium (chalk), magnesium (dolomite) and as a constituent of many organic compounds. All igneous rocks, when heated strongly under vacuum emit carbon dioxide with other gases like steam or hydrogen; gases escape also during eruptions and in general from crust activity. Carbon dioxide escapes also through natural spring water, after being dissolved into it during a process occurred inside the earth;
- atmosphere includes CO_2 for 0.03% by volume on average (2.3×10^{12} t), but the value may oscillate depending on location, and particularly on quantity of vegetation present and time of the day (higher amount by night). In reality, as reported by Topham *et al.* (2014), level of CO_2 in the atmosphere has risen from a pre-industrial level of 278 ppm to 397 in ppm in 2013, steadily increasing by 1.9 ppm/year. Moreover, National Oceanic and Atmospheric Administration (NOAA) reported for 2021 a global average concentration of 414.72 ppm, setting a new record despite the recent economic drag due to COVID-19 pandemic: every year, human activities release more carbon dioxide into the atmosphere than natural processes can remove, mainly due to burning of fossil fuels, causing the amount of CO_2 in the atmosphere to increase. It it thus clear the necessity of the reduction in generation following artificial activities and the simultaneous development and increasing of capture and abatement technologies;
- hydrosphere comprises oceans, seas, rivers, lakes and, in general, all bodies of water present in the Earth; CO_2 concentration in water is estimated as 5 volumes of gas per 10000 volumes of water, with an overall amount of 1.4×10^{14} t of carbon dioxide.

1.3.1 CO_2 production

The majority of carbon dioxide produced industrially, not accounting for electricity and heat generation plants, comes from ammonia synthesis and hydrogen production processes, and is extracted as a by-product. Obviously, it is not recovered at 100%. Furthermore, CO_2 is a component of all flue gases produced by complete combustion of carbonaceous fuels with typical concentrations of 10-18 vol%: in order to recover some of it, after gases are cooled and cleaned by passing through a water scrubber, they are put in contact with an alkaline carbonate solution or an amine solution which absorbs it. Some examples of solvents are monoethanolamine (MEA),

Table 1.4: Selection of physical data of carbon dioxide. Adapted from Topham *et al.* (2014)

Property	Value	Unit	Conditions
Molar mass	44.010	g/mol	
Gas density	1.977	kg/m^3	273.15 K, 0.1 MPa
Molar heat c_p	37.13	$J\,mol^{-1}\,K^{-1}$	298.15 K
Entropy S_0	213	$J\,mol^{-1}\,K^{-1}$	
Heat of formation ΔH	-393.51	kJ/mol	
Free energy of formation ΔG_0	-394.20	kJ/mol	
Critical data			
Temperature	304.19	K	
Pressure	7.383	MPa	
Density	468	kg/m^3	
Triple point			
Temperature	216.58	K	
Pressure	518	kPa	
Heat of vaporization	347.86	J/g	
Heat of fusion	195.82	J/g	
Sublimation point			
Temperature	194.23	K	
Pressure	98.07	kPa	
Heat of sublimation	573.02	J/g	
Thermal conductivity	16.4	$mW\,m^{-1}\,K^{-1}$	298.15 K, 1 atm
Dielectric constant ε	1.58		273.15 K

diethanolamine (DEA), methyl-diethanolamine (MDEA) and potassium carbonate (K_2CO_3). Large quantities of CO_2 are also generated by fermentation process, and up to 80% of this gas produced can be recovered: in this way, after being passed through water scrubber to remove entrained undesired material, impurities are taken out by passing the gas either through an activated charcoal bed or solutions of potassium permanganate ($KMnO_4$) and potassium dichromate ($K_2Cr_2O_7$) (Topham *et al.*, 2014).

1.3.2 Carbon Capture Utilization and Storage (CCUS)

More recently, in the perspective of GHG emissions mitigation, significant efforts have been spent in terms of research and development of solutions involving Carbon Capture Storage (CCS) and Carbon Capture Utilization (CCU): the idea is to capture large-scale CO_2 emissions and store the gas underground in order not to let the release of it in atmosphere; alternatively, instead of being stored, the gas can be used as a feedstock for some chemical process (e.g methanol synthesis). However, International Energy Agency (IEA) forecast the need of further increasing the employment of carbon capture solutions towards 2070, as depicted in figure 1.3, in order to reach carbon neutrality, namely net-zero CO_2 emissions with reference to the so-called *Sustainable Development Scenario* (IEA, 2020a).

Carbon capture is traditionally performed by absorption of flue gases (industrially derived) in methanol or in amine-based solutions, or absorption by porous solid-phase materials, like

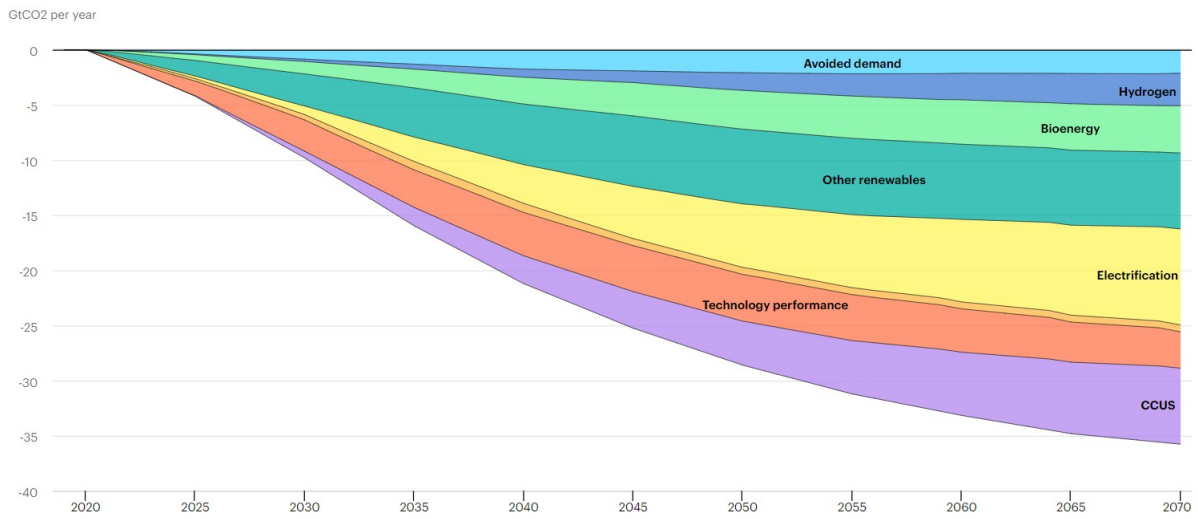

Figure 1.3: Global energy sector CO_2 emissions reductions by measure in the Sustainable Development Scenario relative to the Stated Policies Scenario (source: *IEA*)

zeolites or activated charcoal. Other minor separation techniques currently employed are membranes to selectively separate gas streams (ceramic porous, Pd-based or polymeric membranes) or cryogenic separations (at low temperatures CO_2 is cooled and condensed, but requires high concentration streams) (Freund, 2006); a new promising technology that is increasing its application is Direct Air Capture (DAC) that extracts CO_2 from atmosphere. This process will be detailed deeper in chapter 3.
Main difficulties of CO_2 capturing are related to high-stability of the molecule that makes its removal very expensive in terms of energy requirement: in this way ENI, for example, is studying some ionic liquids to save energy and reduce emissions with respect to traditional absorption by amines; furthermore, it is carrying out a research together with MIT to develop high-efficiency electrochemical systems and is developing technologies to couple green hydrogen generation with chemical reduction of CO_2 to methanol (reaction 1.2).

IEA reported that in 2020 41 $MtCO_2$/year had been captured and in the same period of time a total of 40 millions USD have been invested in CCU start-ups; anyway, for an hypothetical Net Zero Scenario to be achieved in 2030, even if project developers announced over 200 new capture facilities to be operating by 2030 reaching 220 $MtCO_2$/year captured, 1286 $MtCO_2$/year more would be required as it can be seen in figure 1.4 (IEA, 2022).

1.4 Global warming and International policy framework

Climate change is a long-term shift in temperatures and weather patterns and it may occur naturally, for example as result of variations in solar cycle. Anyway, since 1800s human activities have been recognized as the main driver of climate change, primarily due to industrial revolutions and related activities largely employing carbonaceous energy sources like coal, oil and gas; in particular, burning fossil fuels has been recognized as the first cause of increasing

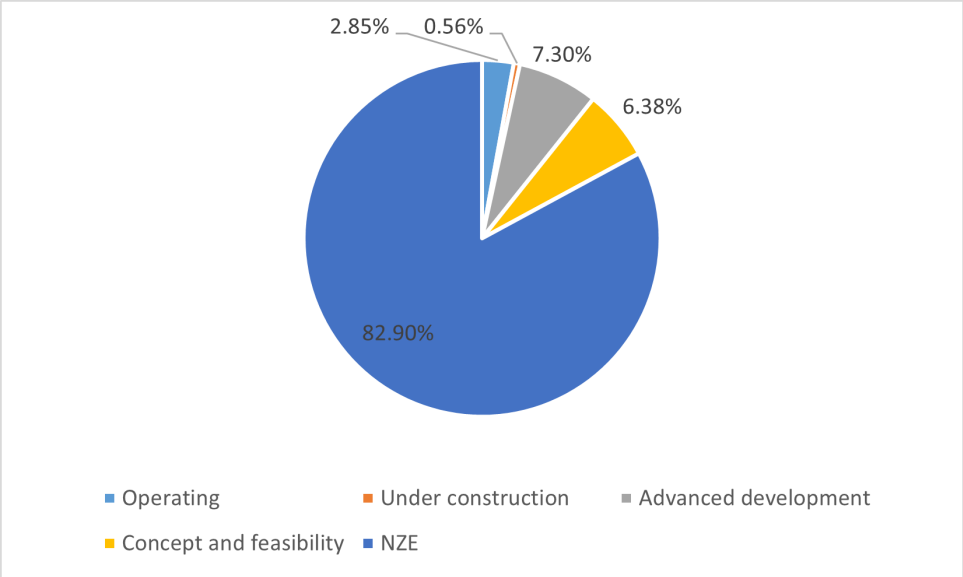

Figure 1.4: Capacity of large-scale CO_2 capture projects, current and planned vs. the Net Zero Scenario (data from *IEA*)

Earth temperature of 1.1 °C from late 1800s to today and the last decade (2010-2020) was the warmest ever (IPPC, 2021 and WMO, 2021). Consequences of these phenomena, include droughts, water scarcity, severe fires, sea levels rising, flooding, polar ice melting, catastrophic storms.
UN underline that, following a series of reports, thousands of scientists and government reviewers agreed that limiting global temperature rise to no more than 1.5 °C would help to maintain a livable climate but policies currently in place point to a 2.8 °C temperature rise by the end of the century; some countries cause a major impact to planet, indeed the 10 countries with largest emissions contribute 68 percent while the 100 least-emitting just for 3 percent.

196 parties at COP 21 (or CMP 11 or United Nations Climate Change Conference, UNCCC) in 2015 signed a legally binding international treaty, *Paris Agreement* that entered into force on 4 November 2016: the goal established was to limit global warming below 2 °C, preferably to 1.5 °C compared to pre-industrial levels. In this way, parties, represented by countries, need to start reducing GHG emissions, reaching global peaking as soon as possible, in order to achieve a world climate neutrality by mid-century thus achieving this long-term temperature goal.
Following this policy low-carbon solutions and new markets established very rapidly and in UNFCCC's opinion, with substantial financial assistance provided by the parties, trend seems to evidence that by 2030 these solutions could be competitive in sectors representing over 70% of global emissions, particularly for what regards power and transport sectors that cause the major carbon impact, as can be seen in figure 1.5, even with a general increase in emissions of over 60% along the period 1990-2019.

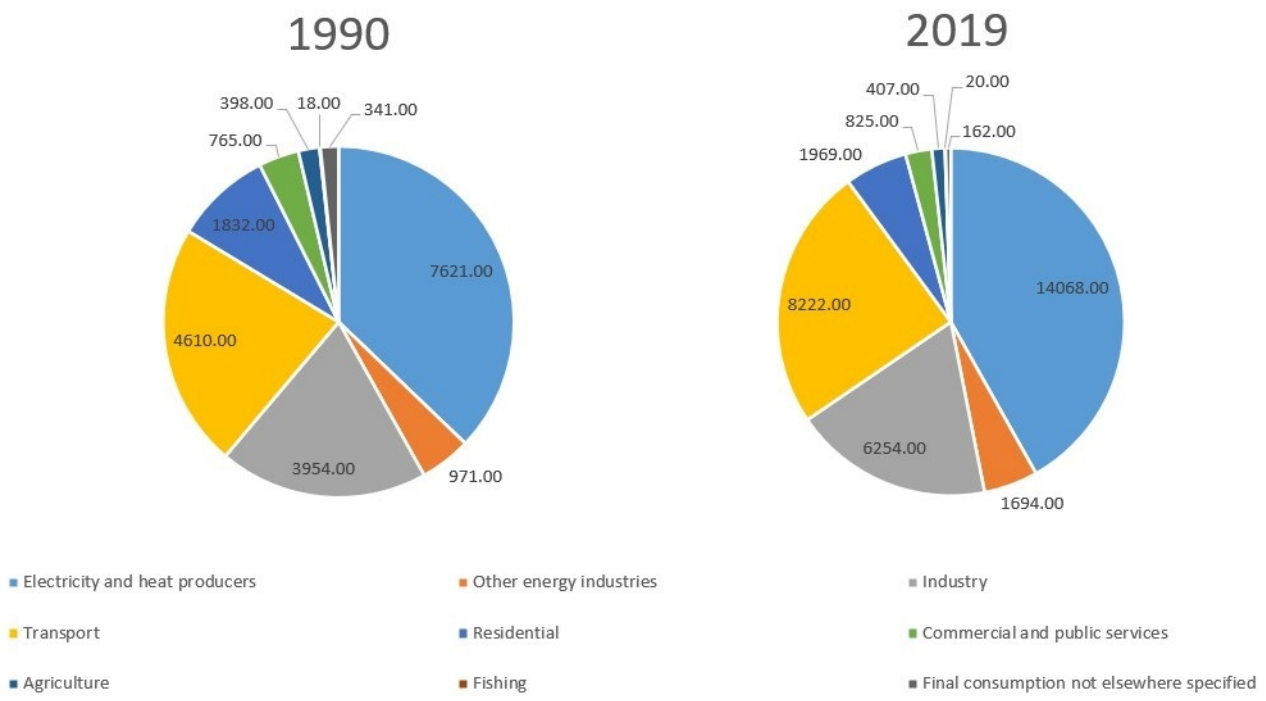

Figure 1.5: CO_2 emissions by sector for World in 1990 and 2019 in $MtCO_2$ (source: *IEA*)

1.4.1 EU environment policy

International standard ISO 14001 on environmental management systems gives a definition of environment policy: "*intentions and directions of an organization related to environmental performance, as formally expressed by its top management*". European Union, taking the role of organization in this context, since 1972 has been developing policies and programmes to fight for solving problem related to GHG emissions and climate change:

- European Council held in Paris in 1972, at which Heads of State or Government decided for the need of a Community environment policy flanking economic expansion and called for an Environmental Action Programme (EAP);
- after the first 3 Action Programmes, in 1987 Single European Act (SEA) included environmental protection as a priority to be managed at a European level, officialized by Treaty of Maastricht in 1993;
- Treaty of Amsterdam (1999) established the duty to integrate environmental protection into all EU sectoral policies with a view to promotion of sustainable development.;
- Sustainable Development Strategy (SDS) in 2001, setting objectives and concrete actions for seven key priority challenges for the period until 2010 (climate change, clean energy, etc...);
- Treaty of Lisbon (2009), introduced a specific goal, the need of combating climate change;
- in 2016 Commission published a document entitled "Next steps for a sustainable European future - European action for sustainability", in response to United Nations' *Agenda for*

Figure 1.6: UN Sustainable Development Agenda

Sustainable Development (figure 1.6) adopted at the September 2015, outlining how to integrate it into EU policy priorities;

- European Green Deal presented in December 2019 and continuously updated, coupled with economic measures related to COVID-19 pandemic, established that one third of the 1.8 million euro investments from the NextGenerationEU Recovery Plan and EU's seven-year budget will finance it. The goal of this policy is to reduce net GHG emissions by at least 55% by 2030, compared to 1990 levels;
- 8th Action Programme started in 2021 towards 2030, endorsing and building on environmental and climate objectives of European Green Deal. Main objective, in this way, is to achieve the 2030 GHG reduction target and climate neutrality by 2050.

1.5 Strategies for carbon emission mitigation and application to methanol synthesis

UN reported 3 broad categories of action as important, in order to soften effects of climate change: cutting GHG emissions, adapting to climate impacts and financing required adjustments. While a huge group of countries are committing to net zero emissions by 2050, about half of emissions must be already cut by 2030 to keep warming below the desired level (1.5 °C): in this way, fossil fuel production must decline by roughly 6 percent per year between 2020 and 2030 and switching energy systems from fossil fuels to renewables, like solar or wind, will further reduce the emissions driving climate change (IPCC, 2022). Climate action requires significant financial investments by governments and businesses: one critical step is for

industrialized countries to fulfill their commitment to provide $100 billion a year to developing countries so they can adapt and move towards greener economies.

Intergovernmental Panel on Climate Change (IPCC) in Sixth Assessment Report considers the importance of achieving net-zero CO_2 emissions from the industrial sector adopting all mitigation options like demand management, energy and material efficiencies, circular material flows, transformational changes in production processes, by using low and zero GHG electricity, hydrogen, fuels and carbon management, and abatement technologies; indeed, it is included as priority the development of CCS and deploying carbon dioxide removal (CDR) methods to counterbalance residual GHG emissions; as underlined by Erans *et al.* (2022), negative emissions technologies (NET) employment are fundamental to reach goal set by Paris Agreement, a specific CDR technology that results in net-negative CO_2 emissions, e.g. it is powered by renewable energy and captured CO_2 is stored, can be defined as a NET, and examples may be bioenergy with carbon capture and storage (BECCS) or direct air carbon capture and storage (DACCS).

Considering that carbon intensity of methanol production from natural gas can be evaluated as about 500 kg of CO_2-eq per t of methanol produced, as reported by IRENA and Methanol Institute (2021), the necessity of introduction and development of "greener" processes is evident. Among solutions that can be employed as alternative routes to methanol synthesis, are:

- Biogas reforming to methanol synthesis: biogas is a product of anaerobic digestion systems that treat vegetable or animal biomass and its use, instead of "fossil methane", is considered in order to substitute a non-renewable raw material with a natural feedstock. It is composed of 25:50 vol% CO_2 and 50:75 vol% CH_4, and can be considered as a net-zero emission fuel because it does not produce more carbon dioxide than what assimilated during life by vegetable or animal from which biomass originates. The reforming reaction, as in the case of methane from natural gas, produces a syngas from which methanol is obtained according to reaction (1.1);

- Biomass steam gasification to methanol synthesis: another way through which a syngas is generated from a natural feedstock, alternatively to fossil-based methane. Methanol is obtained through the same reaction as before, potentially reducing GHG emissions and thus carbon impact of the process;

- Methanol synthesis via CO_2 hydrogenation: innovative way that, through reactions (1.2) and (1.3), potentially produces methanol as a negative emission technology when employing captured CO_2 and green H_2, generated via water electrolysis. Technology is not so mature due to high costs of raw materials and limited CO_2 conversion, but in the next years, with decreasing costs of carbon-free technologies and important financial commitments (e.g. public funding), along with technical improvements, may start substituting old high-emissions methanol plants.

1.6 Aim of the thesis

Methanol is nowadays produced almost exclusively from fossil fuels, with consequences to environment and climate change; since the necessity of reducing carbon impact of industrial processes, in general, and more specifically of chemicals such as methanol, as is the case of this work, mitigation measures or total reduction of CO_2 emissions need to be set as a target, and this objective should be achieved as soon as possible. In literature several alternatives are presented to make methanol production "greener", especially CO_2 hydrogenation. However, there are not works where a thorough comparison between them is presented. The objective of this thesis is to fill this lack.

In particular, a comparison of different alternatives with standard process of methanol synthesis, i.e. from syngas produced via MSR, is made from an economic and carbon impact point of view. Results are obtained through process modeling and simulation, starting from available industrial and/or academic data reported in literature, in order to accurately represent the different processes. To this aim, all the processes considered were simulated in Aspen Plus® V 12.1, carefully selecting thermodynamic and kinetic models; heat integration has been performed by means of pinch analysis. Based on the material and energy balances obtained by a target methanol production, economic and carbon impact assessments have been made, so to provide a critical comparison of the different alternatives considered.

Future perspectives and possible improvements of the work are finally presented.

Chapter 2

Process Modeling and Key Assumptions

In this chapter the process simulation software adopted to simulate the processes is presented along with thermodynamic and kinetic models used for methanol synthesis reactor. Then, comprehensive details of the processes and related simulations are presented, considering industrial examples and literature works, with related assumptions needed to simplify the problems. Five processes are considered: MSR to methanol, biogas reforming to methanol, biomass steam gasification to methanol, two methanol production processes via CO_2 hydrogenation, where CO_2 is captured via DAC process, and H_2 is produced by electrolysis, via alkaline water (AW) electrolysis and polymer electrolyte membrane, or proton exchange membrane (PEM) electrolysis.

2.1 Process Simulator

The five methanol production processes are implemented and modeled in Aspen Plus® v12.1 software from AspenTech®, a steady-state process simulator (PS) which enables to automatically write and solve material and energy balances, after fulfilling required specifications needed to perform the calculations, specifically:

- all components involved in the process;
- physical property models to represent properties of the components, and to calculate mixture properties;
- process flowsheet, blocks (units) and streams;
- chemical reactions and conversions/kinetics;
- operating conditions of unit operation models;
- temperature, pressure, flowrate and composition of the feed streams.

Components can be retrieved from Aspen Plus databanks, thermodynamic models are built-in

options in the software and unit operations need to be represented by a model through Aspen Plus Model Library.

After the required input is complete, PS is capable to run the simulation and possibly to converge to a solution: in case of convergence, values of all the state variables for both blocks and streams are obtained (temperature, flowrate and composition); if PS does not converge, additional optional data can be specified by the user or, alternatively, convergence method, tolerance or number of iterations can be carefully modified. Aspen Plus solves the process model equation system by the so-called sequential modular approach: each unit is solved sequentially starting from a convenient stream (called tear stream) until convergence is reached.

Other important features of such PS are sensitivity analysis (SA) and design specifications (DS): the first is a quick way to understand the effect of a degree of freedom on the converged values of the process state variables (Bertucco and Barbera, 2021); perturbating the value of a degree of freedom it is possible to evaluate the effect of this change on the solution.

From a mathematical point of view, sensitivity is defined as the partial derivative of state variables with respect to the degree of freedom considered:

$$sens_{i,j} = \frac{\partial x_i}{\partial d_j} \tag{2.1}$$

where i indicates the state variable and j the degree of freedom.

DS is the way of forcing PS to converge a state variable of interest, generally a product variable, into a desired value; more DSs can be set on a single process, and once they have been sequentially converged, they can be kept simultaneously acting as process constraints. With sequential modular approach used by the software, every DS introduces a logical loop in the flowsheet that increases computational burden, since it is also nested with physical recycle loops, complicating more the search for the solution. Anyway, often it is necessary to introduce specifications to reach desired values of purity and flowrate of the product, like in this work as it will described in chapter 3.

In addition, Aspen Energy Analyzer™ v12.1 is utilized to perform heat integration, in order to reduce energy consumption, utilities usage, and the related carbon impact and economic results for the processes considered. Firstly, utilities need to be defined in Aspen Plus and associated to heat exchangers, then through *Activated Energy Analysis* the software calculates potential energy savings following some default assumptions; finally, Aspen Energy Analyzer allows the user to transfer data from Aspen Plus, in order to create and improve a Heat Exchanger Network (HEN).

2.2 Thermodynamic models

After making a comprehensive review of previous works (table 2.1), Soave-Redlich-Kwong (SRK) thermodynamic model is chosen for property estimation in the simulation for pure gases and liquids, and for mixtures, except for methanol purification section, where the Non-Random Two-Liquid (NRTL) model is chosen to better represent Vapor-Liquid equilibria of polar mixtures at low pressures.

2.2.1 Equation of state model

An equation of state (EoS) is an algebraic relation between pressure, volume and temperature, used to estimate the volumetric behaviour of gases and liquids as a function of temperature and pressure. A cubic EoS is thus defined when it is expressed as a cubic function of the molar volume.

In 1949 Redlich and Kwong proposed an improvement to volumetric behaviour of Van der Waals (VdW) EoS and to account for a temperature dependency on the attractive parameter:

$$P = \frac{RT}{V - b} - \frac{aT^{-0.5}}{V(V + b)} \tag{2.2}$$

As for VdW, values of parameters a and b of pure components are determined from critical temperature and pressure: critical volume calculation is not necessarily correct, in fact Redlich-Kwong (RK) EoS predicts the critical compressibility factor Z_c as equal to 0.333, independently of the component; calculation of vapor pressure, similarly to VdW EoS, is a prediction, as no extra adjustable parameters are present in the EoS (Bertucco and Barbera, 2021).

Experimental density variations from the ideal gas to compressed liquid, with the saturation and critical conditions between them, suggest that both the EoSs are inadequate (Poling *et al.*, 2001).

Soave in 1972 introduced an α function for the RK EoS, from which SRK model is defined as:

$$P = \frac{RT}{V_m - b} - \frac{a\alpha(T)}{V_m(V_m + b)} \tag{2.3}$$

which allowed to strongly improve the performance of the EoS.

Thus, Aspen Plus RK-SOAVE thermodynamic model is chosen. In the software, with respect to original SRK model, several important modifications have been introduced:

- a volume translational concept introduced by Peneloux and Rauzy is used to improve molar liquid volume calculated from the cubic EoS;
- improvement in the speed of computation for equation based calculation is achieved by using composition independent fugacity;

- optional Kabadi-Danner mixing rules for improved phase equilibrium calculations in water-hydrocarbon systems;
- optional Mathias alpha function.

This EoS can be used for hydrocarbon systems that include the common light gases, such as H_2S, CO_2, N_2, etc. The form of the EoS is the same as equation (2.3), where $a = a_0 + a_1$.

a_0 represents the standard quadratic mixing term:

$$a_0 = \sum_{i=1}^{n} \sum_{j=1}^{n} x_i x_j \sqrt{a_i a_j}(1 - k_{ij}) \tag{2.4}$$

while a_1 is an additional, asymmetric (polar) term:

$$a_1 = \sum_{i=1}^{n} x_i \sum_{j=1}^{n} x_j \left[\left((a_i a_j)^{\frac{1}{2}} l_{j,i} \right)^{\frac{1}{3}} \right]^3 \tag{2.5}$$

The mixing rule for b parameter is:

$$b = \sum_i x_i b_i \tag{2.6}$$

Single components parameters are function of absolute temperature and critical properties: $a_i = f(T, T_{ci}, p_{ci}, \omega_i)$ and $b_i = f(T, T_{ci}, p_{ci})$.

The two binary interaction parameters are defined in the same way:

$$k_{ij} = k_{ij}^{(1)} + k_{ij}^{(2)} T + \frac{k_{ij}^{(3)}}{T} \tag{2.7}$$

with $k_{ij} = k_{ji}$, and:

$$l_{ij} = l_{ij}^{(1)} + l_{ij}^{(2)} T + \frac{l_{ij}^{(3)}}{T} \tag{2.8}$$

where in general, $l_{ij} \neq l_{ji}$

For best results, the binary parameter k_{ij} must be determined from phase equilibrium data regression, e.g Vapor-Liquid Equilibrium (VLE) data. The Aspen Physical Property System also has built-in k_{ij} for a large number of component pairs in the SRK-ASPEN databank, regressed by AspenTech.

2.2.2 Activity coefficient model

NRTL model calculates liquid activity coefficients, it is recommended for highly non-ideal chemical systems, and it is suitable for using in VLE applications: in this regard, for the vapor phase, the fugacity coefficients are generally computed by means of Hayden-O'Connell (HOC) method, a predictive model that does not require any binary data, but only pure component properties.

From thermodynamics, activity coefficients are estimated through excess Gibbs free energy that can be expressed in three ways (Bertucco and Barbera, 2021):

- by polinomial expansions, according to the Wohl method;
- with models using local composition concept, introduced by Wilson in 1961;
- by fully predictive models.

NRTL is based on Wilson's approach that proposed two relevant improvements with respect to polynomial methods:

- interactions among molecules are expressed in terms of binary parameters only;
- temperature dependency of these parameters is made explicit through a Boltzmann-like equation.

Liquid phase activity coefficients are computed with Aspen Plus NRTL model as:

$$\ln \gamma_i = \frac{\sum_j x_j \tau_{ji} G_{ji}}{\sum_k x_k G_{ki}} + \sum_j \frac{x_j G_{ji}}{x_k G_{kj}} \left[\tau_{ij} - \frac{\sum_m x_m \tau_{mj} G_{mj}}{\sum_k x_k G_{kj}} \right] \tag{2.9}$$

where binary interaction parameters are defined as:

- $G_{ij} = \exp\left(-\alpha_{ij}\tau_{ij}\right)$
- $\tau_{ij} = a_{ij} + \frac{b_{ij}}{T} + e_{ij} \ln\left(T\right) + f_{ij}T$
- $a_{ij} = c_{ij} + d_{ij}(T - 273.15\ \mathrm{K})$
- $\tau_{ii} = 0$
- $G_{ii} = 1$

a_{ij}, b_{ij}, e_{ij} and f_{ij} are unsymmetrical, so that a_{ij} may not be equal to a_{ji}, etc.

Parameters a_{ij}, b_{ij}, c_{ij}, d_{ij}, e_{ij}, f_{ij} can be determined from VLE regression data. Aspen Physical Property System has a large number of built-in binary parameters for the model; binary parameters have been regressed using data from Dortmund Databank by using EoSs.

Table 2.1: Review of thermodynamic models adopted in literature for different operating conditions and methanol synthesis processes (unless differently stated commercial catalysts $Cu/ZnO/Al_2O_3$ are employed)

Article	Thermodynamic model	Methanol synthesis process
Adil *et al.* (2022)	PENG-ROB and SRK	Thermodynamic analysis for synthesis from Biomass-derived syngas
Al-Kalbani *et al.* (2016)	*unknown*	CO2 hydrogenation via captured CO_2 and electrolysis H_2
Butera *et al.* (2020)	RK-SOAVE, PR-BM and SR-POLAR	Straw gasification and electrolysis
Kanuri *et al.* (2021)	PSRK	CO2 hydrogenation analysis of operating parameters and catalysts comparison
Kiss *et al.* (2016)	RK-SOAVE and NRTL	CO2 hydrogenation via a highly active Cu/Zn/Al/Zr fibrous catalyst
Leonzio *et al.* (2019)	RK-SOAVE and NRTL	CO2 hydrogenation
Meunier *et al.* (2020)	RK-ASPEN, Henry's law; ELEC-NRTL, Dortmund modified UNIFAC	CO_2 hydrogenation via MEA-captured CO_2 and H_2 from water electrolysis
Santos *et al.* (2018)	PENG-ROB and NRTL	Synthesis from biogas
Van-Dal and Bouallou (2013)	RKSMHV2 and NRTL-RK	CO_2 hydrogenation via captured CO_2 from flue gas and H_2 from electrolysis
Vita *et al.* (2018)	*unknown*	Thermodynamic analysis on methanol synthesis from biogas
Yang *et al.* (2022)	RK-SOAVE and NRTL	CO_2 hydrogenation via captured CO_2 from flue gas and H_2 from electrolysis

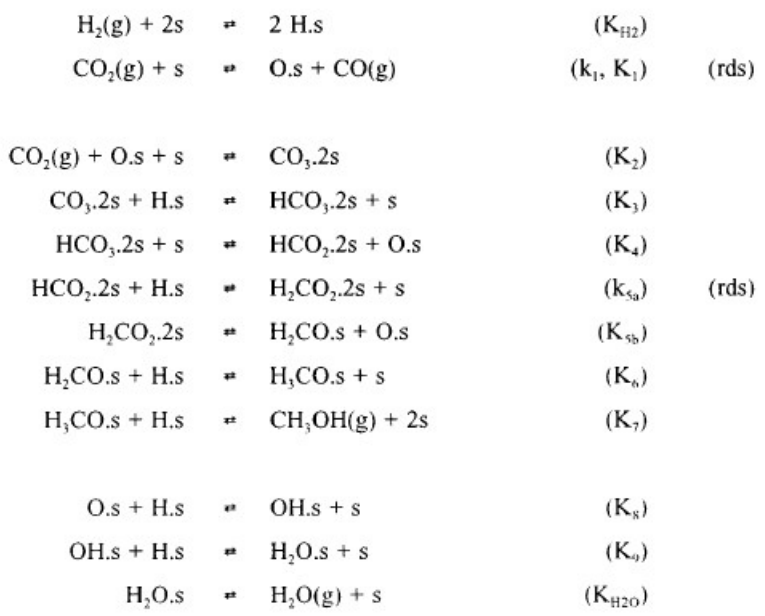

Figure 2.1: Reaction scheme for the synthesis of methanol and the reverse water gas shift reaction. rds, rate determining step (Vanden Bussche and Froment, 1996)

2.3 Kinetic model of methanol synthesis

The approach used for determining catalytic and heterogeneous reaction mechanisms is usually the *Langmuir-Hinshelwood*, coming from ideas proposed by Hinshelwood, based on Langmuir's principles for adsorption. Since this approach was popularized by Hougen and Watson in 1943, kinetic model occasionally includes their names. Langmuir-Hinshelwood-Hougen-Watson (LHHW) kinetic model consists of first assuming a sequence of steps in the reaction, next, rate laws are written for the individual steps (assuming all of these as reversible), and finally a rate-limiting step is postulated in order to eliminate all coverage-dependent terms for steps that are not rate-limiting (Fogler, 2016).

Based on LHHW approach, Vanden Bussche and Froment (1996) developed a steady-state kinetic model for methanol synthesis and water gas shift reaction, starting from previous works and carrying out experimental studies to retrieve kinetic parameters values; experimental data have been obtained in a bench scale setup where methanol synthesis has been performed on a commercial ICI 51-2 $Cu/ZnO/Al_2O_3$ catalyst, with operating temperatures between 180 and 280 °C and at pressures up to 51 bar, while the ratio p_{CO}/p_{CO_2} ranged from 0 to 4.1.

Resulting kinetic equations are:

$$r_{CH_3OH} = \frac{k_1 p_{CO_2} p_{H_2} [1 - p_{CH_3OH} p_{H_2O} / (K_1^* p_{CO_2} p_{H_2}^3)]}{p_{CO_2} + K_{H_2O} p_{CO_2} p_{H_2O} + K'' p_{H_2O}} \tag{2.10}$$

$$r_{rWGS} = \frac{k_2 p_{H_2} p_{CO_2} [1 - p_{CO} p_{H_2O} K_3^* / (p_{CO_2} p_{H_2})]}{p_{CO_2} + K_{H_2O} p_{H_2O} p_{CO_2} + K'' p_{H_2O}} \tag{2.11}$$

Starting from the assumption that CO_2 is the main source of carbon in methanol, the authors presented the different elementary reaction steps to be considered and the nomenclature for equilibrium (K_i) and rate (k_i) constants, that are all reported in figure 2.1. Under the hypothesis of pseudo-steady-state for the concentration of the different surface intermediates, and upon the introduction of the rate determining steps, following expressions are obtained for the rate of methanol synthesis and rWGS reaction:

$$r_{CH_3OH} = k'_{5a} K'_2 K_3 K_4 K_{H_2} p_{CO_2} p_{H_2} \left(1 - \frac{1}{K_1^*} \frac{p_{H_2O} p_{CH_3OH}}{p_{H_2}^3 p_{CO_2}}\right) \beta^3 \tag{2.12}$$

$$r_{rWGS} = k'_1 p_{CO_2} \left(1 - K_3^* \frac{p_{H_2O} p_{CO}}{p_{CO_2} p_{H_2}}\right) \beta \tag{2.13}$$

where partial pressures are expressed in bar and reaction rates in $\mathrm{mol\,s^{-1}kg_{cat}}^{-1}$.

β is the normalized concentration of the free active sites and can be expressed as:

$$\beta = \frac{1}{1 + (K_{H_2O}/K_8 K_9 K_{H_2})(p_{H_2O}/p_{H_2}) + \sqrt{K_{H_2} p_{H_2}} + K_{H_2O} p_{H_2O}} \tag{2.14}$$

Equilibrium constants K_1^* and K_3^* are thermodynamically determined and taken from Graaf *et al.* (1986):

$$\log_{10} K_1^* = \frac{3066}{T} - 10.592 \tag{2.15}$$

$$\log_{10} \frac{1}{K_3^*} = \frac{-2073}{T} + 2.029 \tag{2.16}$$

Kinetic and remaining equilibrium constants are expressed following Arrhenius and Van't Hoff expressions, respectively:

$$K_i = k_i = A_i \exp \frac{B_i}{RT} \tag{2.17}$$

where B_i represents either activation energy (E) or enthalpy ($-\Delta H$), or a combination of those. Values assumed by the parameters are reported in table 2.2.

Van-Dal and Bouallou (2013) rearranged kinetic equations in order to directly implement them in Aspen Plus, creating a compatible kinetic model; LHHW kinetic model from Aspen Plus is considered by incorporating thermodynamic expressions into kinetic constants and modifying units of measure of the expressions to suit software requirements.

Rearranged expressions are here reported, considering that pressures are given in Pa, temperatures in K and reaction rates in $\mathrm{mol\,s^{-1}kg_{cat}}^{-1}$:

Table 2.2: Parameter values for the steady-state kinetic model (Vanden Bussche and Froment, 1996)

Constant expression	Parameters	Values
$\sqrt{K_{H_2}}$	A	0.499
	B	17197
K_{H_2O}	A	6.62×10^{-11}
	B	124119
$\frac{K_{H_2O}}{K_8 K_9 K_{H_2}}$	A	3453.38
	B	-
$k'_{5a} K'_2 K_3 K_4 K_{H_2}$	A	1.07
	B	36696
k'_1	A	1.22×10^{10}
	B	-94765

$$r_{CH_3OH} = \frac{k_1 p_{CO_2} p_{H_2} - k_6 p_{H_2O} p_{CH_3OH} p_{H_2}^{-2}}{(1 + k_2 p_{H_2O} p_{H_2}^{-1} + k_3 p_{H_2}^{0.5} + k_4 p_{H_2O})^3} \tag{2.18}$$

$$r_{rWGS} = \frac{k_5 p_{CO_2} - k_7 p_{H_2O} p_{CO} p_{H_2}^{-1}}{1 + k_2 p_{H_2O} p_{H_2}^{-1} + k_3 p_{H_2}^{0.5} + k_4 p_{H_2O}} \tag{2.19}$$

$$\ln k_i = A_i + \frac{B_i}{T} \tag{2.20}$$

They also reconsidered the activation energies of reactions, readjusted by Mignard and Pritchard (2008), to extend the applicability of the model up to an operating pressure of 75 bar.

The same choice is made for this work, starting from a review of literature (tables 2.4 and 2.5), as for thermodynamic models, and considering operating conditions to validate its applicability. In such tables, unless differently stated, commercial catalysts $Cu/ZnO/Al_2O_3$ are employed; moreover, carbon oxide ratio (COR) and stoichiometric number (SN) are defined as:

$$COR = \frac{y_{CO_2}}{y_{CO_2} + y_{CO}} \tag{2.21}$$

$$SN = \frac{y_{H_2} - y_{CO_2}}{y_{CO_2} + y_{CO}} \tag{2.22}$$

Table 2.3: Parameters of the rearranged kinetic model (Van-Dal and Bouallou, 2013)

k_1	A_1	-29.87
	B_1	4811.2
k_2	A_2	8.147
	B_2	0
k_3	A_3	-6.452
	B_3	2068.4
k_4	A_4	-34.95
	B_4	14928.9
k_5	A_5	4.804
	B_5	-11797.5
k_6	A_6	17.55
	B_6	-2249.8
k_7	A_7	0.1310
	B_7	-7023.5

Table 2.4: Review of kinetic models adopted in literature for different operating conditions and methanol synthesis processes (I)

Article	Operating conditions range	Methanol synthesis process and reactor	Reference kinetic model
Adil *et al.* (2022)	225 °C 82 bar *different molar ratios*	Biomass-derived syngas (Lurgi-type isothermal reactor)	Graaf *et al.* (1988)
Asif *et al.* (2018)	150-300 °C 10-80 bar CO2:H2=6-88 (wt.%)	CO_2 hydrogenation (PFR with constant inlet temperature)	Vanden Bussche and Froment (1996) Graaf *et al.* (1988)
Al-Kalbani *et al.* (2016)	265 °C *unknown* *unknown*	CO_2 hydrogenation (Lurgi-type isothermal reactor)	Vanden Bussche and Froment (1996)
Butera *et al.* (2020)	230-260 °C 80.7-85 bar H_2:CO_2=2 (mol%)	Straw gasification combined with water electrolysis (Lurgi-type isothermal reactor)	*unknown*
Kiss *et al.* (2016)	200-300 °C 1-100 bar H_2:CO_2=3-12 (mol%)	CO_2 hydrogenation via a highly active Cu/Zn/Al/Zr fibrous catalysts (Isothermal multitubular PFR)	Graaf *et al.* (1988) with kinetic data from An *et al.* (2009)
Leonzio *et al.* (2019)	200-280 °C 15-55 bar CO:CO_2=1-2:1-2 (mol%)	CO_2 hydrogenation (Lurgi-type isothermal reactor)	Vanden Bussche and Froment (1996)
Meunier *et al.* (2020)	250 °C 80 bar H_2:CO_2=3 (mol%)	CO_2 hydrogenation (CO_2 captured via MEA) (Adiabatic PFR)	Graaf *et al.* (1988) *(B2-C3 model)*
Meyer *et al.* (2015)	238-263 °C 81 bar H_2:CO_2=70-80:20-30 (mol%)	CO_2 hydrogenation (Pseudo-homogeneous shell tube PFR)	Vanden Bussche and Froment (1996) Graaf *et al.* (1988)
Nestler *et al.* (2020)	230 °C 50-80 bar COR=0.25-1, SN=1.5-3.5	Kinetic studies (Lurgi-type isothermal reactor)	Graaf *et al.* (1988) with kinetic parameters of Henkel (2011)

Table 2.5: Review of kinetic models adopted in literature for different operating conditions and methanol synthesis processes (II)

Article	Operating conditions range	Methanol synthesis process	Reference kinetic model
Park *et al.* (2014)	250-340 °C 50-90 bar *different molar ratios*	Kinetic studies on CO and CO_2 hydrogenation (PBR-modeled microreactor)	Graaf *et al.* (1988) with an additional DME kinetic model from Ng *et al.* (1999)
Peréz-Fortes *et al.* (2016)	210-288 °C 76 bar CO_2:H2:CO=75:13:12 (wt.%)	Integrated CCU process with purchased H_2 (adiabatic PFR)	Van-Dal and Bouallou (2013)
Peter *et al.* (2012)	190-250 °C 5-60 bar *different syngas compositions*	Kinetic modeling of CO CO_2 hydrogenation (fixed bed PFR microreactor)	*several previous works*
Santos *et al.* (2018)	200-260 °C 60-80 bar *unknown*	Biogas to methanol (Lurgi-type isothermal reactor)	Vanden Bussche and Froment (1996)
Seidel *et al.* (2018)	200-300 °C 50-100 bar *different molar ratios*	Kinetic modeling of CO CO_2 hydrogenation (CSTR micro-Berty reactor)	Vollbrecht (2007)
Van-Dal and Bouallou (2013)	210-284 °C 75.1-75.7 bar H_2:CO:CO_2=92:4.5:3.5 (mol%)	CO_2 hydrogenation (adiabatic PFR)	Vanden Bussche and Froment (1996) with readjusted parameters of Mignard and Pritchard (2008)
Vita *et al.* (2018)	250 °C 100 bar SN=2	Thermodynamic analysis on synthesis from biogas	Graaf *et al.* (1988)
Yang *et al.* (2022)	200 °C 80 bar H_2:CO_2=3	CO_2 hydrogenation (isothermal PFR)	Graaf *et al.* (1988) with kinetic data from Kiss *et al.* (2016) and Asif *et al.* (2018)

2.4 Methanol production processes and assumptions

In the following sections , the five processes considered in this thesis and the corresponding assumptions are described in detail. In all cases, a methanol production of 100000 t/yr (i.e. 382.5 kmol/h) has been taken as the base of calculations.

2.4.1 Methane steam reforming to methanol

Industrially, methanol is produced from natural gas, or pure methane, following the process scheme reported in figure 2.2: a mixture of CO, H_2 and CO_2 is produced by steam reforming, a process in which natural gas and steam are mixed and reacted in a reformer operated at 16 bar; natural gas enters the process at 30 °C and steam at 210 °C, mixture is preheated to 450 °C by exhaust gases from the furnace (i.e. the reformer) and is introduced in the reformer where the following reaction occurs:

$$CH_4 + H_2O \rightleftharpoons CO + 3\,H_2 \qquad (\Delta H_{298\ K} = -206.36\ \text{kJ/mol}) \tag{2.23}$$

Another reaction, 1.13, occurs with the formation of H_2 and CO_2. The product gas leaves the reformer at 855 °C and 16 bar: even though steam reforming is carried out at a high temperature, a catalyst is required, due to the high stability of methane, to accelerate the reaction; the catalyst is contained in tubes that are placed inside the furnace heated by the combustion of a fuel, typically natural gas. In general, a furnace contains 500-600 tubes with a length of 7-12 m and an inside diameter of between 70 and 130 mm (Moulijn *et al.*, 2013)

From an energetic point of view, energy efficiency in the process is improved by recovering heat from the burner exhaust gas, which leaves the furnace at 960 °C; this gas is cooled in a series of heat exchangers that preheat the reformer feed, as already mentioned, then produces super-heated steam at 48 bar and 100 °C superheat, from boiler feed water (bfw) at 30 °C, and also preheats combustion air to 300 °C. Superheated steam is used to drive turbines elsewhere in the process or it can be exported to generate electricity. Product gas leaving the reformer contains water that should be removed to reduce the amount of gas that must be compressed, and to minimize the impact on subsequent conversion of CO and CO_2 to methanol, considering equilibria (1.1), (1.2) and (1.3). Heat is removed from the gas by generating superheated steam, cooling the gas at a temperature of 15 °C higher than that of the steam, then 3 steps occur in both recovering heat and reducing water content:

1. heat recovery for use downstream in the process;
2. cooling by ambient air in an air cooler;
3. use of cooling water to reduce temperature of syngas to 35 °C.

Condensed water is collected in a condensate drum, and makeup gas compressor increases the

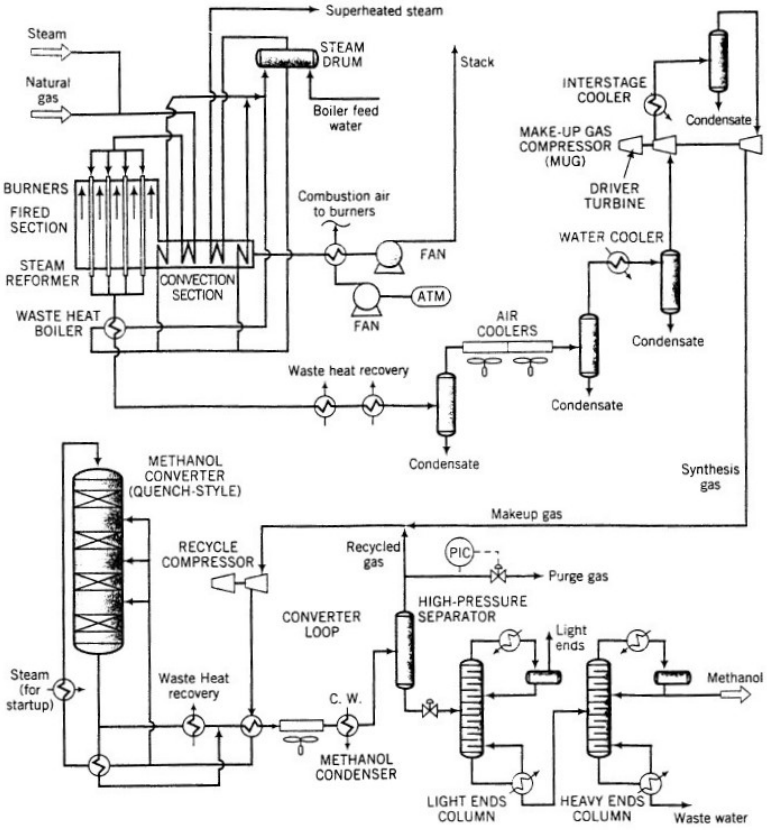

Figure 2.2: Flowchart for overall methanol synthesis process (Felder and Rousseau, 2005)

pressure of the gas from 16 to 75 bar in 2 stages; between the stages, gas is cooled to 100 °C by using cooling water and removing any condensate formed. The compressed gas is introduced into the converter loop where it is combined with recycle gas: this loop is composed of a recycle compressor to compensate pressure drops, methanol synthesis reactor, heat exchangers, a methanol condenser, and a gas-liquid separator (flash drum). After recycle and fresh gas are blended, mixture is heated to 130 °C by a partially cooled product stream leaving the reactor: recycle to feed ratio in this process is 7.8. Feed mixture is then split into two streams: 30% is sent to another heat exchanger where its temperature is raised to 220 °C by a fraction of the product stream and injected into the first stage of methanol reactor; remaining 70%, which is still at 130 °C, is injected at various locations along the reactor.

The product gas leaving the reactor is partially cooled by being split into two streams: one, as already mentioned, is used to heat the feed stream, and the other passes through a waste-heat recovery unit. Afterwards, they recombine and are further cooled in an air-cooled exchanger, before being brought to 35 °C by cooling water: at this point, a liquid consisting of methanol and dissolved gases is separated from the gas stream in a flash drum and sent to the purification system; uncondensed gases are then split, with a portion that is purged from the system, and the remainder that forms the recycle gas (Felder and Rousseau, 2005).

Methanol purification, generally, requires 2 towers: the first one, named *topping column*, removes the light ends (mainly by-products generated during methanol synthesis, and dissolved

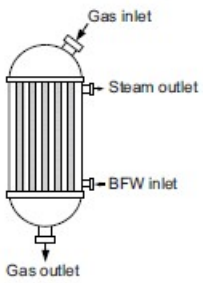

Figure 2.3: Schematic of Lurgi reactor for methanol production

light gases), the second one, named *refining column*, separates methanol and water, and any other by-products less volatile than methanol; methanol is recovered, almost pure, as the overhead product of the second column. More rarely, other configurations may be adopted as reported by Dybkjaer *et al.* (2006), with 3 or 4 columns, in the so-called *double stage distillation* where, other than a topping column and two refining columns, there is a column for ethanol recover: one of the two columns is operated at a slightly higher pressure, in order to integrate heat exiting the condenser of the high-pressure column with reboiler duty of the low-pressure column, with a potential energy savings of 30% in terms of overall distillation energy requirement.

Moreover, several configurations may be adopted for what regards the reactor for methanol synthesis (Dybkjaer *et al.*, 2006 and Moulijn *et al.*, 2013):

- quench reactor: several catalytic beds are present and installed in series, where feed is distributed between each bed. Reaction temperature is controlled by the introduction of the feed at different stages, but catalyst effectiveness factor is low;
- adiabatic reactor: series of fixed bed reactors where heat removal is performed downstream of each reactor by medium-pressure (MP) steam, with a higher efficiency with respect to the previous case;
- boiling water reactor: shell-tube heat exchanger with catalyst contained inside tubes. An example is Lurgi reactor reported in figure 2.3, where cooling is provided by bfw in order to keep nearly isothermal conditions. For large plants several reactors need to be employed in parallel;
- gas-cooled reactor: exchanger-type reactor coupled and adjacent to a boiling water reactor. On one side of the exchanger, feed of boiling water reactor is preheated, on the other side there is catalyst, and effluent from boiling water reactor reaches equilibrium at a lower temperature. Coupling these 2 reactors, single-pass conversions are very high, but, due to the low temperatures of gas-cooled reactor, the rate of reaction is small and amount of catalyst needed increases as a consequence;
- integrated gas-cooled reactor: with respect to the previous case, there is only one reactor whose design is similar to the one of boiling water reactor. Feed gas, in this case, is preheated in concentric tubes, inserted inside tubes containing catalyst of boiling water

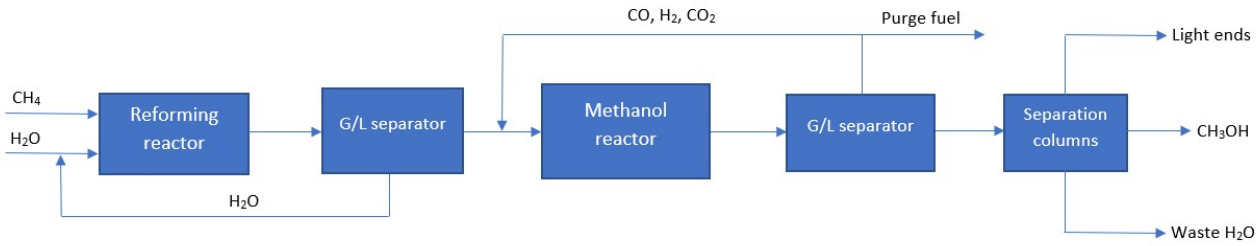

Figure 2.4: BFD of methane steam reforming to methanol process

reactor. Due to mechanical complexity, this configuration is affected by high capital costs.

- radial flux reactor: cooled by a flux of boiling water, but for this configuration catalyst is charged shell-side, and water circulates through tubes. Synthesis gas feed is distributed through the shell, and is collected in a central tube. If production is needed to be increased, solution is just increasing reactor height while, in terms of efficiency, this configuration is between boiling water reactor and adiabatic reactor.

- slurry reactor: solid catalyst is suspended in an inert hydrocarbon liquid, while the feed gas passes through the bed in the form of bubbles. Catalyst remains in the reactor and the hydrocarbon liquid, after being separated from the gas phase, is recycled via a heat exchanger. Temperature control is very efficient, due to the presence of inert hydrocarbon that limits temperature rise; result is a higher single-pass conversion, reducing syngas compression costs. Largest dimensions of the reactor are needed due to the limitations in catalyst loading, that can not exceed 50 wt.% of slurry-phase concentration.

MSR to methanol process, as already underlined, represents the reference for this work to make a comparison with the other processes: anyway, the aim is not to carry out a detailed simulation of the process, but to quantify the material and energy balance of the main process units. In this way, some simplifications and assumptions have been considered in building, firstly, process block flow diagram (BFD), represented in figure 2.4, and then the complete process flowsheet. More in details, from the BFD, a preliminary look at the process can be given: methane and steam are fed to the reforming reactor in a precise molar ratio, then, after the reactor, by lowering the pressure, product gas and liquid water are separated; condensed water is recycled back to generate steam, and gases go to methanol synthesis section. Products exiting the methanol reactor go to a gas/liquid phase separator where liquid is directed to purification units section, and gas is recycled back to the methanol reactor inlet, with a partial purge to avoid inert accumulation. The purification section is formed by two distillation columns, from which light ends exit as the overhead product of the first column, and bottom product of such column goes to a second column, where pure methanol is obtained as the overhead product, while wastewater is available as the bottom one.

Considering the reformer reaction, the following choices have been made in building the model:

- feed is constituted of water and pure methane (already desulfurized) at ambient temper-

Table 2.6: Typical reformer conditions for industrial syngas-based processes (readapted from Moulijn *et al.*, 2013)

				Composition (vol%)[1]			
Process	H_2O/C (mol/mol)	T_{exit} (°C)	p_{exit} (bar)	H_2	CO	CO_2	CH_4
Hydrogen	2.5	850	27	48.6	9.2	5.2	5.9
Hydrogen[2]	4.5	800	27	34.6	5.3	8.0	2.4
Ammonia	3.7	800	33	39.1	5.0	6.0	5.5
Methanol	3.0	850	17	50.3	9.5	5.4	2.6
Aldehydes/alcohols	1.8	865	17	28.0	25.9	19.7	1.1
Reducing gas	1.15	950	5	70.9	22.4	0.9	1.5

ature and pressure;

- steam to carbon (S/C) ratio is set equal to 3. This value generally ranges from 2.5 to 4.5 mol H_2O per mol CH_4 (with the higher limit applied to higher hydrocarbons feeds, such as naphta), the reason is to prevent carbon formation that results in two avoidable situations: first, coke deposition on the active sites of the catalyst that leads to deactivation, then, heat transfer limitations following the formation of *hot spots* on the reformer tubes. Carbon formation occurs at high temperatures (> 650 °C), following the reaction of steam cracking that generates alkenes (equation 1.18), which in turn form carbon through the following reactions (Moulijn *et al.*, 2013):

$$C_nH_{2n} \longrightarrow n\,(C + H_2) \tag{2.24}$$

- thermodynamics suggests to lead the reaction at high temperatures, due to endothermicity of the reaction, and low pressures considering that reaction increases the number of moles; however, since most applications require syngas at elevated pressure, among these methanol synthesis, modern steam reformers operate at pressures far above the atmospheric one, despite the fact that this is thermodynamically unfavorable. The advantages are lower syngas compression costs and smaller volumes needed for the reforming reaction; to counterbalance negative effect on the equilibrium, steam reforming is carried out at very high temperatures, almost reaching limits imposed by materials of construction. Starting from information reported in table 2.6, a constant temperature of 850 °C and pressure of 17 bar are considered for reforming reaction in this work: heat absorbed by reaction is compensated by burning natural gas in the furnace, at 1000 °C exiting at 960 °C;

- WGS reaction (1.13) is also considered in the simulation, because it occurs spontaneously in the reaction environment, even if with a quite low conversion of CO, due to thermodynamic constraints. For pure hydrogen synthesis, WGS reaction is performed in two

[1] Rest is H_2O
[2] From naphta

separated reactors (a high-temperature and a low-temperature one) in order to increase the H_2/CO ratio of the syngas, to finally obtain pure hydrogen, via Pressure Swing Adsorption (PSA). In this work, and, in general, for MSR to methanol processes, since there is no need of pure hydrogen to get methanol, WGS reactors are not employed;

- In Aspen Plus, the reactor is simulated considering a RSTOIC model unit. Reactions are considered to occur in series, considering that there is no CO in the reactor feed and thus WGS reaction starts occurring only when just a little amount of CO is produced from MSR reaction;
- Considering the absence of precise conversion data coming from industry, an estimation is performed for the 2 reactions considered, in order to implement these information in the software. To this aim, thermodynamic equilibrium constants are retrieved from Felder and Rousseau (2005):

  1. MSR reaction:

$$K_{p_{(2.23)}} = \frac{y_{\mathrm{CO}} y_{\mathrm{H_2}}^3}{y_{\mathrm{CH_4}} y_{\mathrm{H_2O}}} P^2 \tag{2.25}$$

$$\log_{10} K_{p_{(2.23)}} = -\frac{11769}{T(\mathrm{K})} + 13.1927 \tag{2.26}$$

  2. WGS reaction:

$$K_{p_{(1.13)}} = \frac{y_{\mathrm{CO_2}} y_{\mathrm{H_2}}}{y_{\mathrm{CO}} y_{\mathrm{H_2O}}} \tag{2.27}$$

$$\log_{10} K_{p_{(1.13)}} = \frac{1197.8}{T(\mathrm{K})} - 1.6485 \tag{2.28}$$

Equations are solved numerically in MATLAB from MathWorks® platform, and conversion values obtained are $X_{\mathrm{CH_4}} = 87.0\%$ for MSR reaction and $X_{\mathrm{CO}} = 15.5\%$ for WGS (the code is provided in appendix A).

Moreover, in a preliminary phase, thermodynamic conversion values have been also considered for methanol synthesis section calculations, prior to implementing kinetics in the software; such values have been retrieved and estimated from Chang *et al.* (1986), even if they refer to a precise composition of the feed of the methanol reactor (15% CO, 8% CO_2, 74% H_2 and 3% CH_4). Since methanol synthesis is currently performed at temperatures between 220 °C and 300 °C, and pressures between 50 and 100 bar, the choice made in this work is a constant reaction temperature of 252 °C, and a pressure of 75 bar; a recycle-to-purge ratio of 9 is finally chosen.

In methanol production from syngas or via CO_2 hydrogenation, side reactions reported in figure 2.5 usually occur: in this work, apart from WGS reaction, the others are neglected. Indeed, as reported in Dybkjær *et al.* (2006), process is very efficient and catalyst selectivity is very high, reaching values of about 99.9% versus by-products formation.

Methanol synthesis section, in general, is the same for all the processes: for this reason, assumptions explanation will not be replicated in next sections. Complete processes flowsheets

	ΔG° (kcal/mol)	ΔH° (kcal/mol)
*** DESIRED REACTION ***		
$CO + 2\,H_2 \rightleftharpoons CH_3OH$	+12.1	-24.5
$CO_2 + 3\,H_2 \rightleftharpoons CH_3OH + H_2O$	+15.8	-15.3
*** OTHER REACTIONS ***		
$CO + H_2O \rightleftharpoons CO_2 + H_2$	-3.7	-9.1
$CO + 3\,H_2 \rightleftharpoons CH_4 + H_2O$	-15.8	-52.2
$2\,CO + 2\,H_2 \rightleftharpoons CH_4 + CO_2$	-19.5	-61.3
$CO + H_2 \rightleftharpoons HCHO$	+16.1	-5.1
$HCHO + H_2 \rightleftharpoons CH_3OH$	-4.0	-19.5
$2\,CH_3OH \rightleftharpoons CH_3OCH_3 + H_2O$	-1.4	-4.6
$2\,CO \rightleftharpoons CO_2 + C$	-16.7	-4.14

Figure 2.5: Desired and side reactions occurring in methanol synthesis from syngas (Modesti, 2021)

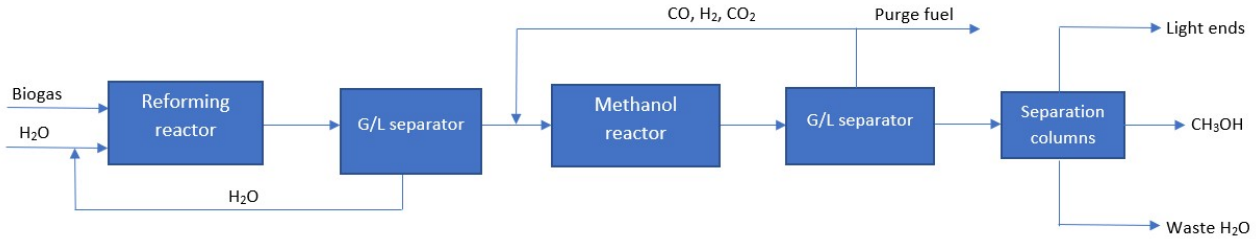

Figure 2.6: BFD of biogas reforming to methanol process

will be detailed in the next chapter, as well as equipment specifications.

2.4.2 Biogas reforming to methanol

Biogas reforming to methanol process represents an alternative to MSR to methanol, in terms of feedstock: instead of using natural gas, a fossil fuel, biogas can be used as a source of CH_4, with some consequences on the choices of reactor operating conditions, and subsequent 2-phase separator. Many works are present in literature, carrying out experimental campaigns on biogas reforming to generate "green" syngas. In this work, biogas is assumed to be composed of CO_2 and CH_4 in a molar ratio of 0.65 (about 60 mol% of CH_4 and 40 mol% of CO_2); a summary of the articles found in literature considering this composition is reported in table 2.8, with related operating conditions of the reforming process, and CH_4 conversion data.

As reported in Zhao *et al.* (2020), bi-reforming or tri-reforming reactions can interest the more generic biogas reforming process, where the first one is the combination of the classical MSR

reaction (2.23) and the methane dry reforming (MDR) reaction, in which reforming is operated by CO_2 naturally present in biogas, instead of externally added steam, according to:

$$CH_4 + CO_2 \rightleftharpoons 2\,CO + 2\,H_2 \qquad (\Delta H_{298\ K} = 247\ kJ/mol) \tag{2.29}$$

Tri-reforming involves also a PO reforming reaction, that occurs when O_2 is injected in the reformer, as:

$$CH_4 + \frac{1}{2}\,O_2 \rightleftharpoons CO + 2\,H_2 \qquad (\Delta H_{298\ K} = -36\ kJ/mol) \tag{2.30}$$

Considering the articles reported in table 2.8, bi-reforming is performed in the works of Ahmed *et al.* (2015), Effendi *et al.* (2005), Ghosh *et al.* (2019), Rahmat *et al.* (2020), and Roy *et al.* (2018); instead, oxygen is added to perform also PO reforming in the works of Di Marcoberardino *et al.* (2018), Galvagno *et al.* (2013), Izquierdo *et al.* (2012), Tuna *et al.* (2018), and Vita *et al.* (2018).

Different catalysts and operating conditions are being investigated because, mainly, four side reactions usually occur, affecting conversions and catalyst performance:

- CO disproportionation:

$$2\,CO \longrightarrow C + CO_2 \tag{2.31}$$

- CO methanation:

$$CO + 3\,H_2 \longrightarrow CH_4 + H_2O \tag{2.32}$$

- CO_2 methanation:

$$CO_2 + 4\,H_2 \longrightarrow CH_4 + 2\,H_2O \tag{2.33}$$

- CO reduction:

$$CO + H_2 \longrightarrow C + H_2O \tag{2.34}$$

In this work PO reaction is not taken into account, considering just steam reforming, with dry reforming occurring naturally due to the presence of CO_2 in the biogas composition, favoured by reaction conditions. Based on experimental data, side reactions are neglected, as it will be explained later on.

The BFD of the biogas bi-reforming to methanol process (referred commonly, in this work, as biogas reforming) is reported in figure 2.6: biogas and steam are fed to the reforming reactor in a precise molar ratio, then, after reaction is complete, product gas and liquid water are separated in a flash drum; water is recycled back to generate steam, and gases go to methanol synthesis section. Products exiting methanol reactor go to another gas/liquid phase separator where liquid is directed to the purification units section, and gas is recycled back to the methanol reactor inlet, with a partial purge to avoid inert accumulation. Purification section is formed by two distillation columns, from which light ends exit as the overhead product of the first

column, and bottom product of such column goes to a second column, where pure methanol is obtained as the overhead product, while wastewater is available as the bottom one.

Among works presented in table 2.8, experimental data are taken in accordance to Ahmed *et al.* (2015).

For the biogas reforming to methanol process the following choices have been made in building the model:

- feed is constituted of water at ambient temperature and biogas at 37 °C (general outlet temperature of a mesophilic digester). Pressure is the atmospheric one;
- steam to carbon (S/C) ratio equal to 1.28. In the reference article this value ranges from 1.28 to 3.86 mol H_2O / (mol CH_4 + mol CO_2), but better performances in terms of methane conversion are obtained at S/C=1.28;
- thermodynamics suggests to lead the reforming reactions at high temperatures (being both endothermic) and low pressures, considering that the number of moles increases; however, differently from the case of MSR to methanol, reactions are carried out at atmospheric pressure, considering that conversion data from literature are available only at that pressure, and extrapolation can not be performed, neither correlations or other models are available from literature for estimations at different pressures. The reformer operates at a constant temperature of 650 °C for the same reasons: heat absorbed by reaction is compensated by burning natural gas in the furnace, at 800 °C exiting at 760 °C;
- WGS reaction (1.13) is also considered in the simulation, because it occurs spontaneously in the reaction environment, even if with a quite low conversion of CO, due to thermodynamic constraints. In this case, 3 reactions need to be considered, instead of 2 of the MSR to methanol process, with MSR and MDR occurring in parallel, and WGS in series. Since it is not possible to set this in a single RSTOIC reactor unit in Aspen Plus, 2 different reactors are considered in the simulation: the first one, reforming reactor, in which reactions (2.23) and (2.30) occur, and the second one, the WGS reactor, in which just reaction (1.13) occurs. WGS reaction, as already mentioned in MSR to methanol process, starts occurring only when just a little amount of CO is produced from MSR and MDR reactions. However, this is simply a simulation artifact, while a single reactor is considered when performing the economic analysis;
- conversion data are recalculated starting from the reference work of Ahmed *et al.* (2015): considering that in the article the presence of by-products at the reformer outlet is neglected, an error of 10% emerges from carbon mass balance; consequently, either global CH_4 (for both reforming reactions) or CO conversion data, or both of these, are affected by an error with respect to experimental data. In a first instance, CH_4 conversion of MSR reaction and CO_2 conversion of MDR are assumed as fixed, and the error is attributed entirely to WGS reaction: the result is a relative error of CO product yield of almost 20%

(table 2.7). From this consideration, the need of a distribution among also CO_2 species arises by solving an optimization problem;

- considering, instead, only the global CH_4 conversion as not affected by errors, CH_4 conversion of MSR reaction, and consequently CO_2 conversion of MDR reaction, and CO conversion of WGS reaction are recalculated by a least-squares optimization model that minimizes the sum of square relative errors of the 4 species involved in the reaction, with respect to experimental products yields: anyway, methane is considered not to be affected by an error in yield calculation, thus number of species actually involved is equal to 3. Starting from experimental products yields reported in table 2.7, values are recalculated by setting a guess value of CH_4 conversion in MSR reaction, and of CO conversion in WGS reaction, with the difference that represents the error of the model with respect to experimental data:

$$e_i = y_i^{calc} - y_i^{exp} \tag{2.35}$$

where i is one of the three species involved, and y stands for the product yield ($\mathrm{mol_i/mol_{CH_4}}$).

Calculated products yields are obtained from the 2 conversion values choices, assuming as the base of calculation a molar flowrate of CH_4 equal to 1 kmol/h:

$$\begin{cases} Y_{\mathrm{H_2}}^{calc} = 3 \cdot \vec{x}_{\mathrm{CH_4}}^{(2.23)} + 2 \cdot \vec{x}_{\mathrm{CH_4}}^{(2.30)} + \vec{x}_{\mathrm{CO}}^{(1.13)} \cdot (\vec{x}_{\mathrm{CH_4}}^{(2.23)} + 2 \cdot \vec{x}_{\mathrm{CH_4}}^{(2.30)}) \\ Y_{\mathrm{CO_2}}^{calc} = 0.65 - \vec{x}_{\mathrm{CH_4}}^{(2.30)} + \vec{x}_{\mathrm{CO}}^{(1.13)} \cdot (\vec{x}_{\mathrm{CH_4}}^{(2.23)} + 2 \cdot \vec{x}_{\mathrm{CH_4}}^{(2.30)}) \\ Y_{\mathrm{CO}}^{calc} = \vec{x}_{\mathrm{CH_4}}^{(2.23)} + 2 \cdot \vec{x}_{\mathrm{CH_4}}^{(2.30)} - \vec{x}_{\mathrm{CO}}^{(1.13)} \cdot (\vec{x}_{\mathrm{CH_4}}^{(2.23)} + 2 \cdot \vec{x}_{\mathrm{CH_4}}^{(2.30)}) \\ Y_{\mathrm{CH_4}}^{calc} = 1 - \vec{x}_{\mathrm{CH_4}}^{(2.23)} - \vec{x}_{\mathrm{CH_4}}^{(2.30)} = y_{\mathrm{CH_4}}^{exp} \end{cases} \tag{2.36}$$

where $(\vec{x}_{\mathrm{CH_4}}^{(2.23)})^T$ and $\vec{x}_{\mathrm{CO}}^{(1.13)}$, which indicate conversion of CH_4 in reaction (2.23) and conversion of CO in (1.13), respectively, assume 200 evenly spaced values in the interval [0,1]; $\vec{x}_{\mathrm{CH_4}}^{(2.30)}$ is calculated as the difference between $X_{\mathrm{CH_4}}^{global}$ and $\vec{x}_{\mathrm{CH_4}}^{(2.23)}$.

At this point, a 200x200 square matrix is defined as $X = (\vec{x}_{\mathrm{CH_4}}^{(2.23)})^T \cdot \vec{x}_{\mathrm{CO}}^{(1.13)}$

Element-wise relative error is defined as the ratio between the error and the experimental product yield, for a generic species s:

$$(\mathcal{E}_{r,s})_{i,j} = \frac{(E_s)_{i,j}}{y_s^{exp}} = \frac{(Y_s^{calc})_{i,j} - y_s^{exp}}{y_s^{exp}} \qquad i,j \in [0,200] \tag{2.37}$$

where $s = \mathrm{H_2}, \mathrm{CO_2}, \mathrm{CO}$.

The optimization problem, as already stated, consists of the minimization of an objective function F^{obj}, defined as the sum of square relative errors (SSRE):

Table 2.7: Experimental vs calculated yields and relative errors before and after applying optimization model (mol_i/mol_{CH_4})

		Before optimization		After optimization	
Species	Experimental	Calculated	Relative error	Calculated	Relative error
H_2	2.280	2.484	0.08225	2.558	0.10851
CO	0.700	0.868	0.19324	0.794	0.11893
CO_2	0.637	0.637	0.00000	0.694	0.08148
CH_4	0.162	0.162	0.00000	0.162	0.00000

$$\min F^{obj} = \min_{i,j} \sum_{s} (\mathcal{E}_{r,s})^2_{i,j} = \min_{i,j} \sum_{s} \left(\frac{(Y_s^{calc})_{i,j} - y_s^{exp}}{y_s^{exp}} \right)^2 \tag{2.38}$$

where bounds constraints are present, and they are represented by X matrix dimensions, in terms of i rows and j columns.

Dealing with vectors, for 2 conversion values, and matrices, for calculated products yields, the results of the problem consists of a 2-elements vector; such elements correspond to i, j values corresponding to the position in X matrix of the following optimal conversion values: $x_{CH_4}^{(2.23)}$ equal to 0.7236 and $x_{CO}^{(1.13)}$ equal to 0.1658. All of these calculations are performed in MATLAB platform (code is provided in the Appendix **??**).

The detailed process flowhseet and corresponding units specifications are better described in chapter 3.

Table 2.8: Review of biogas conversion data from literature for different biogas compositions and operating conditions. When conversion data are not reported in the article, calculated values are presented

Article	CH_4:CO_2	Temperature (°C)	Pressure (bar)	S/C ratio	Catalysts	CH_4 conversion (%)
Ahmed *et al.* (2015)	0.66-1.82	590-685	1.01-1.72	1.28-3.86	4 (wt.%) Rh/La-Al_2O_3	66.8-99.0
Di Marcoberardino *et al.* (2018)	1.30-1.71	800	12-14	4.00	*unknown*	92.6 (*calc.*)
Effendi *et al.* (2005)	1.50	650-850	1.01	0.67-1.67	11.5 (wt.%) Ni/Al_2O_3	> 98
Galvagno *et al.* (2013)	1.50	800	1.00	1.20	Ni/Al_2O_3	~ 100 (*calc.*)
Ghosh *et al.* (2019)	1.50	900	15	2.50	-	94.1
Izquierdo *et al.* (2012)	1.50	800	1.01	1-3	*various*	76.2-99.8
Rahmat *et al.* (2020)	1.00-2.00	600-900		1-3	Ni-$MgAl_2O_4$	$\sim 80 - 96$
Roy *et al.* (2018)	1.50	600-850	1.01	1.50	1.31 (wt.%) Pd-Rh/$CeZrO_2$-Al_2O_3	50.0-95.0
Tuna *et al.* (2018)	1.00-1.50	650-850	1.00	1.50	7.4 (wt.%) Ni/$NiAl_2O_4$/γ-Al_2O_3 and 3.1 (wt.%) Ru/γ-Al_2O_3	-
Vita *et al.* (2018)	1.00-2.30	400-900	1.00	0-4	*unknown*	18.0-100

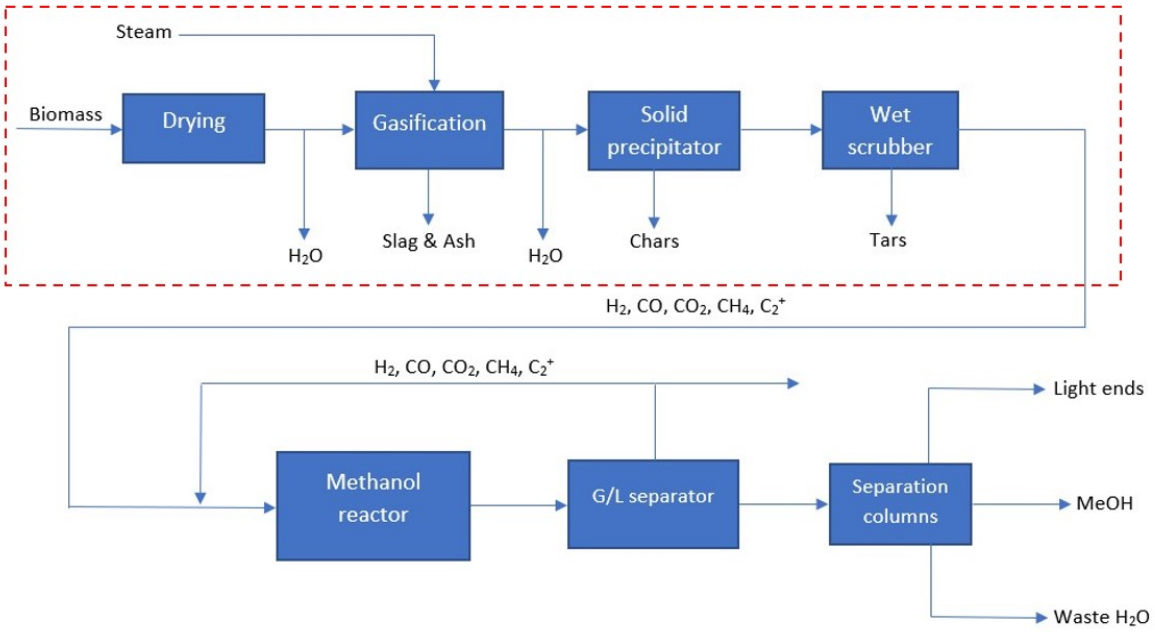

Figure 2.7: BFD of biomass steam gasification to methanol process

2.4.3 Biomass steam gasification to methanol

Biomass steam gasification to methanol process represents another alternative to MSR to methanol process, in terms of feedstock: biomass, a natural organic feedstock, substitutes fossil-based methane in generating syngas.

Gasification consists of several elementary chemical reactions, beginning with the partial oxidation of a lignocellulosic feedstock (cellulose, hemicelluloses, and lignin), when using biomass as feedstock with a gasifying agent such as air, oxygen, steam, or a combination of oxygen and steam. Volatile compounds, released by burning the feedstock, partially oxidize to yield combustion products, such as H_2O and CO_2. Feedstock pyrolysis continues with burning feedstock, and when reaching higher temperatures gasification occurs, providing a product gas mixture composed of CO, CO_2, H_2O, H_2, CH_4, other gaseous hydrocarbons, tars, char, inorganic constituents, and ash, owing to thermal decomposition and partial oxidation of the pyrolysis vapours (Subramani *et al.*, 2015); char is the solid yield of pyrolysis, and it is mainly constituted of carbon ($\sim$ 85%), while tar is the liquid yield, a black tarry fluid containing up to 20% of water, and that consists mainly of homologous phenolic compounds (Basu, 2010).

A simplified BFD of the process is reported in figure 2.7: after biomass is gasified, and syngas is purified from solid particles (chars) and liquid contaminants (tars), the gaseous mixture enters the methanol reactor; at this point, synthesis process occurs, and product gas is directed to a gas/liquid phase separator (flash drum) where liquid goes to purification section, and gas is recycled back as the methanol reactor inlet, with a partial purge to avoid inert accumulation. Purification section is formed by two distillation columns, from which light ends exit as the overhead product of the first column, and bottom product of such column goes to second column, where pure methanol is obtained as the overhead product, while wastewater is available

Table 2.9: Typical levels of tar in biomass gasifier by type (Basu, 2010)

Gasifier Type	Average tar concentration in product gas (g/Nm^3)	Tar as % of biomass feed
Downdraft	< 1.0	< 2.0
Fluidized bed	10	1-5
Updraft	50	10-20
Entrained flow	negligible	

as the bottom one.

In Morandin and Harvey (2015) an additional MSR is performed because CH_4 represents an inert in methanol synthesis, and CO_2 is removed via rectisol process using the same methanol, to not shift methanol synthesis reactions equilibria. In the same work and in that of Pala *et al.* 2017, WGS reactor is integrated in the process to increase H_2 content in the syngas. The biomass to methanol process considered in this work is kept at a base level, thus the design choices just mentioned are not considered, leaving to further studies a possible comparison or improvement, following different ways and alternatives.

The gas composition of the products is heavily influenced by the gasification agent, operating parameters, catalyst usage, and feedstock composition. The latter is relevant on design and operation of the process, indeed it is well known that lignin is harder to gasify with respect to cellulose, due to its ordered aromatic structure, and thus due to its high chemical stability; furthermore, gas composition at the outlet of the gasifier depends on the nature of the inlet.

Starting from some considerations on parameters influencing gasification process (Subramani *et al.*, 2015), choices adopted for the biomass to methanol process are presented:

- gasifying agent: air is the most commonly used agent for heat and power generation. Produced gas has a very low H_2 content (8-14 vol%) and calorific value (4-7 MJ/m^3). Oxygen produces a higher quality gas, with a lower heating value (LHV) between 10 and 18 MJ/m^3, but is quite expensive, and thus suitable only for small-scale applications. Steam generates a syngas with a high H_2 content (30-60 vol%) and a moderate LHV (10-16 MJ/m^3), but with this agent an external energy supply is needed for the gasifier, because of endothermic reactions involved in the process. Another drawback is high tar content in syngas, requiring catalytic reforming to clean syngas for further applications (e.g. methanol synthesis): as suggested by Basu (2010), upper limit of tar content is 0.1 g/Nm^3, while typical levels vary depending on the choice of the reactor (table 2.9);

- operating temperature: most of the reactions are endothermic, temperatures typically employed are higher than 700 °C. By increasing temperature, the concentration of syngas increases while that of the other species, such as CO_2, CH_4, and H_2O decreases; temperature control is important, because otherwise problems of sintering, buildup, erosion, and corrosion may arise;

- operating pressure: with a high-pressure operation, size of the gasifier is greatly reduced, and syngas compression costs, in the case of subsequent methanol production, are reduced (as seen for MSR to methanol process). From an economic point of view, the use of pressurized systems is more suitable for large-scale plants;

- use of catalysts: important role in tar and char reduction during gasification, with the result of improving the quality of the product gases. Natural or synthetic catalysts can be used: dolomite and olivine are the most widely used natural catalysts, while 3 main classes of synthetic are used:

    1. alkali-based: expensive but they enhance gasification rates;

    2. nickel-based: high activity for steam reforming of hydrocarbons and tars, leading to a high-quality syngas. Drawbacks are related to high coke formation in the gasifier environment, at high temperatures, which blocks catalyst active sites;

    3. noble metal-based: highly resistant to carbon deposits, but very expensive.

Starting from these considerations, steam is selected as the gasifying agent for this work; experimental data are taken from Pfeifer *et al.* (2011), considering the choice of the gasifying agent, and that experimental campaign is carried out on a pilot plant, employing a dual fluidized-bed gasifier (DFBG). In general, with this reactor design, and the usage of a catalyst, tar catalytic reforming is performed leading to a huge reduction in its content, reaching values next to the target for the synthesis of methanol, from a biomass-based syngas ($< 0.1 g/Nm^3$).

In the reference work, DFBG represented in figure 2.8 is employed. DFBG, with respect to a single fluidized bed, is divided into two zones, including a gasification zone (bubbling bed) and a combustion zone (fast fluidized bed); endothermic heat required for the gasification is supplied by the combustion reaction, by circulating bed material. A schematic of this mechanism is reported in figure 2.9.

For a process simulation purpose, the upper section of the process, indicated by the dotted-line rectangle in figure 2.7, is not modeled, and a syngas stream at operating temperature and pressure, and with composition taken from experiments of Pfeifer *et al.* (2011) is considered as the process inlet. The material and energy balances associated with biomass gasification and syngas pre-treatment are calculated based on the reference paper (Pfeifer *et al.*, 2011). In that work, olivine, a natural mineral, is used as catalyst to reform tars, and thus as a heat carrier, in a 100 kW pilot rig: it operates with a steam to fuel ratio ranged between 0.5 and 1.2, and with temperatures between 650 and 870 °C. Different fuels are tested, as well as bed materials, temperature, steam to fuel ratio, and moisture content in the fuel: for this work, experimental data coming from wood chips gasification, at 850 °C with olivine as catalyst (100 kg), are taken into consideration; furthermore, the steam to fuel ratio equals 0.8 and fuel flowrate fed to the gasifier is 22.5 kg/h_{db} (db, dry biomass).

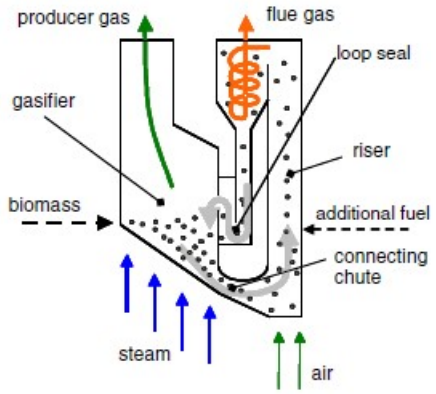

Figure 2.8: Dual fluidized-bed gasifier (Pfeifer *et al.*, 2011)

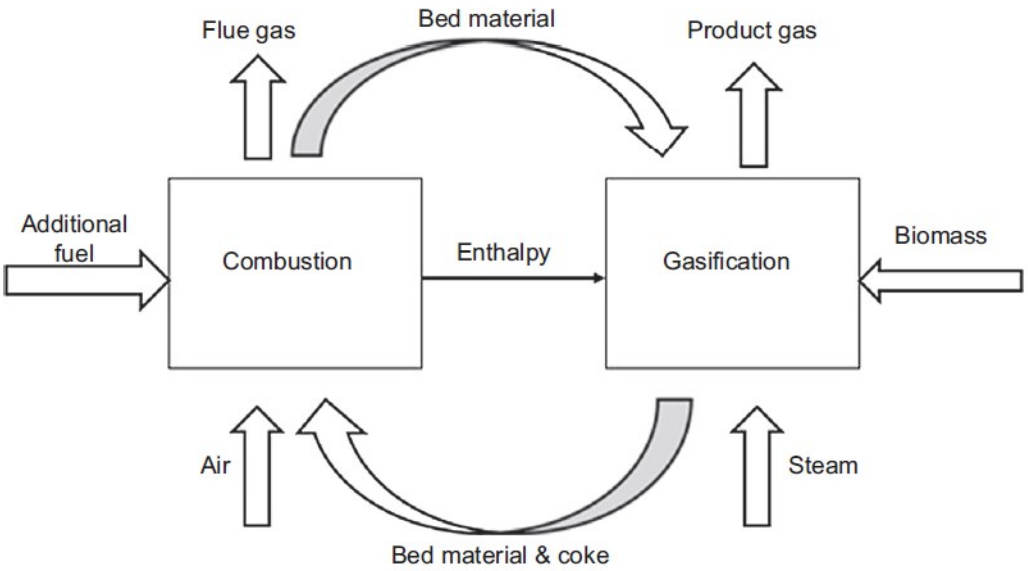

Figure 2.9: Principle of the dual fluidized-bed gasifier (Subramani *et al.*, 2015)

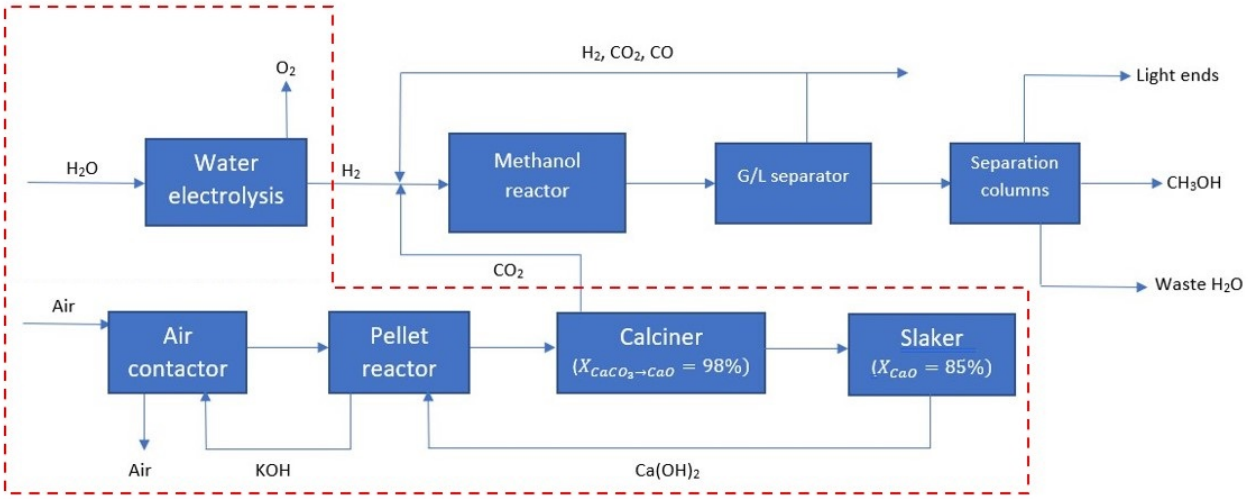

Figure 2.10: BFD of CO_2 hydrogenation processes

2.4.4 CO_2 hydrogenation

Finally, the possibility to produce methanol from CO_2 hydrogenation is taken into consideration: CO_2 is captured via DAC, based on the work of Keith *et al.* (2018), while H_2 is produced via water electrolysis. Two different technologies are considered, namely AW electrolysis and PEM electrolysis, based on the works of Buttler and Spliethoff (2018) and Jang *et al.* (2022). The general BFD is reported in figure 2.10, where the only relevant difference between the 2 processes is the type of electrolizer, and corresponding operating conditions and parameters.

In general, CO_2 captured via DAC process enters the process at ambient temperature and pressure, while H_2 coming from the electrolysis unit enters at specific operating temperature and pressure of the electrolyzer. Then, gaseous hydrogen and carbon dioxide go to methanol synthesis section; products exiting methanol reactor are directed to a gas/liquid phase separator, where liquid is directed to purification units section, and gas is recycled back to constitute the methanol reactor inlet, without the need of a purge, since inerts are neglected. Purification section is formed by two distillation columns, from which light ends exit as the overhead product of the first column, and bottom product of such column goes to a second column, where pure methanol is obtained as the overhead product, while wastewater is available as the bottom one.

Below are presented the assumptions made to describe the 2 CO_2 hydrogenation processes:

- DAC process: the work of Keith *et al.* (2018) is considered, with the process presented in figure 2.11. CO_2 is captured from the atmosphere in the air contactor, by using an alkali aqueous solution with ionic concentrations of roughly 1.0 M OH^-, 0.5 M CO_3^{2-}, and 2.0 M K^+. CThe carbonate ion (CO_3^{2-}) is removed from the solution by causticization in the pellet reactor: in particular, in this fluidised bed reactor, the ion is precipitated by reaction with Ca^{2+} to form calcium carbonate ($CaCO_3$), while the Ca^{2+} is replenished by dissolution of calcium hydroxide ($Ca(OH)_2$); $CaCO_3$, in the form of pellets, is suspended in the capture solution, coming from air contactor, while a slurry of 30 wt.% of calcium hydroxide is injected into the bottom of reactor vessel. Afterwards, the $CaCO_3$ is directed

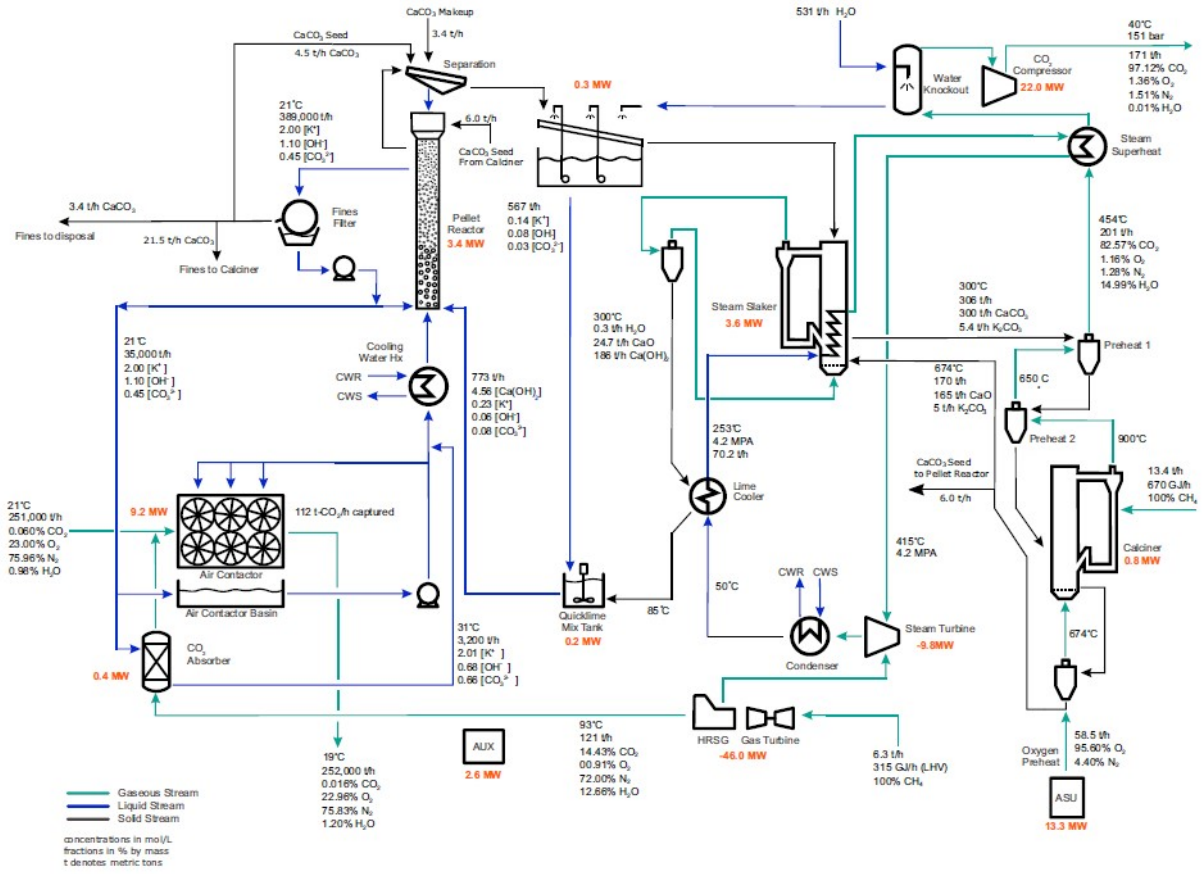

Figure 2.11: Overview of process showing mass and energy balances (Keith *et al.*, 2018)

to the calciner, a large steel vessel lined internally with refractory bricks, where fluidizing gas is supplied into the bottom of the equipment through a distribution plate, and natural gas is directly injected just above that plate; here calcium carbonate is calcined to liberate CO_2, producing calcium oxide (CaO). CaO is finally hydrated or "slaked" to produce $Ca(OH)_2$, that is needed in the pellet reactor: the reaction is carried out in the steam slaker, a refractory lined bubbling/turbulent fluid bed that is fluidized by recirculating steam flow.

CO_2 exiting from calciner at atmospheric pressure is finally compressed to 151 bar: anyway, since this compression step is not aimed for this work, the performances and energy requirements of the process are evaluated following scenario D described in the reference article, i.e. when considering a CO_2 output at atmospheric pressure. Reactions involved in the process can be represented by the two connected loops presented in figure 2.12;

- AW electrolysis: it is mature technology applied at large-scale since the beginning of the 20th century. Electrodes are immersed in a liquid electrolye separated by a diaphragm; usually the electrolyte is a 25-30 wtpercent aqueous KOH-solution. The product gas quality, after drying, typically ranges from 99.5 to 99.9%, and from 99 to 99.8% for O_2 (Buttler and Spliethoff, 2018). Partial reactions occurring at the electrodes are 1.20 and 1.21, and a general layout of the process is depicted in figure 2.14. Typical operating

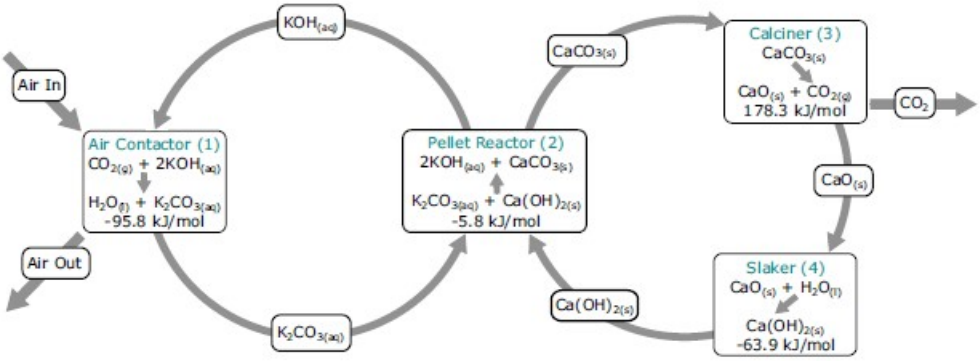

Figure 2.12: Process chemistry and thermodynamics (Keith *et al.*, 2018)

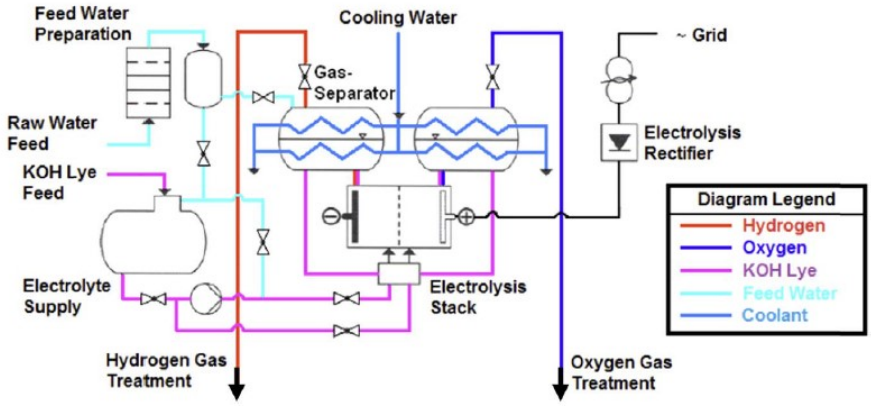

Figure 2.13: Layout of an alkaline electrolysis system (Buttler and Spliethoff, 2018)

conditions are a cell temperature of 60-90 °C, and a typical pressure of 10-30 bar: in this work it is assumed to work at 90 °C and 30 bar, in order to reduce gaseous hydrogen compression ratio for subsequent methanol synthesis.

- PEM electrolysis: introduced by General Electric in the 1960s. A proton exchange membrane (material is Nafion® in most cases) separates the two electrodes which are usually mounted on the membrane forming the membrane electrode assembly. Due to corrosive acidic regime provided by the membrane, the use of noble metal catalysts is required (e.g. iridium for the anode and platinum for the cathode). Water is supplied at the anode and is partially transported to the cathode side, due to the electro-osmotic effect (Buttler and Spliethoff, 2018). The following partial reactions occur at the electrodes:

$$Cathode: \qquad 2\,H^+ + 2\,e^- \longrightarrow H_2 \tag{2.39}$$

$$Anode: \qquad H_2O \longrightarrow \frac{1}{2}\,O_2 + 2\,H^+ + 2\,e^- \tag{2.40}$$

Global cell reaction is the same as AW electrolysis (1.22).

The polymeric membrane allows to obtain a higher purity hydrogen, with respect to AW

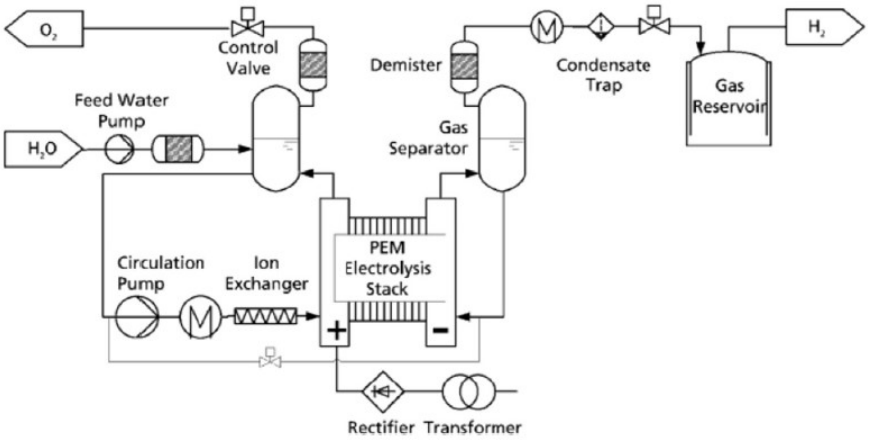

Figure 2.14: Layout of a PEM electrolysis system (Buttler and Spliethoff, 2018)

electrolysis, typically greater than 99.99% after drying. Typical operating conditions are a cell temperature of 50-80 °C and a typical pressure of 20-50 bar: in this work it is assumed to work at 80 °C and 50 bar to reduce gaseous hydrogen compression ratio for subsequent methanol synthesis.

For a simulation purpose, sections of the process inside the dotted-line rectangle in figure 2.10 are not considered rigorously modeled, but the outlet streams are taken as the raw materials for methanol synthesis via CO_2 hydrogenation; CO_2 exits DAC process at ambient temperature and pressure, while hydrogen exits AW or PEM electrolizer at operating conditions of such systems. The material and energy balances for DAC and electrolysis are taken from the reference articles.

Reactants molar flowrates are calculated considering a methanol reactor stoichiometric feed: dealing with CO_2 hydrogenation (reaction 1.2), a H_2:CO_2 ratio equal to 3 is needed.

Chapter 3

Process Simulation and Results

In this chapter the results of simulations carried out in Aspen Plus software for the five processes are presented, starting from the flowsheets and the description of unit operation models used. Then, Aspen Activated Energy Analysis and pinch analysis procedures and results are presented. Finally, results obtained from the simulations are validated and compared to previous works from literature.

3.1 Simulation methods

Considering the BFDs, design choices, and assumptions presented in chapter 2, Aspen Plus flowsheets are created for the five processes, and the following unit operation built-in models are employed:

- mixers: MIXER is used to represent the combination of material streams that are characterized by the same temperature and pressure (no heat or work exchange is considered);
- splitters: FSPLIT is used to separate material streams, when purge is needed for the process. Recycle and purge streams represent the typical outlets of the splitter that require the definition of the molar fraction of the inlet in one between the two streams;
- heat exchangers: HEATER is used to model the process side of a heat exchanger (heater/-cooler);
- separators: FLASH2 is used to model a 2-streams outlet partial vaporization process (i.e. flash process), by performing rigorous distillation calculations;
- columns: DSTWU and RADFRAC are used for shortcut and rigorous calculations, respectively. The procedure followed in this work for distillation columns design is detailed in section 3.1.1.
- reactors: two different models are employed for reforming and methanol synthesis reactors:
  - RSTOIC: the reformers in MSR to methanol and BR to methanol processes are

modeled specifying the stoichiometry of the main reactions and conversion values, following the assumptions described in chapter 2. Isothermal conditions are assumed;

  - RPLUG: the methanol synthesis reactor is rigorously modeled as a PFR, starting from the built-in generalized LHHW kinetic model. In particular, the Lurgi-type reactor is modeled in the software with a specified temperature, constant at the inlet value of 252 °C; the kinetic model described in chapter 2 is implemented, considering a multi-tubular configuration with 810 tubes, 12 m long, and with a diameter of 60 mm, as in the work of Kiss *et al.* (2016). Furthermore, 865 kg of catalyst are loaded, with a bed voidage assumed as equal to 0.98;

- pressure changers: four models are used depending on the phase of the stream for which pressure has to be changed, and depending on whether pressure has to be increased or decreased:

  - PUMP: it is used to simulate a pump or a hydraulic turbine, when considering liquid streams and, particularly, in the water recycle loops of MSR and BR to methanol processes;

  - MCOMPR: when the total compression ratio is higher than 4 a multistage compressor with intermediate cooling is needed, and this built-in model can be employed, assuming isoentropic compression, and considering a 72% efficiency. The number of stages depends on the total compression ratio, and the compression ratio should be the same for all the stages;

  - COMPR: it is used to simulate a single-stage compressor, when a multi-stage one is not needed. Same considerations about isoentropic compression and efficiency as of multi-compressor are valid;

  - VALVE: it is used to decrease the pressure of a stream; in particular for this work, it is applied to the feed stream of the first distillation column for which pressure needs to be decreased from 75 bar to atmospheric pressure.

3.1.1 Distillation columns design

In the preliminary phase of the design of a distillation column to be implemented in Aspen Plus, it is convenient to perform a Winn-Underwood-Gilliland shortcut calculation by using DSTWU built-in model, valid for a single-feed, two-product column, with a partial or total condenser. Carrying out the shortcut simulation, given the value of reflux ratio, the number of theoretical stages is calculated, or viceversa: in this work, a reflux ratio 1.2 times the minimum one is considered, thus the calculated and the actual number of theoretical stages are obtained. The choice of this value of reflux ratio depends on techno-economic considerations and it is usually taken in the range of 1.15-1.25 times the minimum value.

Reflux ratio is the ratio between the amount of liquid returned to the column and the amount of

distillate withdrawn, and its minimum value is calculated by the so-called Underwood equation; instead, the minimum number of theoretical stages needed for a desired separation is calculated by an empirical equation, i.e. the Fenske equation. More details can be found in Luyben (2013).

A more sophisticated version of these equations is used by the software for DSTWU short-cut simulation, as from Sandler (2015):

$$\frac{N - N_{min}}{N + 1} = 1 - \exp\left(\frac{1 + 54X}{11 + 117.2X} \cdot \frac{X - 1}{X^{0.5}}\right), \; X = \frac{R - R_{min}}{R + 1} \tag{3.1}$$

The equation relates the minimum number of stages N_{min}, and the minimum reflux ratio R_{min} to the actual number of stages N and the actual reflux ratio R. The actual number of stages is defined starting from the calculated one, by the introduction of an efficiency value that accounts for the fact that complete vapor-liquid equilibrium may not be achieved on each tray or stage.

Other fundamental inputs needed for the shortcut simulation are the choice of a pressure for the condenser and reboiler, which in this work is set to the atmospheric one, and the definition of separation specifications, to be presented as the key components recoveries in the distillate. Considering volatility of the species involved in each process, and their molar fractions in the columns feed, a heavy key component and a light one are individuated for each one of the two columns involved in the process, as follows:

- Topping column (or lightends column): indicated as DIST-1 in all the processes; CO_2 represents the light key component, while CH_3OH is considered as the heavy key component;
- Refining column (or methanol column): indicated as DIST-2 in all the processes; CH_3OH represents the light key component, while H_2O the heavy one.

Recoveries can be related to composition specifications, required for the distillate and residue streams, by solving material balances for the two key components. Naming R the residue and D the distillate, assuming a unitary feed F, the overall and single species balances can be written as follows:

$$R + D = F = 1 \tag{3.2}$$

$$z_i F = y_i D + x_i R \tag{3.3}$$

Fractional recovery of the i species in the distillate is thus defined as:

$$R_i = \frac{y_i D}{z_i F} \tag{3.4}$$

For the lightends column, recoveries to be input in DSTWU model are calculated starting from

the composition specifications of 90 mol% of CO_2 in the distillate and 99.8 mol% of CH_3OH in the residue; for the methanol column, the composition specifications of 99.9 mol% for CH_3OH in the distillate, and for H_2O in the residue, are assumed. Moreover, DSTWU column feed is assumed as bi-component for the shortcut simulation purpose, and feed conditions are set to the pressure of 1 atm and boiling temperature of the bi-component mixture.

Results obtained from shortcut simulation are then input in RADFRAC rigorous simulation model, that requires:

- reflux ratio: actual value calculated from DSTWU model;
- distillate rate or distillate to feed ratio: they are retrieved from DSTWU model calculations;
- number of stages and feed stage: approximated by excess to the higher whole number from the actual value obtained from DSTWU;
- condenser type: a partial condenser was used in the lightends column, and a total one in the methanol column;
- condenser and reboiler pressure: same as in DSTWU, atmospheric pressure for both the heat exchangers.

Rigorous distillation column simulation results and input specifications can be found in appendix **??**.

3.1.2 Energy analysis and heat integration

In this work, the final step of the Aspen Plus simulation has been represented by the introduction of utilities needed to cool or heat streams interested by the presence of a heat exchanger, or a reactor in which heating or cooling needs to be provided; a comprehensive list of utilities used for the five processes is presented in tables 3.1 and **??**, as they are named in the simulations. The utilities, in the software, are defined starting from built-in models, represented by the *type* denomination reported in the tables; details about their cost, reported in the tables, are presented in chapter 4.

With regard to the choice of utilities, and their use in the processes, they can be distinguished by the scope:

- heating:
  - FURNACE: it represents the NG burnt in a furnace to heat reactants in MSR to methanol and BR to methanol processes. Moreover, it is used to provide heating to reforming reactors in both these processes, interested by an overall endothermic reaction at high temperatures. In table **??**, natural gas utility is distinguished between the use in MSR and BR to methanol processes, due to the fact that in the latter lower temperatures are required;

Table 3.1: Aspen Plus utilities input data and assumption

	AMMONIA	CW	LP-STEAM	HP-STEAM
Type	Refrigerant	Cooling water	High-pressure steam	Low-pressure steam
Purchase price ($/t)	-	0.01208	11.7008	20.4128
Energy price ($/kWh)	0.04535	-	-	-
Heating/cooling value (kJ/kg)	-4.47830	-	2009.50	1469.90
Inlet temperature (°C)	-25	25	125	260
Outlet temperature (°C)	-24	35	124	259
Minimum approach temp. (°C)	3	5	7	7

	FURNACE (MSR)	FURNACE (BR)	R-152A	REFWATER
Type	Fired heat	Fired heat	Refrigerant	Cooling water
Purchase price ($/t)	-	-	-	-
Energy price ($/kWh)	0.01416	0.01416	0.04535	0.04535
Heating/cooling value (kJ/kg)	47700	47700	-1.57112	-
Inlet temperature (°C)	1000	800	-50	20
Outlet temperature (°C)	960	760	-49	25
Minimum approach temp. (°C)	25	25	3	5

  - HP-STEAM: it represents high-pressure steam that is needed to provide heating to the feed of methanol synthesis reactor, whose operating temperature is 252 °C. To this aim, a very high pressure steam needs to be produced with a saturation pressure of 46.923 bar. Cost analysis and a complete description of the steam production system is presented in chapter 4;
  - LP-STEAM: it represents low-pressure steam that is needed to provide modest heating when temperatures are lower than about 120 °C, as are the cases of column reboilers in all the processes. It is characterized by a saturation pressure of 2.322 bar;

- cooling:
  - AMMONIA: ammonia (NH_3) is used as a refrigerating agent to provide cooling when temperatures reach values below 10 °C, such as in topping column condensers;
  - CW: it represents cooling water that is generally used to cool down liquid and gas streams, or to condensate vapours. It is assumed to be available at 25 °C, exiting the heat exchanger at 35 °C, thus it is employed for cooling streams up to 40 °C, while temperatures below this threshold require refrigeration. This utility is also used for intermediate cooling in multi-stage compression;
  - R-152A: it represents the refrigerant gas 1,1-difluoroethane, a hydrofluorocarbon usually referred as R-152a. It substitutes ammonia in biomass to methanol process,

where lightends column condenser operates at -27.3 °C, a temperature for which ammonia usage as a refrigerant is not feasible;

– REFWATER: it indicates refrigerated water, employed when mild refrigeration needs to be provided, i.e. with temperatures above 5 °C. In this work it is available at 20 °C and used only in biomass to methanol process prior to heat integration.

Once assigned all the utilities, and with a converging simulation, Energy Analysis is carried out in Aspen Plus in order to evaluate the possible energy and cost savings, by heat integration, which limits the employment of the utilities.

The methanol synthesis reactor duty is neglected in the heat integration procedure, while in chapter 4 for techno-economic and carbon impact assessments, boiler feed water is considered to provide the actual cooling needed for the reactor; even cooling water employed in intermediate cooling of multi-stage compressors is not accounted for heat integration.

Afterwards, these results are transferred to Aspen Energy Analyzer (AEA), a tool from AspenTech that helps performing the pinch analysis, a technique for optimising HEN design via heat integration; the objective is minimizing the use of utility streams, by employing the minimum number of exchangers, via an algorithm properly defined (e.g. MUMNE from Turton *et al.* 2018).

In pinch analysis, HENs featuring minimum utility usage are called Maximum Energy Recovery (MER) networks; in MERs heat is never transferred through the pinch point, a temperature dividing the process temperature range in two regions, so that heating utilities can be used only above the pinch, while cooling utilities only below it. The pinch point can be individuated from composite curves, a temperature vs duty plot, or from the Grand Composite Curve (GCC), a temperature vs enthalpy diagram, whenever a minimum temperature difference ΔT_{min} is chosen, generally taken as 10 °C for a first estimate; this temperature difference sets the distance between the hot stream line and the cold stream line in the composite curves diagram.

MERs design starts from the principle that the following golden rules have to be satisfied:

- heat is never transferred across the pinch, cold utilities are never used above the pinch, and hot utilities are never used below the pinch;
- immediately below the pinch, heat capacity flowrate of the hot stream (CP_H) has to be higher, or at least equal, to the heat capacity flowrate of the cold stream (CP_C);
- immediately above the pinch, the opposite situation must hold ($CP_H \leq CP_C$).

Heat capacity flowrate CP_s of a generic stream s is defined as the product between the mass flowrate of that stream ($\dot{m}_s$) and its specific heat capacity ($c_{p,s}$). Away from the pinch, there is more flexibility to make matches, so the inequalities are not needed to hold.

Furthermore, if above the pinch the number of hot streams (S_H) is larger than the number of cold streams (S_C), or below the pinch the number of cold streams is larger than the number of

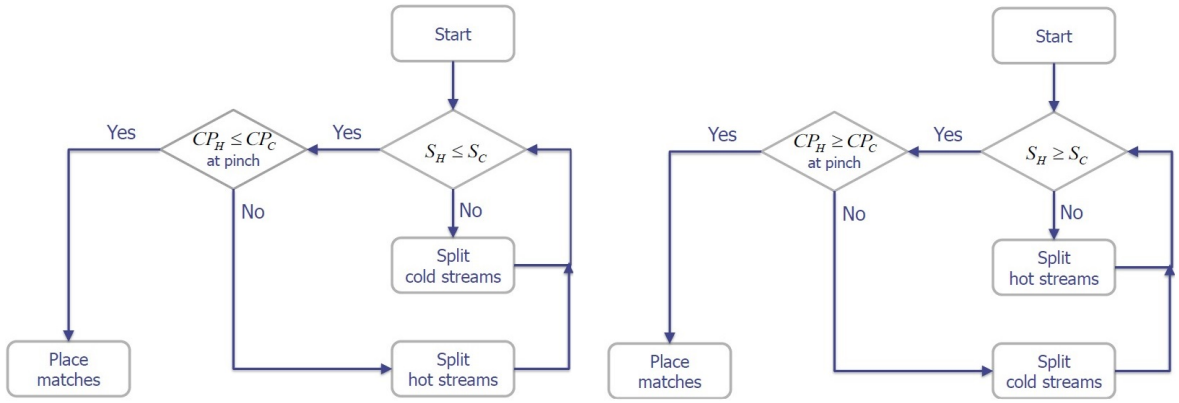

(a) *Above the pinch* **(b)** *Below the pinch*

Figure 3.1: Energy Targeting algorithms (Bezzo, 2020)

hot streams, then some pinch matches are impossible: in the first case the solution is to split the cold stream(s) until the inequality is satisfied, while in the second case the solution is to split the hot stream(s). The algorithms reported in figure 3.1 summarize the steps required to respect all of these mentioned rules, in order to design an appropriate MER network: this procedure is called energy targeting.

In this work, considering the solutions given by AEA, the following procedure is adopted for all the processes:

- Aspen Plus simulation data are imported in the AEA environment, where it is displayed by default the so-called *Base Case Simulation* where heat exchangers work just with utilities, so the minimum number of them is presented;
- pinch temperature is automatically determined by the software, as well as composite curves and GCC are built by default from AEA;
- since energy use (in terms of utilities usage) increase with ΔT_{min} proportionally, but, on the other hand, heat exchanger area is roughly proportional to ΔT_{min}, assuming that energy cost is proportional to energy usage, and that heat exchanger cost is proportional to its surface area, an optimum value needs to be found. Optimising this cost is called supertargeting, and in AEA a diagram of the so-called *total cost index target* vs ΔT_{min} is automatically created after entering the range to be analized (5 to 40 °C and the step-size increment (0.5 °C);
- after the choice of the optimal ΔT_{min}, the definitive composite curves and GCCs are drawn for each process. The respective plots are reported in **??**;
- immediately above the pinch temperature the total number of hot and cold streams is considered, and corrected by splitting if needed, in order to follow the golden rule on inequality of the number of streams. Utility streams are not considered at the moment, thus in these calculations their amount is not considered;
- the same procedure is repeated for the streams immediately below the pinch temperature;

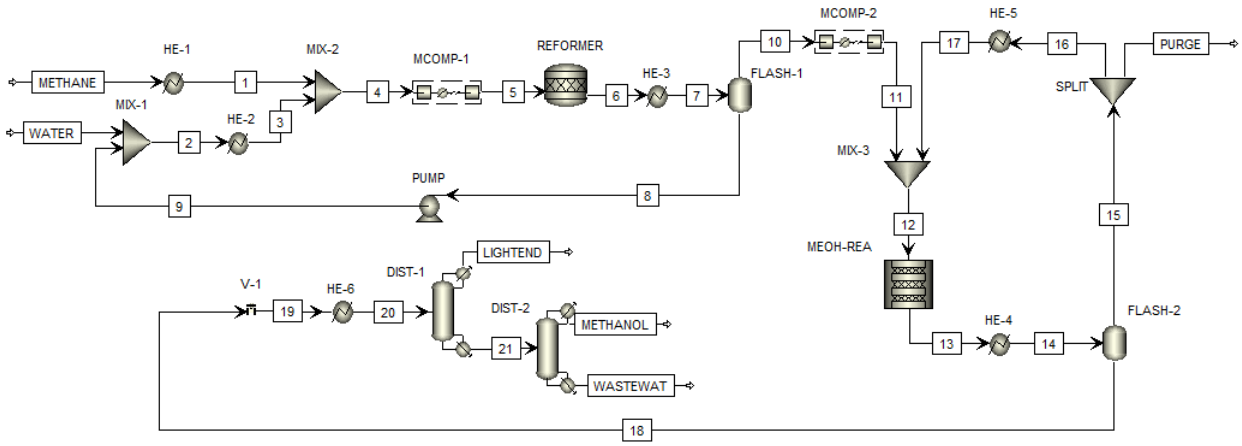

Figure 3.2: Aspen Plus process flowsheet of MSR to methanol process

- first matches are placed at the pinch in order to satisfy the golden rules, then it is possible to move away from that point to place the other matches;
- once a match has been chosen, the exchanger load need to be maximized (i.e., one of the stream has its duty satisfied), following the so-called *tick-off rule*;
- several scenarios are considered in order to minimize utilities usage, while not increasing too much capital costs for HEN design, thus keeping low the total costs of MER network.

3.2 Process flowsheets description and pinch analysis results

In this section Aspen Plus flowsheets are presented for all the processes, with some equipment details; stream conditions and compositions are presented in the stream tables that are reported in appendix C for all the five processes. Then, pinch analysis procedure and HEN diagrams finally obtained are reported for each process: initially streams splitting and heat capacity flowrates are defined, then matches below and above the pinch are explained.

3.2.1 Methane steam reforming to methanol

Considering the process flowsheet depicted in figure 3.2, natural gas is assumed to be composed of pure methane, and it is fed at ambient temperature and pressure, along with water at the same conditions. Then, temperature is increased up to 600 °C (in HE-1 and HE-2), before the reactants are mixed and compressed in a multi-stage compressor (MCOMP-1): since pressure is risen from the atmospheric one to the operating pressure of the steam reforming reactor (17 bar), 3 stages are employed with an intermediate cooling that in the last stage lowers the temperature to 850 °C. Steam reforming reaction occurs in REFORMER furnace, and the products exiting the reactor pass through a heat exchanger (HE-3) that lowers temperature to 40 °C. A gas-liquid separation is carried out in a flash drum (FLASH-1) that works at the same

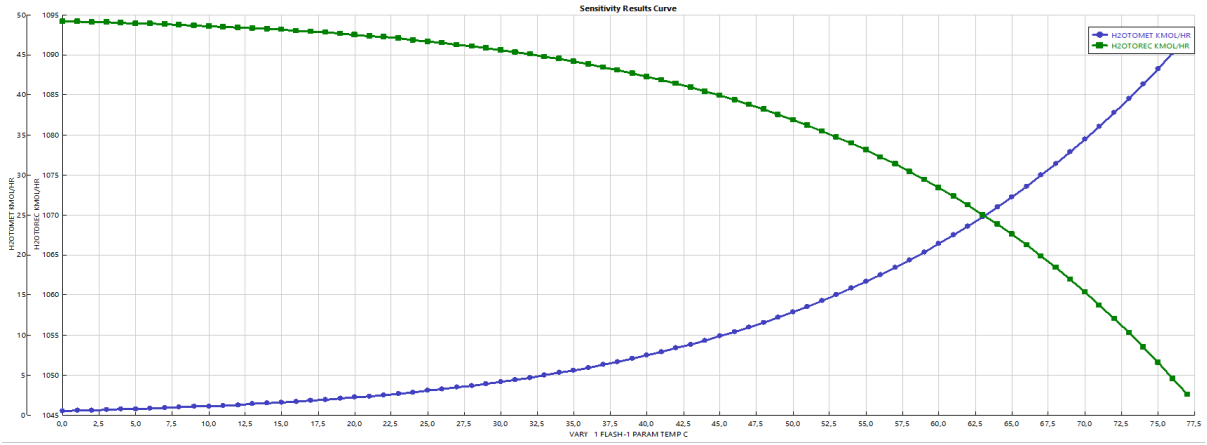

Figure 3.3: Sensitivity analysis on flash separation effectiveness by varying temperature at a pressure of 17 bar

Table 3.2: Multi-stage compressors simulation results for MSR to methanol process

	MCOMP-1			MCOMP-2	
	Stage 1	Stage 2	Stage 3	Stage 1	Stage 2
Exit temperature (°C)	811.592	811.744	868.906	140.081	269.419
Exit pressure (bar)	2.594	6.641	17.000	35.707	75.000
Shaft power (kW)	6285	6285	6634	1730	2301
Head developed (m)	43158	43155	45553	24211	32199
Volumetric flow (m^3/h)	157350	61447.4	25369.9	3184.37	2016.05
Cooling temperature (°C)	600	650	850	140	252
Cooling duty (kW)	-6295	-4871	-599.6	-1.416	-309.1

pressure of the reactor. The choice of temperature is based on the sensitivity analysis results depicted in figure 3.3, where the profiles of water recovered as a liquid, and remaining in the gaseous state, in terms of molar flowrates, are plotted in the range between 0 and 77 °C. A temperature of 40 °C ensures a good compromise between the effectiveness of separation and a reasonable temperature to avoid using expensive refrigeration systems. Liquid water is recycled back and, after being depressurized to atmospheric conditions, is mixed with water initially fed to the process; the vapor phase exiting the flash vessel is compressed to the operating pressure of methanol synthesis reactor (MCOMP-2) in 2 stages with intermediate cooling, thus reaching operating conditions of the reactor (252 °C and 75 bar). Multi-stage compressors profiles and data are reported in table 3.2.

The product gas exiting the methanol synthesis reactor (MEOH-REA) is cooled down to 40 °C in HE-4, while pressure is kept at 75 bar to avoid an expansion, and the successive need to re-compress the gas exiting the FLASH-2 separation unit that is recycled back to methanol synthesis section, thus avoiding the related higher capital and operating costs. The gaseous outlet of the flash unit is partially purged (10 %), while the rest is heated in HE-5 to 252 °C, and then mixed with stream 11; the liquid stream exiting the flash drum, mainly constituted of methanol and water, is de-pressurized to atmospheric pressure, and heated in HE-6 to 62

Table 3.3: Streams crossing the pinch split fractions and heat capacity flowrates for MSR to methanol process

Stream name	T_{in} (°C)	T_{out} (°C)	CP (kW/°C)	Split fraction 1	Split fraction 2	Split fraction 3	Split CP (kW/°C) 1	Split CP (kW/°C) 2	Split CP (kW/°C) 3
HOT STREAMS									
6_To_7	850	40	77.00	0.5	0.4	0.1	38.50	30.80	7.70
13_To_14	252	40	196.60	0.3	0.7		58.98	137.6	
COLD STREAMS									
2_To_3	35	600	72.12	0.5	0.5		36.06	36.06	
METHANE_To_1	25	600	6.18						
16_To_17	40	252	63.85						
Reboiler DIST-2	82.7	94.6	706.2						

°C, which is the boiling temperature of stream 20. This stream represents the feed of the first column DIST-1, where volatile gases exit as the overhead product, and leave the process to be burnt in flare (LIGHTEND stream). The liquid bottom product of the column, stream 21, is fed to the second distillation column (DIST-2), where methanol is obtained as a liquid from the total condenser (METHANOL stream), while the bottom product is mainly constituted of water that is treated as a waste (WASTEWAT stream); in this column DSs are set on methanol productivity (382.464 kmol/h) and mass purity (99.85 wt.%), by varying the user-input data of such column, namely the reflux ratio and the distillate-to-feed ratio. These parameters are that obtained from the shortcut distillation method, modeled as DSTWU in the software, and performed for both columns to obtain the necessary input data to rigorously simulate them. The procedure and assumptions adopted have been reported in section **??**.

Pinch temperature of the process is 97.7 °C, and the optimal ΔT_{min} has been estimated to be 15 °C. Six streams are spread across the pinch temperature ideal line, and they are reported in table 3.3 where, as in AEA, hot streams to be cooled are marked with red colour, while cold streams that need to be heated are marked with blue color.

From the data reported in such table, the golden rules about the number of hot and cold streams are satisfied, both above and below the pinch, after splitting some of them, considering that their number is finally equal to 5. Considering the golden rules on heat capacity flowrates, the following matches can be placed at the pinch, in the initial phase of the analysis:

- below the pinch: 6_To_7 split 1 is matched with 2_To_3 split 1, 6_To_7 split 3 is matched with METHANE_To_1;
- above the pinch: 13_To_14 split 1 is matched with 16_To_17 stream, 13_To_14 split 2 is matched with the reboiler of DIST-2 column;

Afterwards, other 3 matches are placed and in figure 3.4 the complete HEN diagram is reported for the process. Energy consumption results, before and after the heat integration, considering the different utilities used in the process, are reported in table 3.4.

Table 3.4: Load and mass flowrate of the different utilities required, making a comparison before and after heat integration in the MSR to methanol process

Utility	Before heat integration		After heat integration	
	Load (kW)	Mass flowrate (kg/h)	Load (kW)	Mass flowrate (kg/h)
Hot utilities				
Natural gas	35190	2655.85	10180	768.302
Low-pressure steam	8151	14602.4	2618	4690.12
High-pressure steam	13532	33141	7052.2	17270.8
Cold utilities				
Ammonia	312	250809	312	250809
Cooling water	66320	5711770	29290	2522584

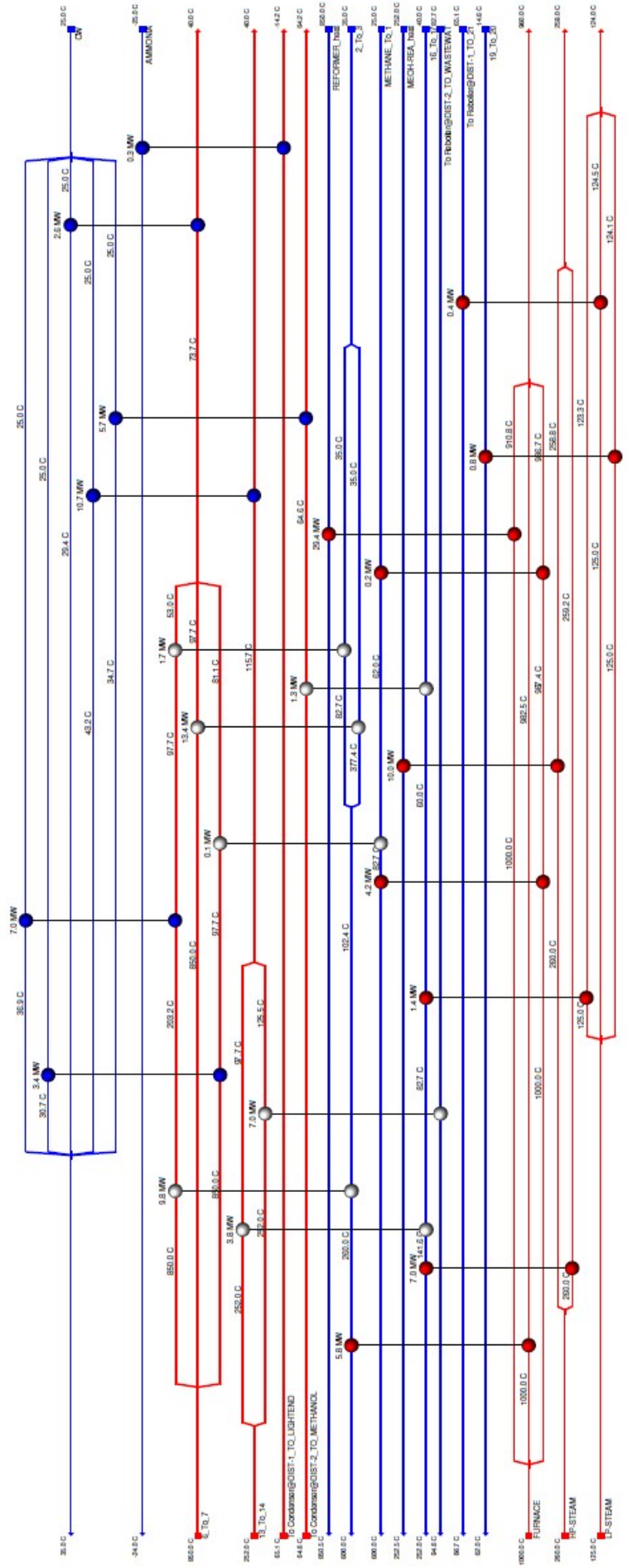

Figure 3.4: HEN diagram for Methane Steam Reforming to methanol process

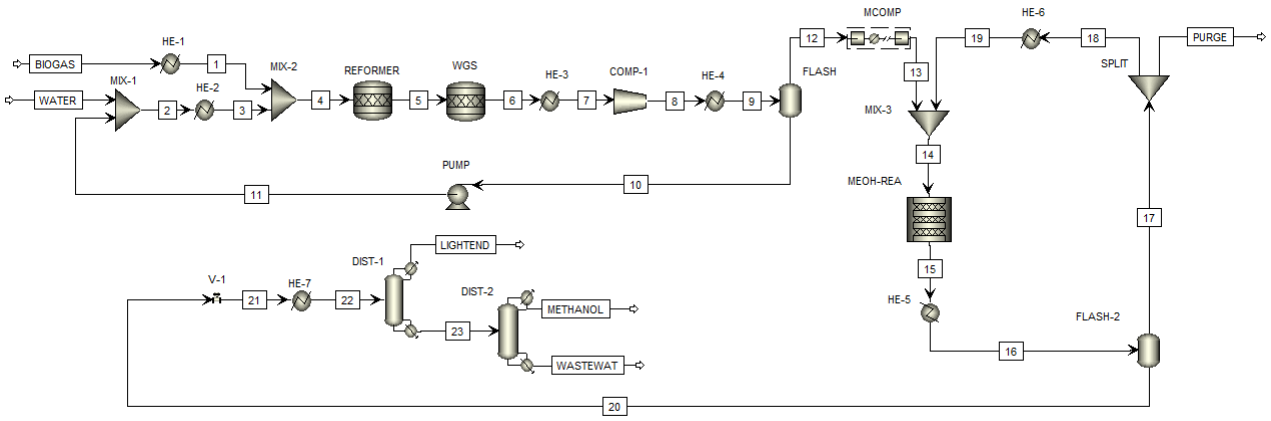

Figure 3.5: Aspen Plus process flowsheet of BR to methanol process

3.2.2 Biogas reforming to methanol

Considering the process flowsheet depicted in figure 3.5, biogas is fed at typical outlet conditions of a mesophilic digester (37 °C and 1 atm), along with water at ambient conditions. Then, temperature is increased up to 650 °C (HE-1 and HE-2), before the reactants are mixed and fed to the atmospheric reforming reactor (REFORMER) followed by the WGS reactor: as explained in chapter 2, the configuration of 2 reactors in series is a simulation artifact to go beyond PS solving method issues. Afterwards, reaction products pass through a heat exchanger (HE-3) that lowers the temperature to 250 °C, before the gases are compressed to the pressure of 5 bar in a single-stage compressor (COMP-1) with subsequent cooling to 40 °C in HE-4; stream 9 is then directed to a gas-liquid separator, represented by a flash drum (FLASH-1) that works at 5 bar. The choice of temperature is based on the sensitivity analysis results depicted in figure 3.6, where the profiles of water recovered as a liquid, and water that remains in the gaseous state, in terms of molar flowrates, are plotted in the range between 3 and 61 °C. Also in this case, 40 °C represents a good compromise between the effectiveness of separation and a reasonable temperature, in order to avoid using expensive refrigeration systems. Liquid water is recycled back and, after being depressurized to atmospheric conditions, is mixed with water fed to the process; vapor phase exiting the flash vessel is compressed to the operating pressure of methanol synthesis reactor (MCOMP-2) in 2 stages with intermediate cooling, thus reaching operating conditions of the reactor (252 °C and 75 bar). Compressors profiles and data are reported in table 3.5.

The product gas exiting the methanol synthesis reactor (MEOH-REA) is cooled down to 40 °C in HE-5, while pressure is kept at 75 bar to avoid an expansion, and the successive need to re-compress the gas exiting the FLASH-2 separation unit that is recycled back to methanol synthesis section, thus limiting the related higher operating costs. The gaseous outlet of the flash unit is partially purged (10 %), while the rest is heated in HE-6 to 252 °C, and then mixed with stream 13; the liquid stream exiting the flash drum, mainly constituted of methanol and water, is de-pressurized to 1 atm, and heated in HE-7 to 63 °C, i.e. the boiling temperature of stream 22. This stream represents the feed of the first column DIST-1, where volatile gases

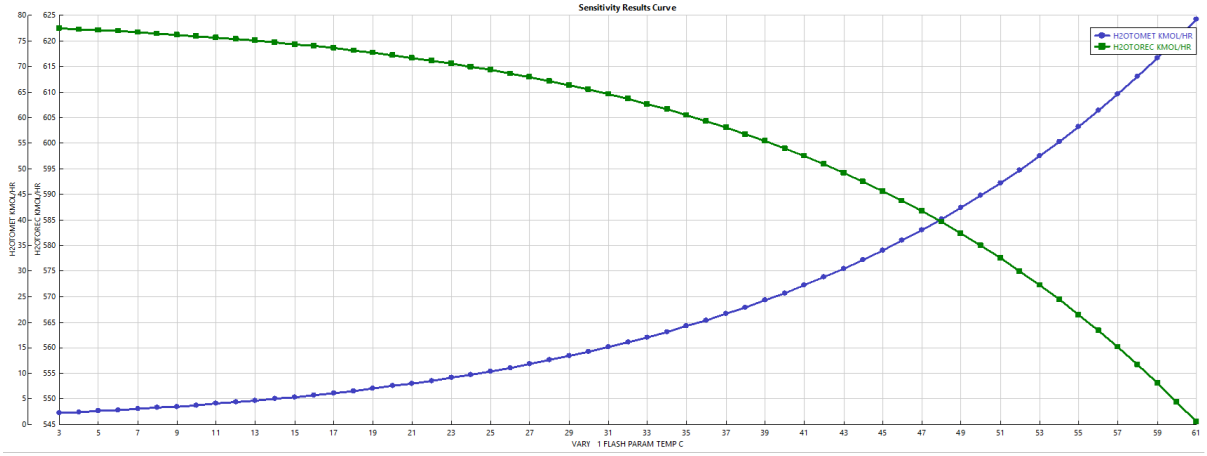

Figure 3.6: Sensitivity analysis on flash separation effectiveness by varying temperature at a pressure of 5 bar

Table 3.5: Single-stage and multi-stage compressors simulation results for BR to methanol process

	COMP-1	MCOMP-2	
		Stage 1	Stage 2
Exit temperature (°C)	588.684	225.718	316.273
Exit pressure (bar)	5.00	19.36	75.00
Shaft power (kW)	7615	2990	3590
Head developed (m)	56963	30101	36144
Volumetric flow (m^3/h)	33334.0	9479.88	2931.00
Cooling temperature (°C)	40	100	252
Cooling duty (kW)	-18493.1	-2054.8	-1090.2

Table 3.6: Streams crossing the pinch split fractions and heat capacity flowrates for BR to methanol process

Stream name	T_{in} (°C)	T_{out} (°C)	CP (kW/°C)	Split fraction			Split CP (kW/°C)		
				1	2	3	1	2	3
HOT STREAMS									
8_To_9	588.7	40	178.0	0.25	0.70	0.05	44.50	124.6	8.90
15_To_16	251.8	40	139.1	0.30	0.70		41.73	97.37	
COLD STREAMS									
2_To_3	33.4	650	39.09	0.95	0.05		37.14	1.955	
BIOGAS_To_1	37	650	8.168						
18_To_19	40	252	41.97						
Reboiler DIST-2	81.8	93.5	850.7						

exit as the overhead product, and leave the process to be burnt in flare (LIGHTEND stream). The liquid bottom product of the column, stream 23, is fed to the second distillation column (DIST-2), where methanol is obtained as a liquid from the total condenser (METHANOL stream), while the bottom product is mainly constituted of water that is treated as a waste (WASTEWAT stream); in this column DSs are set on methanol productivity (382.464 kmol/h) and mass purity (99.85 wt.%), by varying the user-input data of such column, i.e. the reflux ratio and the distillate-to-feed ratio.

Pinch temperature of the process is 91.8 °C, and the optimal ΔT_{min} of the process has been estimated to be 10 °C. Six streams are widespread across the pinch temperature ideal line, and they are reported in table 3.6.

From the data reported in such table, the golden rules about the number of hot and cold streams are satisfied, both above and below the pinch, after splitting some of them, considering that their number is finally equal to 5. Considering the golden rules on heat capacity flowrates, the following matches can be placed at the pinch, in the initial phase of the analysis:

- below the pinch: 8_To_9 split 1 is matched with 2_To_3 split 1, 8_To_9 split 3 is matched with BIOGAS_To_1;
- above the pinch: 15_To_16 split 1 is matched with 18_To_19 stream, 15_To_16 split 2 is matched with the reboiler of DIST-2 column;

Afterwards, other 3 matches are placed and in figure 3.7 the complete HEN diagram is reported for the process. Energy consumption results, before and after the heat integration, considering the different utilities used in the process, are reported in table 3.7.

Table 3.7: Load and mass flowrate of the different utilities required, making a comparison before and after heat integration in the BR to methanol process

Utility	Before heat integration		After heat integration	
	Load (kW)	Mass flowrate (kg/h)	Load (kW)	Mass flowrate (kg/h)
Hot utilities				
Natural gas	23425	1767.95	18715	1412.48
Low-pressure steam	9248	16568	1504	2694.4
High-pressure steam	8897	21790.5	0	0
Cold utilities				
Ammonia	616	494866	616	494866
Cooling water	52373	4510598	31013	2670981

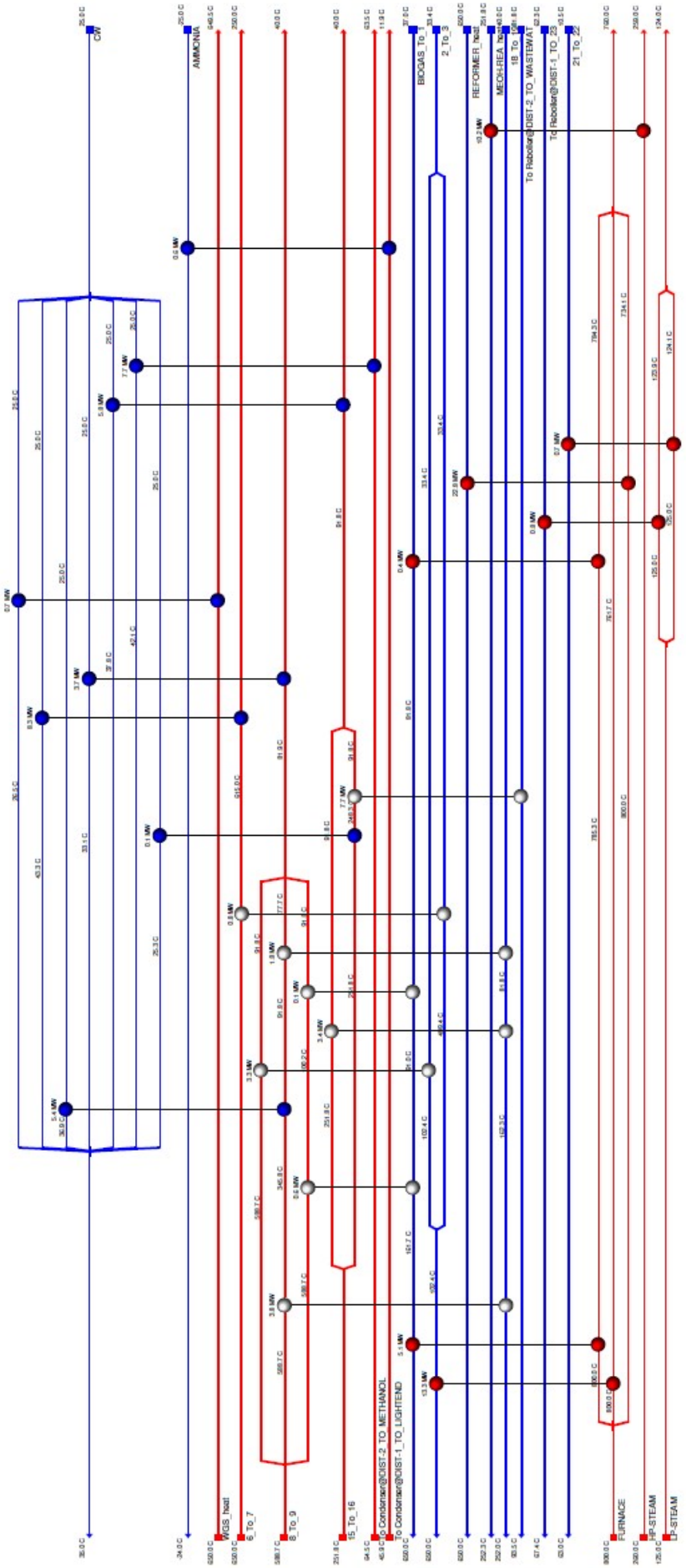

Figure 3.7: HEN diagram for Biogas Reforming to methanol process

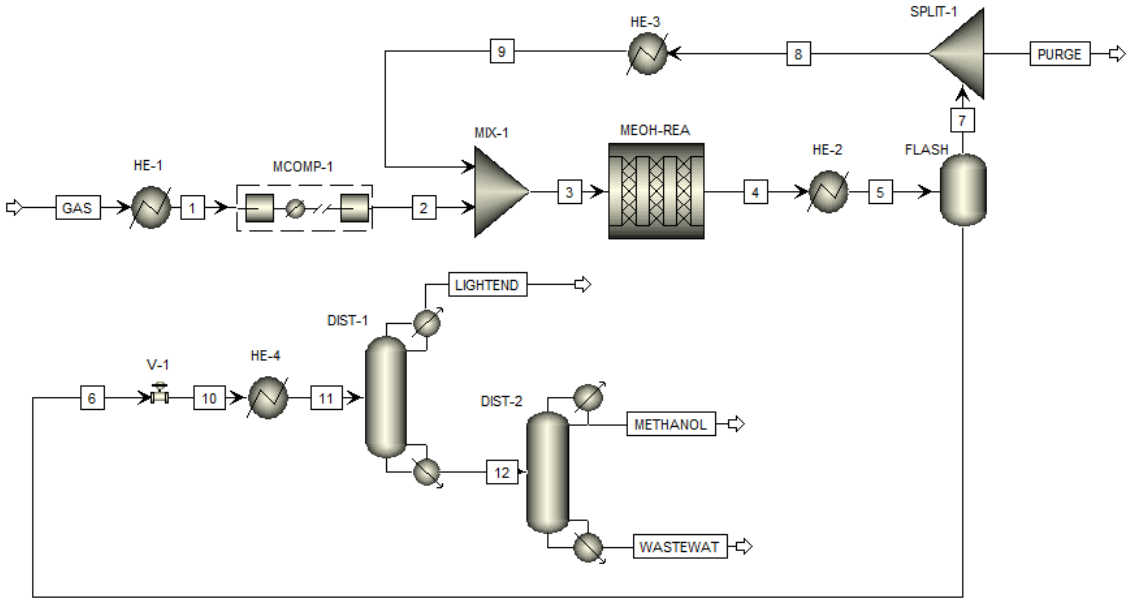

Figure 3.8: Aspen Plus process flowsheet of biomass steam gasification to methanol process

3.2.3 Biomass steam gasification to methanol

Considering the process flowsheet depicted in figure 3.8, biomass steam gasification products ideally represent the feed of the process, entering it at the operating conditions of the gasifier (850 °C and 1 atm). Then, pressure is increased up to 75 bar in a 4-stages multi-compressor (MCOMP-1), exiting at the operating temperature of methanol synthesis reactor (252 °C); multi-stage compressor profiles and data are reported in table 3.8.

The product gas exiting the methanol synthesis reactor (MEOH-REA) is cooled down to 40 °C in HE-2, while pressure is kept at 75 bar to avoid an expansion, and the successive need to re-compress the gas exiting the FLASH-1 separation unit that is recycled back to methanol synthesis section, thus avoiding the related higher operating costs. The gaseous outlet of the flash unit is partially purged (10 %), while the rest is heated in HE-3 to 252 °C and mixed with stream 2; the liquid stream exiting the flash drum, mainly constituted of methanol and water, is de-pressurized to atmospheric pressure, and heated in HE-4 to 36 °C, the boiling temperature of stream 11. This stream represents the feed of the first column DIST-1, where volatile gases exit as the overhead product, and leave the process to be burnt in flare (LIGHTEND stream). The liquid bottom product of the column, stream 12, is fed to the second distillation column (DIST-2), where methanol is obtained as a liquid from the total condenser (METHANOL stream), while the bottom product is mainly constituted of water that is treated as a waste (WASTEWAT stream); in this column DSs are set on methanol productivity (382.464 kmol/h) and mass purity (99.85 wt.%), by varying the user-input data of such column, the reflux ratio and the distillate-to-feed ratio.

There is not a pinch temperature for the process, anyway an optimal ΔT_{min} value of the process has been estimated to be 10 °C, and the GAS_To_1 hot stream (inlet temperature 850

Table 3.8: Multi-stage compressor MCOMP-1 simulation results for biomass steam gasification to methanol process

	Stage 1	Stage 2	Stage 3	Stage 4
Exit temperature (°C)	438.769	438.853	439.093	439.755
Exit pressure (bar)	2.972	8.717	25.57	75.00
Shaft power (kW)	5868	5875	5897	5962
Head developed (m)	26243	26276	26374	26665
Volumetric flow (m^3/h)	123841	42246.4	14428.6	4945.39
Cooling temperature (°C)	252	252	252	252
Cooling duty (kW)	-5869.9	-5881.9	-5916.2	-6011.0

Table 3.9: Load and mass flowrate of the different utilities required, making a comparison before and after heat integration in the biomass steam gasification to methanol process

Utility	Before heat integration		After heat integration	
	Load (kW)	Mass flowrate (kg/h)	Load (kW)	Mass flowrate (kg/h)
Hot utilities				
Low-pressure steam	8749	15673.7	0	0
High-pressure steam	35902	87929.9	17022	41690.0
Cold utilities				
Refrigerant R-152a	573.9	1315011	113.9	260986
Cooling water	27720	2387368	46670	4019426
Refrigerated water	46118	7938110	0	0

°C, outlet temperature 252 °C) is split in two equal streams: 7 matches are finally obtained constituting the HEN illustrated in figure 3.9. Energy consumption results, before and after the heat integration, considering the different utilities used in the process, are reported in table 3.9. Cooling water load is increased after the heat integration, while refrigerated water load is nullified: by the design of the HEN, refrigerated water load has been reduced progressively until reaching the zero value, by employing, in partial substitution, cooling water utility: the need of cooling water is thus increased, after the design and development of the HEN.

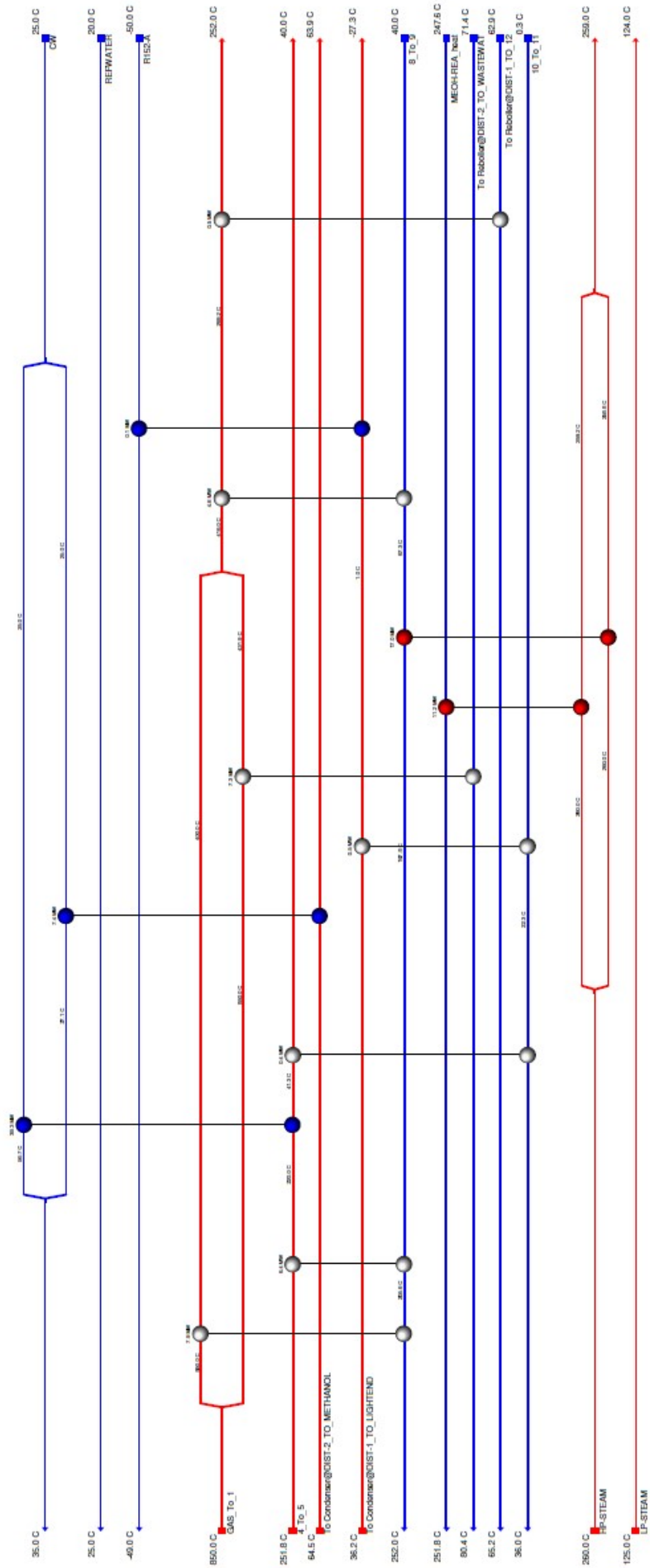

Figure 3.9: HEN diagram for Biomass Steam Gasification to methanol process

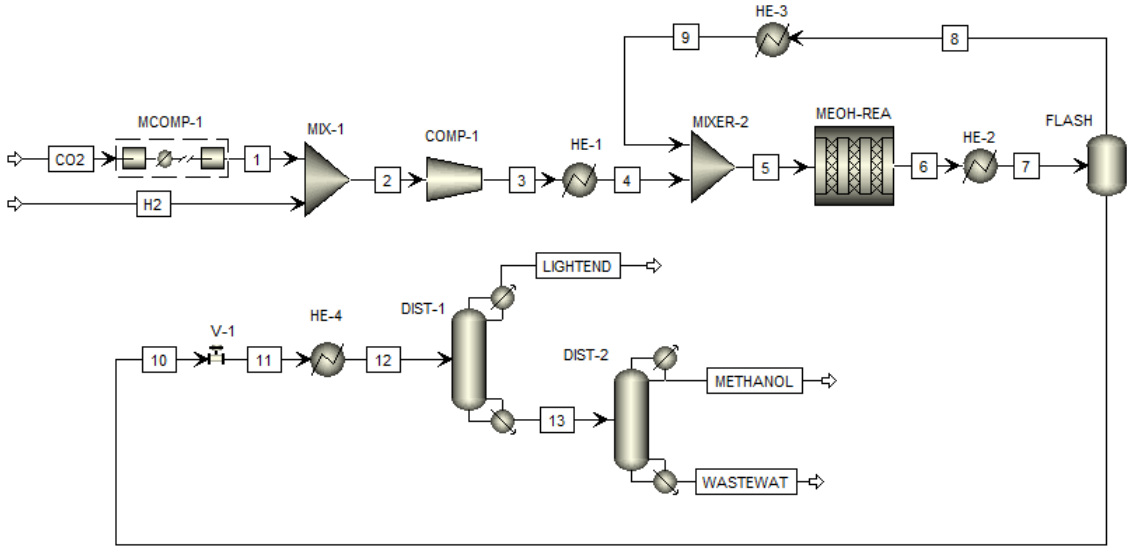

Figure 3.10: Aspen Plus process flowsheet of CO_2 hydrogenation process (AW electrolysis)

3.2.4 CO_2 hydrogenation (AW electrolysis)

Considering the process flowsheet depicted in figure 3.10, hydrogen is fed at typical operating conditions of an AW electrolysis unit, assumed to be 90 °C and 30 bar in this work, while carbon dioxide is fed at atmospheric condition, as it exits from DAC process; afterwards, CO_2 is brought to the same pressure conditions of H_2 feed stream, with a multi-stage compressor (MCOMP-1), before being put in contact with hydrogen, with a further compression step (COMP-1) that rises the pressure up to 75 bar. Compressors profiles and data are reported in table 3.10.

Following the last compression step, HE-1 increases the temperature of stream 3 to the operating one of methanol synthesis reactor (MEOH-REA), i.e. 252 °C, while the product gas exiting the reactor, is cooled to 40 °C in HE-2; instead, pressure is kept at 75 bar to avoid an expansion and the successive need to re-compress the gas exiting the FLASH-1 separation unit that is recycled back to methanol synthesis section. The gaseous outlet of the flash unit is totally recycled (stream 8), it is re-heated in HE-3 to 252 °C, and then mixed with stream 4; the liquid stream exiting the flash drum, mainly constituted of methanol and water, is de-pressurized to atmospheric pressure, and heated in HE-4 to 57 °C, the boiling temperature of stream 12. This stream represents the feed of the first column DIST-1, where volatile gases exit as the overhead product, and leave the process to be burnt in flare (LIGHTEND stream). The liquid bottom product of the column, stream 13, is fed to the second distillation column (DIST-2), where methanol is obtained as a liquid from the total condenser (METHANOL stream), while the bottom product is mainly constituted of water that is treated as a waste (WASTEWAT stream); in this column only the DS on methanol productivity is set (382.464 kmol/h), while mass purity is overcome ($>$ 99.94 wt.%). Only distillate-to-feed ratio is varied to reach the desired productivity.

Table 3.10: Multi-stage compressor MCOMP-1 simulation results for CO_2 hydrogenation process (AW electrolysis)

	MCOMP-1			COMP-1
	Stage 1	Stage 2	Stage 3	
Exit temperature (°C)	135.928	215.758	216.775	215.999
Exit pressure (bar)	3.135	9.697	30.00	75.00
Shaft power (kW)	517.2	623.2	614.1	1915
Head developed (m)	7308.9	8806.6	8677.6	24052
Volumetric flow (m^3/h)	10345.5	4061.77	1291.18	882.645
Cooling temperature (°C)	90	90	90	252
Cooling/heating duty (kW)	-225.156	-645.505	-686.435	540.877

Table 3.11: Streams crossing the pinch split fractions and heat capacity flowrates for CO_2 hydrogenation process (AW electrolysis)

Stream name	T_{in}	T_{out}	CP	Split fraction		Split CP (kW/°C)	
	(°C)	(°C)	(kW/°C)	1	2	1	2
HOT STREAM							
6_To_7	251.6	40	127.1	0.30	0.70	38.13	88.97
COLD STREAM							
8_To_9	40	252	44.23				

Pinch temperature of the process is 103.4 °C, and the optimal ΔT_{min} of the process has been estimated to be 8 °C. Only two streams are widespread across the pinch temperature ideal line, and they are reported in table 3.11.

From the data reported in such table, the golden rule about the number of hot and cold streams is satisfied only below the pinch after splitting, considering that $S_H > S_C$. Taking into consideration the golden rule on heat capacity flowrates below the pinch, only the match between split 2 of 6_To_7 stream and 8_To_9 can be placed at the pinch, in the initial phase of the analysis. Afterwards, other 4 matches are placed, and in figure 3.11 the complete HEN diagram is reported for the process. Energy consumption results, before and after the heat integration, considering the different utilities used in the process, are reported in table 3.12.

Table 3.12: Load and mass flowrate of the different utilities required, making a comparison before and after heat integration in the CO_2 hydrogenation process (AW electrolysis)

Utility	Before heat integration		After heat integration	
	Load (kW)	Mass flowrate (kg/h)	Load (kW)	Mass flowrate (kg/h)
Hot utilities				
Low-pressure steam	11710	20978.4	0	0
High-pressure steam	9916	24285.8	6486	15885.2
Cold utilities				
Ammonia	1160	932496	1160	932496
Cooling water	29570	2546699	14440	1243636

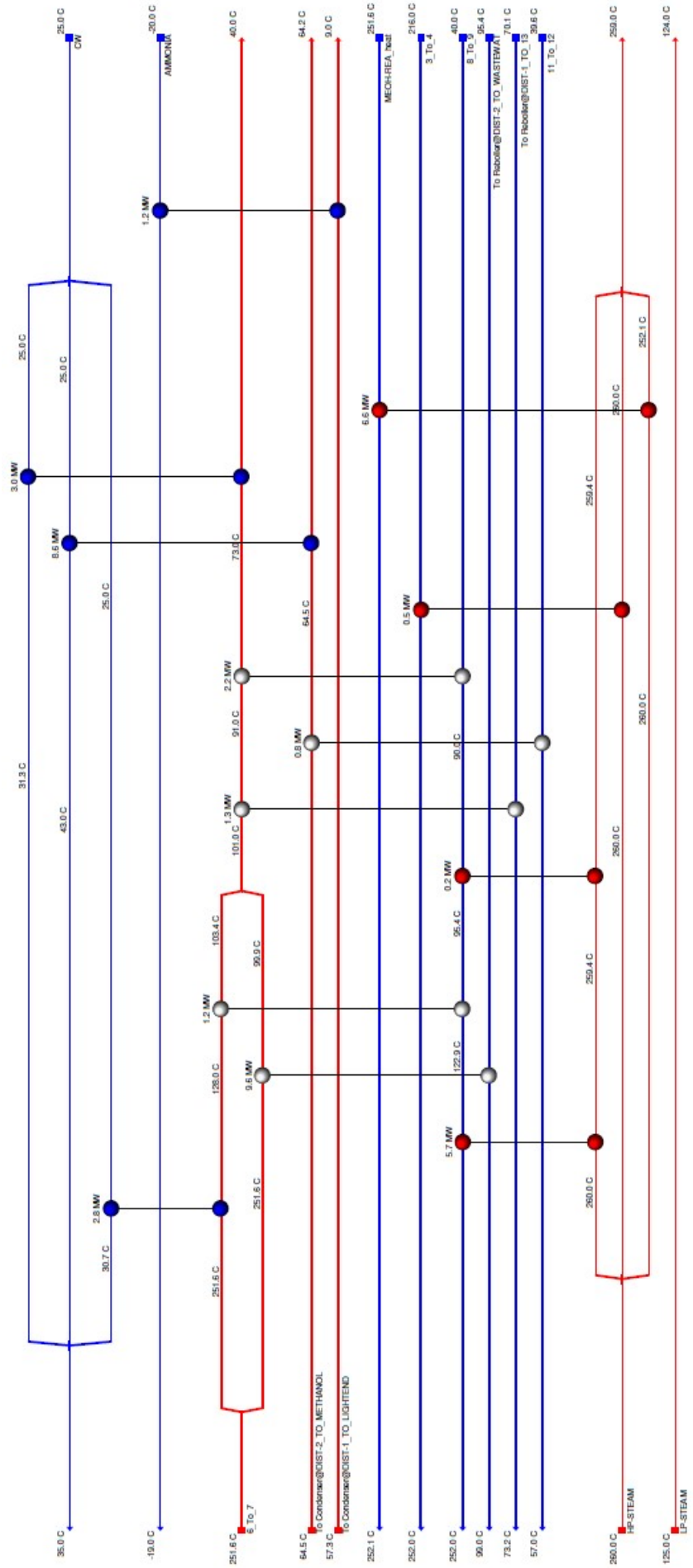

Figure 3.11: HEN diagram for CO_2 hydrogenation process (AW electrolysis

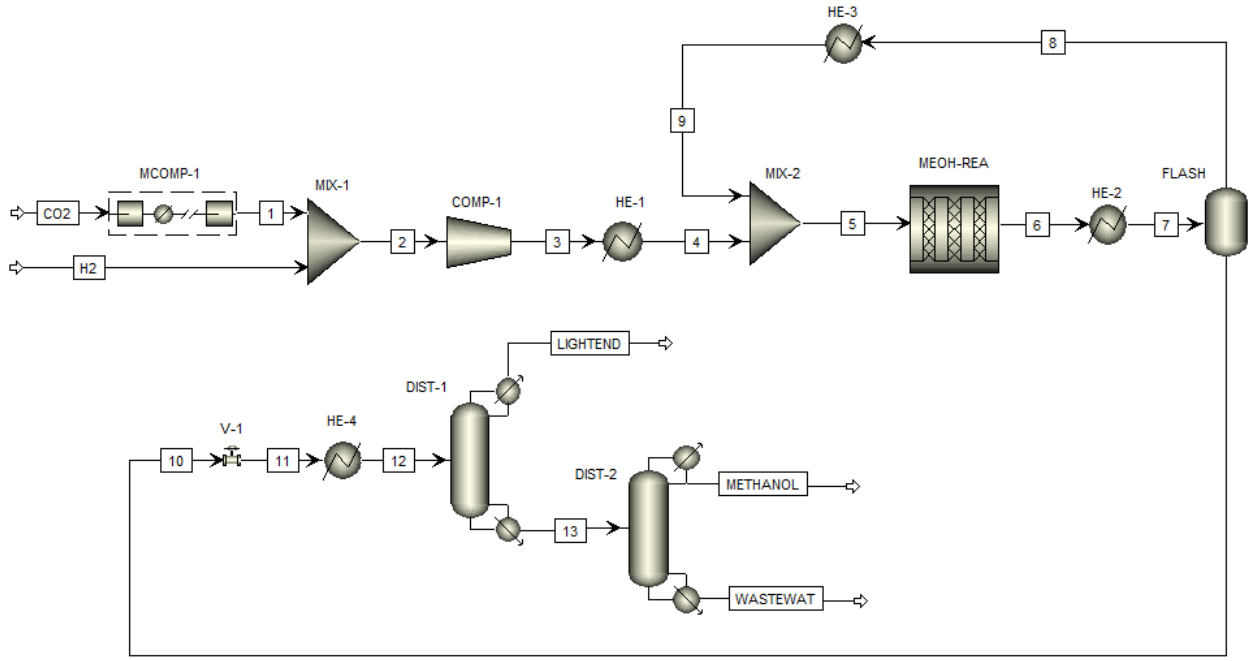

Figure 3.12: Aspen Plus process flowsheet of CO_2 hydrogenation process (PEM electrolysis)

3.2.5 CO_2 hydrogenation (PEM electrolysis)

Considering the process flowsheet depicted in figure 3.12, hydrogen is fed at typical operating conditions of a PEM electrolysis unit, assumed to be 80 °C and 50 bar in this work, while carbon dioxide is fed at atmospheric condition, as it exits from DAC process; afterwards, CO_2 is brought to the same pressure conditions of H_2 feed stream, with a multi-stage compressor (MCOMP-1), before being put in contact with hydrogen, with a further compression step (COMP-1) that rise the pressure up to 75 bar. Compressors profiles and data are reported in table 3.13.

Following the last compression step HE-1 increases the temperature of stream 3 to the operating one of methanol synthesis reactor (MEOH-REA), i.e. 252 °C, while the product gas exiting the reactor is cooled to 40 °C in HE-2; instead, pressure is kept at 75 bar to avoid an expansion and the successive need to re-compress the gas exiting the FLASH-1 separation unit that is recycled back to methanol synthesis section. The gaseous outlet of the flash unit is totally recycled (stream 8), it is re-heated in HE-3 to 252 °C, and then mixed with stream 4; the liquid stream exiting the flash drum, mainly constituted of methanol and water, is de-pressurized to atmospheric pressure, and heated in HE-4 to 57 °C, the boiling temperature of stream 12. This stream represents the feed of the first column DIST-1, where volatile gases exit as the overhead product, and leave the process to be burnt in flare (LIGHTEND stream). The liquid bottom product of the column, stream 13, is fed to the second distillation column (DIST-2), where methanol is obtained as a liquid from the total condenser (METHANOL stream), while the bottom product is mainly constituted of water that is treated as a waste (WASTEWAT stream); in this column only the DS on methanol productivity is set (382.464 kmol/h), while mass purity is overcome ($>$ 99.87 wt.%). Only distillate-to-feed ratio is varied to reach the

Table 3.13: Multi-stage compressor MCOMP-1 simulation results for CO_2 hydrogenation process (PEM electrolysis)

	MCOMP-1			COMP-1
	Stage 1	Stage 2	Stage 3	
Exit temperature (°C)	153.930	223.774	225.622	215.999
Exit pressure (bar)	3.717	13.63	50.00	75.00
Shaft power (kW)	606.3	708.9	692.0	761.953
Head developed (m)	8568.0	10018	9778.0	9567.7
Volumetric flow (m^3/h)	10345.5	3323.19	880.571	714.715
Cooling temperature (°C)	80	80	80	252
Cooling/heating duty (kW)	-364.145	-744.829	-837.786	1918.48

Table 3.14: Streams crossing the pinch split fractions and heat capacity flowrates for CO_2 hydrogenation process (PEM electrolysis)

Stream name	T_{in}	T_{out}	CP	Split fraction		Split CP (kW/°C)	
	(°C)	(°C)	(kW/°C)	1	2	1	2
HOT STREAM							
6_To_7	251.6	40	166.8	0.25	0.75	41.70	125.1
COLD STREAM							
8_To_9	40	252	44.24				

desired productivity.

Pinch temperature of the process is 105.6 °C, and the optimal ΔT_{min} of the process has been estimated to be 10 °C. Only two streams are widespread across the pinch temperature ideal line, and they are reported in table 3.14.

From the data reported in such table, the golden rule about the number of hot and cold streams is satisfied only below the pinch after splitting, considering that $S_H > S_C$. Taking into consideration the golden rule on heat capacity flowrates below the pinch, only the match between split 2 of 6_To_7 stream and 8_To_9 can be placed at the pinch, in the initial phase of the analysis. Afterwards, other 4 matches are placed, and in figure 3.13 the complete HEN diagram is reported for the process. Energy consumption results, before and after the heat integration, considering the different utilities used in the process, are reported in table 3.15.

Table 3.15: Load and mass flowrate of the different utilities required, making a comparison before and after heat integration in the CO_2 hydrogenation process (PEM electrolysis)

Utility	Before heat integration		After heat integration	
	Load (kW)	Mass flowrate (kg/h)	Load (kW)	Mass flowrate (kg/h)
Hot utilities				
Low-pressure steam	11720	20996.3	0	0
High-pressure steam	11295	27663.2	7375	18062.6
Cold utilities				
Ammonia	1156	929280	1156	929280
Cooling water	29590	2548421	13960	1202297

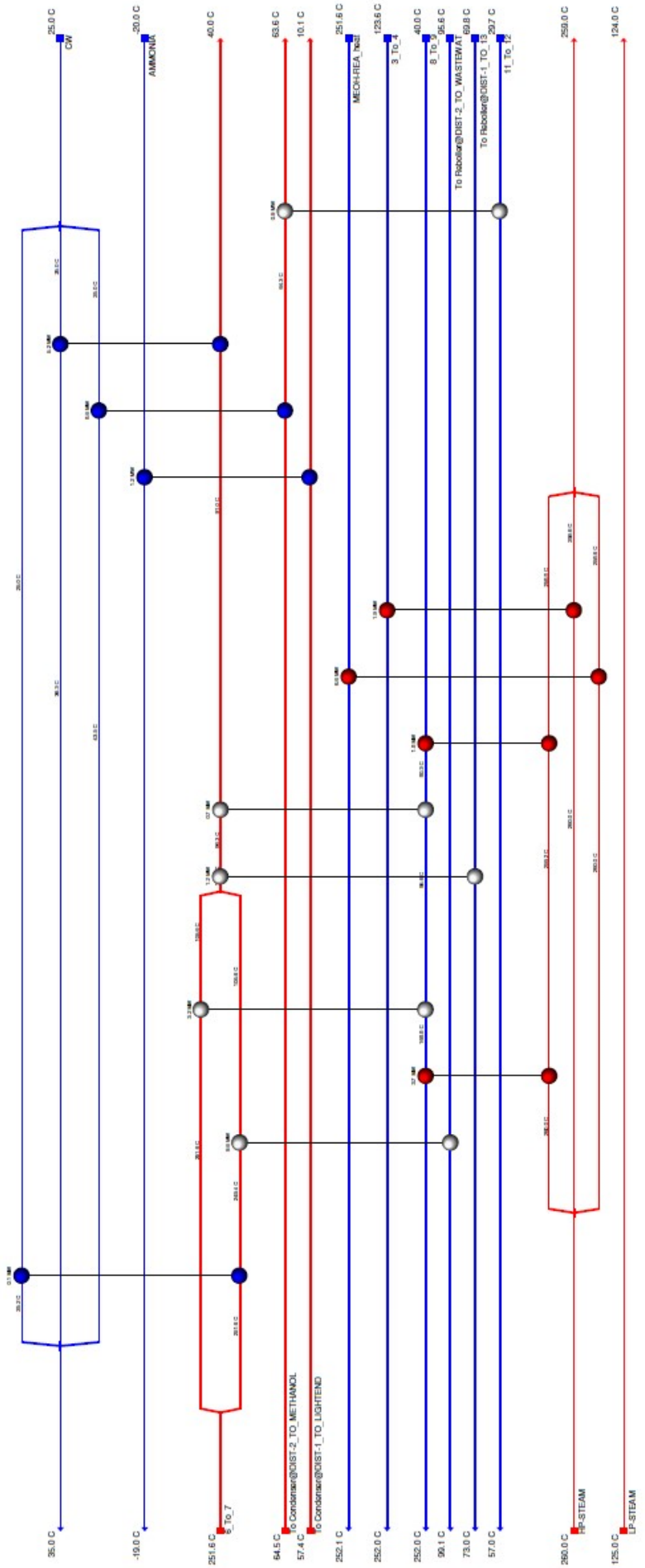

Figure 3.13: HEN diagram for CO_2 hydrogenation process (PEM electrolysis)

3.3 Results assessment and validation

A technological assessment based on Aspen Plus simulation results is performed for each process, and a comparison is made between the five processes. Several indicators are used to evaluate the performances of the processes, and an explanation of their definition is of paramount importance to fully understand the results obtained:

1. single-pass conversion for a generic reactant i is defined as:

$$X_i = \frac{F_i^{in} - F_i^{out}}{F_i^{in}} \tag{3.5}$$

   where F_i^{in} is the molar flowrate at the reactor inlet, and F_i^{out} the molar flowrate at the reactor outlet. In the case of multiple reactions, the global conversion value is considered.

2. overall process conversion for a generic reactant i is instead defined with respect to its fresh feed and to the amount of reactant exiting the process in the purge, or in the products streams:

$$X_i^{overall} = \frac{F_i^{feed} - (F_i^{prod} + F_i^{purge})}{F_i^{feed}} \tag{3.6}$$

   where F_i^{feed} is the molar flowrate of the reactant i in the fresh feed.

3. product yield for a generic product j, with respect to a reactant i:

$$\eta_j^i = \frac{F_j^{out}}{F_i^{in}} \tag{3.7}$$

   if i and j have different stoichiometric coefficients, they should be normalized to the unitary value of them.

4. selectivity of the product j with respect to reactant i:

$$S_j^i = \frac{F_j^{out}}{F_i^{in} - F_i^{out}} \tag{3.8}$$

   if i and j have different stoichiometric coefficients, they should be normalized to the unitary value of them.

5. recycle-to-feed ratio (R/F) is defined from the total molar flowrate of the recycle stream, with respect to the total molar flowrate of the feed stream(s). In MSR and BR to methanol processes, only the methanol synthesis recycle loop is considered for this calculation (the recycle considered is the gaseous stream exiting FLASH-2 unit).

6. Higher Heating Value (HHV) represents the heat developed by the complete combustion,

considering that combustion products are led back to pre-combustion temperature, thus condensing vapors. HHV is calculated from the mass percentages of the atomic components, on a dry basis, following the correlation reported in Green and Southard (2019), validated for various biomass, liquid fuels, and other solid fuels with an average error of 337 kJ/kg:

$$HHV = 349.1\ \%C + 1178.3\ \%H + 100.5\ \%S - 103.4\ \%O - 15.1\ \%N - 21.1\ \%A \text{ kJ/kg} \quad (3.9)$$

where A stands for ash, that, as well as nitrogen and sulfur, are not present in the processes considered in this work.

7. Lower Heating Value (LHV) represents the heat developed by the complete combustion considering that steam is present as a product of the combustion; it is obtained from HHV by subtracting the mass of combustion water, following this correlation:

$$LHV = HHV - \%H \cdot 214 \text{ kJ/kg} \quad (3.10)$$

HHV and LHV are calculated for gaseous streams leaving the process (PURGE and LIGHTEND streams).

8. the average residence time τ, defined as the average time the molecules spend in the reactor, for a PFR reactor is equal to the space time (i.e. time necessary to process one reactor volume of fluid based on entrance conditions). It is thus defined as:

$$\tau = \frac{V}{v_0} \quad (3.11)$$

where V is the reactor volume, and v_0 represents the volumetric flow of the reactor inlet. Typical residence times for production capacities up to 5 million t/y range between 0.5 s and 1 h (Fogler, 2016).

9. total hot utilities load: heating provided by the furnace, high-pressure steam, and low-pressure steam is taken into consideration after the heat integration is carried out. Results are normalized to the mass flowrate of methanol produced (kJ per kg of CH_3OH);

10. total cold utilities load: cooling provided by ammonia, cooling water, refrigerant R-152a, and refrigerated water is taken into consideration after the heat integration is carried out. Results are normalized to the mass flowrate of methanol produced (kJ per kg of CH_3OH);

11. energy savings: total loads of all the utilities, both the cold and the hot ones, are compared between the scenarios before and after heat integration. Results are presented in terms of load savings normalized to the mass flowrate of methanol produced (kJ per kg of CH_3OH),

Table 3.16: Technological comparative assessment of the five methanol production processes simulated

	MSR to methanol	BR to methanol	Biomass to methanol	CO_2 hydrogenation	
				AW el.	PEM el.
Single-pass CO conversion (%)	29.37	46.99	10.28		
Overall CO conversion (%)	99.92	99.89	99.76		
Single-pass CO_2 conversion (%)	43.09	5.956	0.663	24.91	24.93
Overall CO_2 conversion (%)	97.46	77.61	87.19	91.14	91.15
Methanol yield vs CO	0.3845	0.6495	0.1472	3.2670	3.2695
Methanol yield vs CO_2	2.8705	0.2734	0.1028	0.2622	0.2624
Selectivity of CH_3OH vs CO	1.309	1.3823	1.4318		
Selectivity of CH_3OH vs CO_2	6.662	4.5907	15.504	1.0528	1.0528
Recycle-to-feed ratio	3.5963	2.2200	4.7881	3.0142	3.0143
Purge HHV (kJ/kg)	47392	15248	16366		
Purge LHV (kJ/kg)	40585	13521	15078		
Lightends HHV (kJ/kg)	15806	4193	8235	3174	3242
Lightends LHV (kJ/kg)	14208	3930	7714	3016	3075
Residence time (s)	18.093	31.721	10.364	29.341	29.340
Total hot utilities load (kJ/kg)	5820.9	5931.2	4992.3	1905.1	2165.3
Total cold utilities load (kJ/kg)	8682.5	9278.8	13721	4579.0	4434.4
Heat integr. load savings (kJ/kg)	21723	12526	16210	8887.7	9173.7
Heat integr. load savings (%)	59.96	45.16	46.42	57.82	58.16

by considering also the reduction percentage.

It can be easily verified that, provided these definitions, there is a relationship between conversion, product j selectivity and yield, with respect to the same reactant i:

$$\eta_j^i = X_i \cdot S_j^i \tag{3.12}$$

The technological assessment results are presented, by considering the indicators listed above, in table 3.16: here CO is not considered as a reactant in the two CO_2 hydrogenation processes.

Single-pass carbon conversion is then calculated by considering as reactants both CO and CO_2:

$$X_{\mathrm{CO}_x} = \frac{(F_{\mathrm{CO}}^{in} + F_{\mathrm{CO}_2}^{in}) - (F_{\mathrm{CO}}^{out} + F_{\mathrm{CO}_2}^{out})}{F_{\mathrm{CO}}^{in} + F_{\mathrm{CO}_2}^{in}} \tag{3.13}$$

Methanol reactor inlet composition and carbon conversion results are reported, for the five processes, in table 3.17.

Carbon (CO_x) conversion results obtained are then validated, by comparing them with experimental data from Klier *et al.* (1982), and simulation data reported in VandenBussche and Froment (1996) and Mignard and Pritchard (2008), which represent the reference kinetic models as described in chapter 2; the reference plots for comparison are reported in figures 3.14 and

Table 3.17: Single-pass carbon conversion (X_{CO_x}) results, and methanol reactor inlet molar composition for the five processes simulated, considering the 4 main components (minor components are referred as others)

	MSR to methanol	BR to methanol	Biomass to methanol	CO_2 hydrogenation	
				AW el.	PEM el.
Reactor inlet composition (mol%)					
CO	11.67	11.07	21.85	1.958	1.957
CO_2	1.56	26.30	31.30	24.39	24.38
H_2	78.85	50.40	18.54	73.23	73.26
CH_4	7.40	11.37	19.24	0.000	0.000
Others	0.510	0.865	9.077	0.413	0.413
CO_x conversion (%)	30.99	18.11	4.617	23.05	23.07

3.15.

Carbon conversion is largely influenced by the composition of the inlet stream of methanol reactor: the highest is calculated for the classical MSR to methanol process, while the lowest is attributed to biomass to methanol process; hydrogen is present in a quite scarce amount, thus there would be the need to enrich the syngas before entering the methanol synthesis section. In this way, a solution may be represented by the introduction of one or two WGS reactors: in fact, via WGS reaction (1.13), under the best operating conditions for the reaction and the proper catalyst, as reported in figure 3.16 (considering the 2-reactors configuration), the hydrogen-to-carbon monoxide ratio (H_2/CO) is increased. However, as it can be noticed in figure 3.14, even in the case of BR to methanol process, the high concentration of CO_2 in the reactor feed reduces a lot carbon conversion, even with a very high hydrogen concentration. Thus, further studies would be needed to find the optimal syngas composition needed for methanol synthesis from renewable feedstocks.

Instead, with regard to the most innovative routes to methanol production, via CO_2 hydrogenation, carbon conversion is quite good, but single-pass CO_2 conversion is not so high, even with a stoichiometric feed. Indeed, studies and research are in progress to find the optimal operating conditions and to develop new catalysts, that may increase CO_2 conversion and a higher selectivity of methanol versus CO_2. However, considering that a syngas is not needed, temperatures along the process are comprised between the ambient one and the methanol synthesis operating one (252 °C), never crossing the upper limit: the result is a huge reduction of utilities loads needed, for both the hot and cold ones, with respect to the traditional synthesis processes from syngas. Furthermore, the heat integration between process streams, result in a load saving comparable to that of MSR to methanol process ($\sim 58\%$ vs $\sim 60\%$).

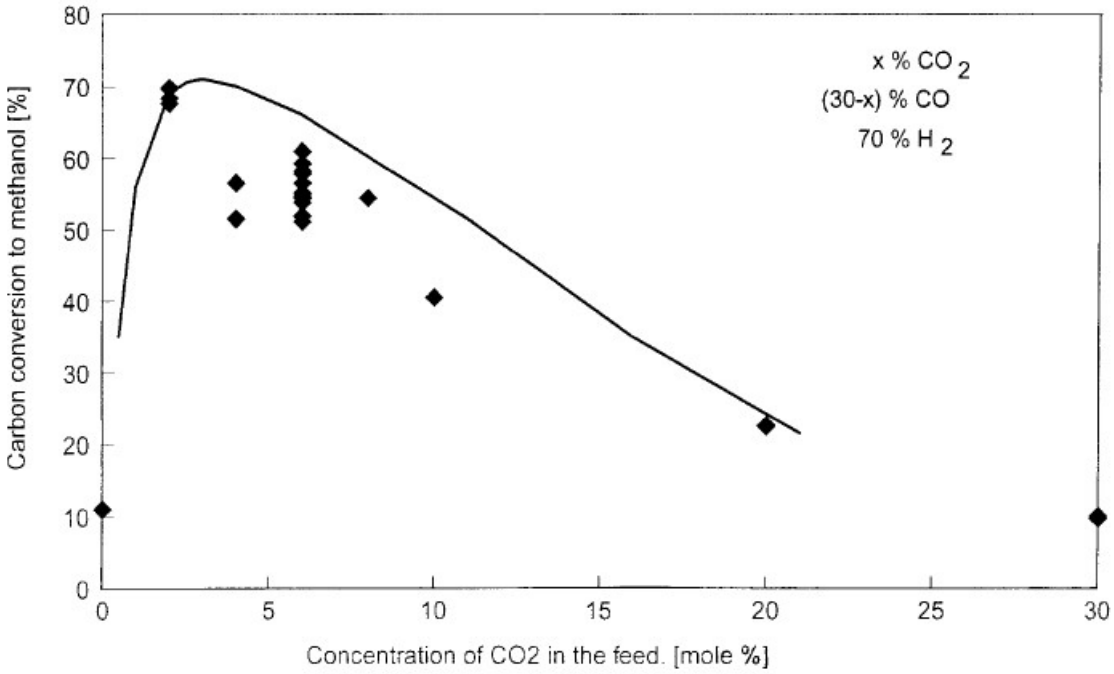

Figure 3.14: Conversion to methanol for different ratios of y_{CO}/y_{CO_2} at $y_{H_2} = 0.7$, 75 bar and 250 °C; experimental results by Klier *et al.* (1982) are represented by the rhombi, while the line represents simulated results using the kinetic model of VandenBussche and Froment, 1996

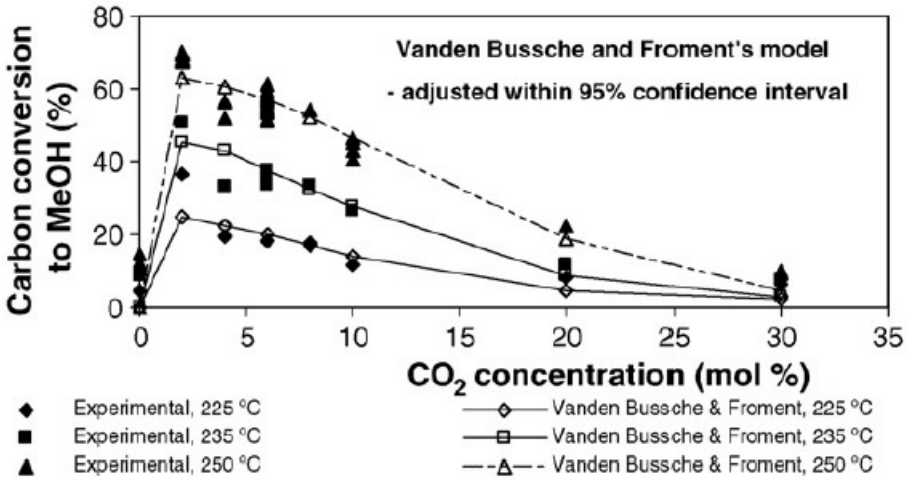

Figure 3.15: Comparison between Klier *et al.* (1982) data and simulation as predicted by Vanden Bussche and Froment (1996) model, after adjustment to two of the original parameters of the model within the 95% confidence interval (Mignard and Pritchard, 2008)

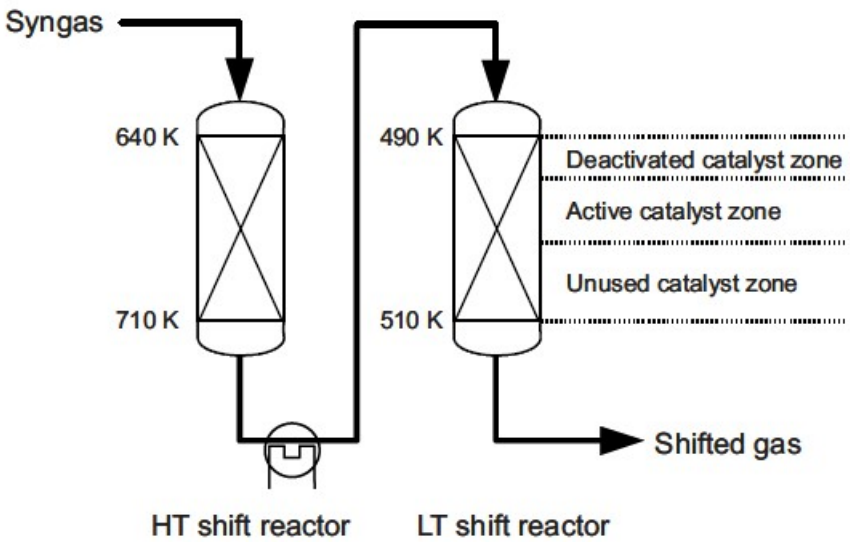

Figure 3.16: WGS reactors with typical temperatures and catalysts profile (Moulijn *et al.*, 2013)

Chapter 4

Economic and Carbon Intensity Analysis

Once a Process Flow Diagram (PFD) is available for a process, in the case of this work an Aspen Plus flowsheet, the economic analysis can be performed for the same process. In this chapter the capital investment needed to build an hypothetical new plant is investigated, for each of the five processes; afterwards, the operating costs that characterize the operation of the plant are calculated, and finally, a profitability analysis for each process is carried out, in order to evaluate if an investment in building a new plant, carrying out the specific process, would be convenient, and which of the methanol synthesis routes considered is more profitable. In the second part of the chapter, the analysis of carbon emissions related to each process is performed, by considering both the direct and the indirect emissions, as explained later.

4.1 Economic analysis

The economic analysis of a process starts from the evaluation of the capital costs (or capital investment), and of the operating costs (or manufacturing costs); they are commonly referred to also as Capital Expenditure (CAPEX), or Operational Expenditure (OPEX), but in this work they will be always indicated as capital costs and manufacturing costs.

Capital costs pertain to the costs associated with the construction of a new plant, or modifications to an existing one. The Total Capital Investment (TCI) is the total asset needed to build a plant, and it can be represented by the sum of three contributions, as reported by Bezzo (2021):

- Fixed Capital Investment (FCI): direct and indirect costs needed for building the plant. They represent money that can not be converted into cash immediately. Indirect costs are related to engineering and plant supervision costs, general construction expenses, contractor's fee (assumed as 10% of ISBL+OSBL in this work), and contingencies (assumed as 10% of ISBL+OSBL); direct costs can be divided in the sum of two contributions:

  - Inside Battery Limits (ISBL), that include purchase and installed costs of equipment, as well as instrumentation, control systems, piping, and electrical equipment.
  - Outside Battery Limits (OSBL) that comprise the costs of buildings, yard improvements, service facilities, and land. They are assumed as 20% of ISBL.

- Working Capital (WC): money needed to operate the plant every day, renewed by selling products and generating new cash. In this work it is assumed as 10% of the sum between ISBL and OSBL.
- Start-up Costs or Start-up Capital (StC): money needed to start up the plant for the first time, when extra labor is needed. In this work it is assumed as 8% of the FCI.

On-site direct costs, represented by ISBL, must consider both the purchase cost of equipment, and the cost of installed equipment, so that ISBL is not the simple sum over all the equipment purchase costs. Typically, the following scaling factors are considered to calculate the actual cost of equipment, that contributes to the calculation of ISBL:

- distillation columns: 3.5 times;
- heat exchangers: 2.5 times;
- compressors: 2.0 times;
- furnaces: 2.0 times;
- other equipment: 2.5 times;

Bare-module cost (C_{BM}) represents the link between purchase and installed cost of equipment, starting from the purchase cost of equipment at base conditions (C_p^0) and correcting it by a bare-module factor (F_{BM}):

$$C_{BM} = C_p^0 F_{BM} \tag{4.1}$$

A typical correlation from Turton *et al.* (2018) represents the bare-module factor as the sum of contributions related to the operating pressure, and material of construction of the equipment considered for cost calculation:

$$C_{BM} = C_p^0 (B_1 + B_2 F_P F_M) \tag{4.2}$$

where B_1 and B_2 are tabulated values, F_P is the pressure factor calculated through another correlation, and F_M is the material factor. Material factor is generally 1 for carbon steel, as it represents the reference for material cost evaluation. Sometimes, in this work, different materials are considered, due to corrosion, or operational constraints:

- titanium-based alloys are employed in the light ends column, due to the huge presence of CO_2 dissolved in liquid water, giving rise to a potential corrosive regime, given by

carbonic acid (H_2CO_3);

- nickel-based alloys are employed in the light ends column condenser, where ammonia is used as a refrigerant. In the case of a shell-and-tube heat exchanger, Nickel alloys are employed in tube-side;
- ceramic materials are used in furnaces, due to the high operating temperatures.

Because of inflation, the cost estimates are needed to be continuously updated with respect to the "base" year, by the use of a cost index: as in Turton *et al.* (2018), Chemical Engineering Plant Cost Index (CEPCI) is used, which for reference year 2001 is equal to 397. In this work economic analysis is referred to year 2020, characterized by a CEPCI equal to 596.

The Cost of Manufacturing (COM) for a process is affected by many factors; it can be expressed on an annual basis, or per unit production of product, and it can be divided in three categories (Bezzo, 2021):

- Direct Manufacturing Costs (DMC) or variable costs of production: they represent operating expenses that vary with production rate, and include the costs of:
  - raw materials consumed by the process: in table 4.1 the assumptions related to the raw materials cost are reported, along with the reference considered. Water used to generate the steam for reforming reactions, in MSR and BR to methanol process, is estimated from process water cost, while methane cost is estimated from the NG cost. Captured CO_2 cost is considered specifically for the DAC process, while the cost of H_2, produced via the two different electrolysis technologies, is considered specifically for those production processes;

Table 4.1: Raw material costs and reference

	Cost (C_{RM})		
Raw material	\$/t	\$/kmol	Reference
Water (H_2O)	0.177	0.003	Turton *et al.* (2018)
Methane (CH_4)	164.8	2.644	NG cost from EUROSTAT
Carbon dioxide (CO_2)	94.00	4.137	Keith *et al.* (2018)
AW hydrogen (H_2)	7600	15.32	Jang *et al.* (2022)
PEM hydrogen (H_2)	8550	17.24	Jang *et al.* (2022)
Biogas	0.978	0.026	IEA (2020b)
Biomass (wood chips)	107.4	0.806	Yao *et al.* (2017)

  - utilities needed for the process: electricity and natural gas are directly involved, while utilities used for heating or cooling process streams, are generated through the employment of either electricity, or natural gas, or a combination of them. A detailed analysis is reported in section 4.1.2;
  - consumables possibly employed (solvents, acids or bases, inert materials, additives, catalysts, ...): in this work only catalysts are used, for reforming reactions and

methanol synthesis. Anyway, their annual cost is assumed to be negligible;

- effluent disposal and treatment: considering a wastewater disposal cost of \$56/1000 m^3 (Turton *et al.*, 2018), and the quite low volumetric flow of the bottom product of methanol column (WASTEWAT stream), the cost of disposal and treatment of waste water is neglected.
- operating labor, considering an operator cost of 50 k\$/year (C_{op}), labor cost (C_{OL}) is calculated as:

$$C_{OL} \cong C_{op} N'_{OL} \cong C_{op}(4.5 N_{OL}) \tag{4.3}$$

where the number of work positions per shift (N_{OL}), is calculated considering the number of processing steps involving particulate solids P (not considered in this work), and N_{np} is the number of non-particulate processing steps:

$$N_{OL} \cong (6.29 + 31.7P^2 + 0.23N_{np})^{0.5} \tag{4.4}$$

where N_{np} takes into account the number of compression stages, towers, reactors, heat exchangers, furnaces; pumps and vessels are not considered in this calculation.

- Fixed Manufacturing Costs (FMC), or fixed costs of production: they are independent of changes in production rate, and they comprise depreciation, maintenance, local taxes and insurance, rent of land/buildings, plant overhead costs, capital charges.
- General Expenses (GE): these costs comprise management, sales, Research and Development, financing functions, and they usually do not vary with productivity.

Manufacturing and associated costs, as well as revenues, are most often calculated on a year basis (\$/yr), as in this work. However, information provided by a PFD, or the Aspen Plus flowsheet, are reported in terms of mass or molar flowrates (kg/h or kmol/h): thus, the fraction of time that a plant is operating per year must be estimated. All the processes considered in this work are designed for continuous operation, but some planned maintenance are always necessary, thus the plant can not operate 24 h/d, and 365 d/yr; considering that, a typical operating time of 340 d/yr is assumed, and it can be translated into 8160 h/yr.

For most calculations the COM is estimated without the effect of depreciation (COM_d), and it is evaluated through the following correlation (Turton *et al.*, 2018):

$$COM_d = 0.18FCI + 2.73C_{OL} + 1.23(C_{RM} + C_{WT} + C_{UT}) \qquad [\$/\text{yr}] \tag{4.5}$$

where C_{RM}, C_{WT}, and C_{UT}, are the overall (annual) costs related to raw materials, wastewater treatment, and utilities, respectively.

Sometimes, the COM is calculated by assuming that there is an annual capital charge related to the capital investment:

$$COM = COM_d + ACCR \cdot FCI \tag{4.6}$$

where ACCR is the annual capital cost ratio, that is usually assumed to be equal to 0.333, following the rule of thumb "annualised capital costs by dividing by three".

The DMC, FMC and GE are calculated through the following correlations (Turton *et al.*, 2018):

$$COM_d = C_{RM} + C_{WT} + C_{UT} + 1.33C_{OL} + 0.069FCI + 0.03COM \tag{4.7}$$

$$FMC = 0.708C_{OL} + 0.068FCI \tag{4.8}$$

$$GE = 0.177C_{OL} + 0.009FCI + 0.160COM \tag{4.9}$$

4.1.1 Costs of utilities

In this section utilities costs assumptions and calculation procedure are explained in details. Following the results anticipated in table 3.1 of the previous chapter, where user-input data for utilities cost definition in Aspen Plus have been reported, the overall operating expenses related to their employment are reported in table 4.7. An anticipation of such results, presented as the single-utility cost voices, is reported in table 4.4 of this section.

Electricity and energy prices are retrieved from European Commission website (provided by the European Statistical Office, EUROSTAT), and are taken as the EU average in year 2020: an electricity price of 0.0453 $/kWh, and a natural gas price of 0.0142 $/kWh are thus assumed in this work. The cost of electricity is relevant to the generation of refrigerants (ammonia and R-152a utilities), and cooling water, but it also contributes to the cost of low-pressure steam, as explained later, or to the operation of compressors; instead, the price of natural gas influences the cost of high-pressure steam, and it is relevant in MSR and BR to methanol processes, where it is burnt in the furnaces for the reactants pre-heating, and the reforming reactors operation.

The following choices and assumptions are adopted for the calculation of the utilities costs:

- ammonia need to be refrigerated to -25 °C, for which a cooling value of 4.478 kJ/kg is estimated. Ammonia purchase cost is considered as negligible with respect to the electricity cost needed for generating the refrigerated fluid;
- R-152a need to be refrigerated to -50 °C, for which a cooling value of 1.571 kJ/kg is calculated. Refrigeration fluid purchase cost is neglected with respect to the electricity cost needed for generating the refrigerated fluid;

- natural gas heating value is estimated from its net calorific value (47.7 MJ/kg).

Cooling water and steam costs are estimated in a more complicate way; a detailed description is provided in the next paragraphs.

Cooling water cost estimation

In the largest chemical plants cooling water is supplied to the process units from a central facility that consists of one or more cooling towers, make-up water and antifouling chemicals streams, and the cooling water feed pumps, as depicted in figure 4.1. A water make-up is needed to compensate water that is loss by evaporation in the cooling tower, the purge is needed due to the accumulation of inorganic material in the circulating loop; chemicals are introduced to reduce the tendency of the water to foul heat exchanger surfaces within the processes.

Cooling water cost is estimated following the procedure reported in Turton *et al.* (2018), considering that a circulating cooling water stream is produced by using a mechanical draft cooling tower. It is assumed to be supplied at 25 °C and to be returned at 35 °C.

Starting from a calculation basis of 1 GJ/h of energy removal from the process units, the mass flowrate of cooling water needed to remove this energy ($\dot{m}_{cw}$) is obtained by solving the following energy balance:

$$\dot{m}_{cw} c_p \Delta T = 1 \times 10^9 \tag{4.10}$$

where a specific heat capacity of water at the temperature of 30 °C is considered ($c_p = 4180\,\mathrm{J\,kg^{-1}\,K^{-1}}$), and the temperature difference (ΔT) between inlet and outlet conditions of cooling water is of 10 °C; a water mass flowrate of 23923.45 kg/h is thus obtained.

The amount of water evaporated from the tower ($\dot{m}_{tower}$) is calculated as:

$$\dot{m}_{tower} = \frac{HeatLoad}{\Delta H_{vap}} = \frac{1 \times 10^9}{2429.8 \times 10^3} = 411.6\,\mathrm{kg/h} \tag{4.11}$$

by considering the latent heat of vaporization of water (ΔH_{vap}) at the average temperature of 30 °C. The amount of water evaporated represents the 1.72% of the mass flowrate of circulating water. Furthermore, assuming a windage loss of 0.3% from the mechanical draft tower, as in the reference work, water that is lost in the blowdown represents the 0.13% of the total mass flowrate of circulating water: 514.4 kg/h of make-up water are needed.

Power required for cooling water pumps is then calculated, by previously evaluating pressure drops around the cooling water loop (ΔP). The overall pressure drop is calculated as the sum of many contributions:

- pipe losses: 103.4 kPa
- exchanger losses: 34.5 kPa

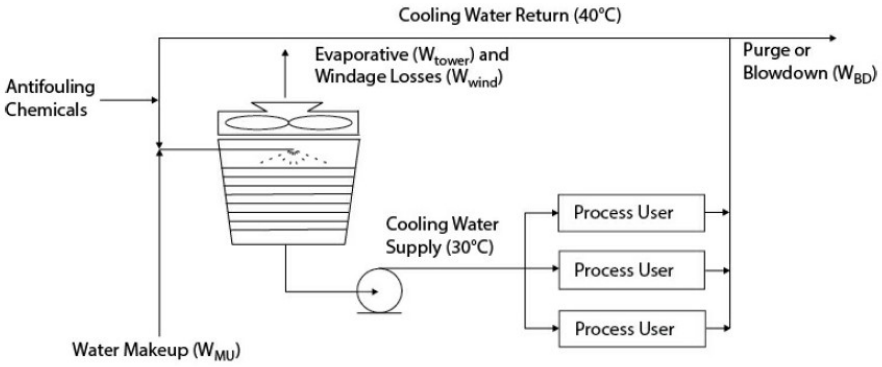

Figure 4.1: Schematic diagram of cooling water loop (Turton *et al.*, 2018)

- control valve loss: 68.9 kPa
- static head due to water pumping to the top of cooling water tower, assumed to be 6 m above the pump inlet: 60.0 kPa

obtaining a final value of 266.8 kPa.

Pump power ($\dot{W}_{pump}$) is calculated as:

$$\dot{W}_{pump} = \frac{1}{\varepsilon}\dot{V}\Delta P = 2.37\,\text{kW} \tag{4.12}$$

by assuming an overall efficiency (ε) of 75%, where $\dot{V}$ is the volumetric flowrate of circulating water. A constant density of water at 30 °C of 996 kg/m^3 is assumed.

The power required for fans is calculated by assuming a surface area needed for the tower (a_{tower}) of 736.27 s m^{-1}, and a fan power per surface (of the tower, K) of 0.3292 kW//m^2:

$$\dot{W}_{fan} = \dot{V}Ka_{tower} = 1.62\,\text{kW} \tag{4.13}$$

The cost of chemicals (C_{ch}) is assumed to be \$0.0347/1000 kg of make-up water, and the cost of process water (C_{pw}) \$0.176/1000 kg (Turton *et al.*, 2018). The overall cost of cooling water (C_{cw}) is obtained as follows:

$$C_{cw} = \frac{1}{\dot{m}_{cw}}[1000C_{el}\cdot(\dot{W}_{pump}+\dot{W}_{fan}) + \dot{m}_{mu}C_{ch} + \dot{m}_{mu}C_{pw}] = 0.012\,\$/\text{t} \tag{4.14}$$

where C_{el} indicates the cost of electricity, as already assumed from EU average price for year 2020, and $\dot{m}_{mu}$ the make-up water flowrate needed.

Steam generation system

Most sites have a pipe network supplying steam at three or more pressure levels for different process uses. A typical steam system is illustrated in figure 4.2

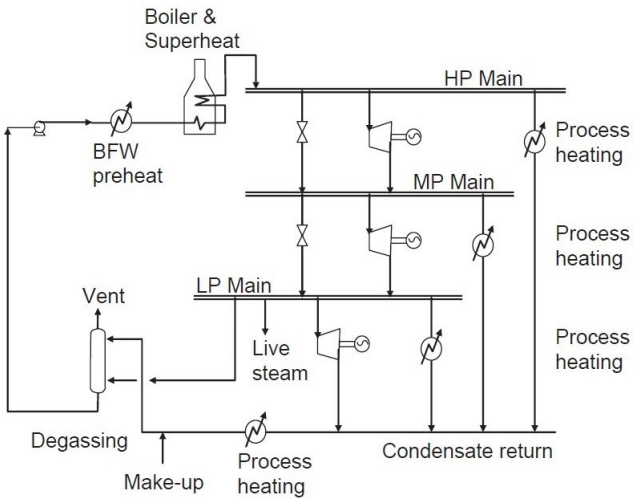

Figure 4.2: Steam system (Towler and Sinnott, 2008)

Boiler feed water is preheated and fed to a boiler, where high-pressure steam is generated and superheated above the dew point to allow for heat losses in the piping. Some of high-pressure steam is used for process heating at high temperatures, while the remainder is expanded either through steam turbines or through let-down valves to form medium-pressure steam. Medium-pressure steam is used for intermediate temperature heating or expanded to form low-pressure steam. Some of low-pressure steam is used for process heating when there are low temperature heat requirements; it can also be expanded in condensing turbines to generate shaft work for process drives or electricity production. When steam is condensed without coming into contact with process fluids, the hot condensate is collected and returned to the boiler feed water system.

The price of high-pressure steam (P_{hps}) can be estimated from the cost of boiler feed water treatment (P_{bfw}), the price of fuel (P_F), and the boiler efficiency η_B (Towler and Sinnott, 2008):

$$P_{hps} = P_F \cdot \frac{dH_b}{\eta_B} + P_{bfw} \tag{4.15}$$

where typical boiler efficiencies range between 0.8 and 0.9, and dH_b is the heating rate that takes into consideration the boiler feed water preheat, the latent heat of vaporization, and the superheat specified.

The prices of medium- and low-pressure steam are usually discounted from the high-pressure steam price, to allow for the shaft work credit that can be gained by expanding the steam through a turbine. Shaft work is priced as equivalent to electricity, thus the value of the shaft work sets the discount between steam at different levels. The procedure followed in price calculations of the three levels of steam is that of Towler and Sinnott (2008).

In this work, the steam conditions reported in table 4.2 are chosen. The superheat temperatures are set to give an adequate margin above the saturation temperature for the high-pressure steam, and also to roughly give the same specific entropy for each steam level; anyway, the actual superheat temperatures of the medium- and low-pressure steam would be higher, due to

the nonisentropic nature of the expansion (a turbine efficiency of 85% is assumed).

Table 4.2: Physical properties for the three steam levels considered in this work

Steam level	High-pressure	Medium-pressure	Low-pressure
Temperature (°C)	260	200	125
Pressure (bar)	46.923	15.549	2.3223
Heating value ($kJ\,kg^{-1}$)	1469.9	1743.7	2009.5
Superheat temperature (°C)	545	350	126
Specific entropy ($kJ\,kg^{-1}\,K^{-1}$)	7.0839	7.0863	7.0887
Specific enthalpy ($kJ\,kg^{-1}$)	3528.2	3146.9	2714.5

The difference in enthalpy between levels, assuming an isoentropic expansion, is as follows:

Isoentropic enthalpy difference (kJ/kg)	381.25	432.46

The actual enthalpy difference is obtained by taking into account the steam turbine efficiency:

Actual enthalpy difference (kJ/kg)	324.06	367.59

The shaft work credit is then obtained by multiplying the enthalpy variation by the electricity price:

Shaft work credit ($/t)	4.0818	4.6301

These values represent the discount that is considered in the estimation of the costs of medium- and low-pressure steams, with respect to the high-pressure steam price that is calculated from equation (4.15); it is assumed that boiler feed water cost is canceled out by a condensate credit coming from the steam generation system. Final costs obtained for the three levels of steam are:

Steam price ($/t)	20.413	16.331	11.701

Steam for turbines

Typically, when compression power needed is above 150 kW, steam is used as a drive for compressors, instead of using electricity. This is the case of multi-stage compressors in the MSR to methanol, BR to methanol, and biomass steam gasification to methanol process.

Following the procedure reported in Turton *et al.* (2018), a 11 bar steam with exhaust at 1 bar is assumed to be used for steam-driven turbines. From table 4.3 a steam requirement of 8.79 kg of steam per kW h of power is obtained, while from figure 4.3 the steam turbine efficiency (η_s) is evaluated case-by-case considering the shaft power of the compressor ($\dot{W}_s$). Steam flowrate required by the drive ($\dot{m}_{sd}$) is then calculated as:

$$\dot{m}_{sd} = \dot{W}_s \frac{8.79}{\eta_s} \tag{4.16}$$

Table 4.3: Theoretical steam requirements (kg/kWh), readapted from Turton *et al.* (2018). (sat.: saturated)

Inlet steam pressure (bar)	11.0	14.8	18.2	28.6	42.4	42.4	59.6	59.6
Superheat in °C	(sat.)	(sat.)	50	170	145	185	165	205
Exhaust pressure								
1 bar	8.79	7.94	6.88	5.08	4.72	4.45	4.22	4.00
1.69 bar	10.87	9.57	8.11	5.77	5.28	4.97	4.67	4.40
3.07 bar	15.24	12.72	10.40	6.91	6.18	5.78	5.35	5.02
4.45 bar	20.86	16.32	12.79	7.97	6.97	6.49	5.93	5.54
5.14 bar	24.45	18.32	14.11	8.50	7.34	6.83	6.20	5.78
5.82 bar	28.80	20.68	15.47	9.05	7.71	7.16	6.45	6.01

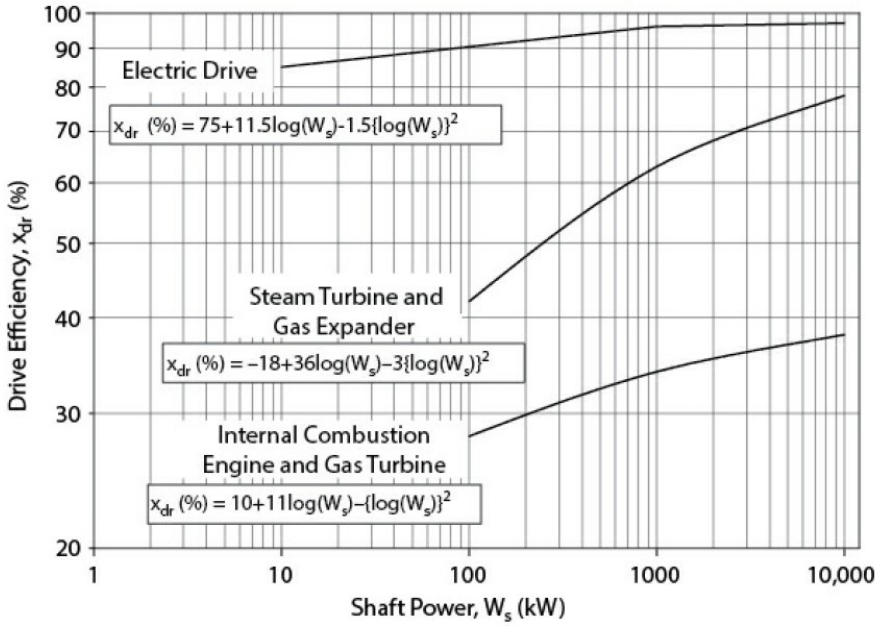

Figure 4.3: Efficiencies for pumps and compressor drives (Turton *et al.*, 2018)

Results summary

Resulting costs of utilities for each process are summarized in table 4.4, where they are divided into hot and cold utilities; the generic term refrigerant refers to ammonia and R-152a, with the latter that is used only in biomass steam gasification to methanol process. The total cost percent of savings is presented for both hot and cold utilities, separately. Cooling water costs comprise also the amount needed for inter-stage cooling in multi-stage compressors.

There are no extra electricity costs in MSR and BR to methanol processes, as well as biomass to methanol, than those needed for generating the utilities; instead, for the two CO_2 hydrogenation processes, there are electricity costs related to compressors, electrolysis units, and DAC process. They are reported in a separate table (4.5), along with costs associated to the steam needed for driving turbines (where steam is used instead of electricity for compressors), and boiler feed water cost for cooling the methanol synthesis reactor. Steam needed for turbines is a 11 bar saturated steam, which cost, reported in Turton *et al.* (2018), is 56 \$/t; boiler feed water price is equal to 0.529 \$/t, and it has been retrieved from Seider *et al.* (2017).

Table 4.4: Utilities annual cost summary, making a comparison before and after heat integration for the five methanol production processes. (NG: natural gas, LPS: low-pressure steam, HPS: high-pressure steam, Ref.: refrigerant, RW: refrigerated water, CW: cooling water, Tot.: sum of hot/cold utilities)

Hot utilities	Final cost (M$/yr)				Cost before heat integration (M$/yr)				Total cost percent
	NG	LPS	HPS	Tot.	NG	LPS	HPS	Tot.	of savings (%)
MSR to methanol	4.6819	0.4286	2.8759	7.9864	7.5719	1.3343	5.5227	14.4289	44.65
BR to methanol	4.8009	0.2461	0.0000	5.0470	7.9781	1.5137	3.6297	13.122	61.54
Biomass to methanol	7.9823	0.0000	6.9447	14.927	7.9823	1.4321	14.647	24.061	37.96
CO_2 hydrogenation (AW el.)	3.1525	0.0000	0.8082	3.9606	3.1525	0.9723	1.9010	6.0256	34.27
CO_2 hydrogenation (PEM el.)	3.1525	0.0000	2.3384	5.4908	3.1525	0.9723	1.9010	6.0255	8.87
Cold utilities	**Final cost (M$/yr)**				**Cost before heat integration (M$/yr)**				**Total cost percent**
	Ref.	RW	CW	Tot.	Ref.	RW	CW	Tot.	of savings (%)
MSR to methanol	0.1154	-	0.3509	0.4664	0.1154	-	0.6650	0.7804	40.24
BR to methanol	0.2278	-	0.2898	0.5176	0.2278	-	0.4711	0.7045	25.94
Biomass to methanol	0.0423	0.0000	0.5969	0.6392	0.2124	17.065	0.4361	17.713	96.39
CO_2 hydrogenation (AW el.)	0.4938	-	0.3368	0.8307	0.4938	-	0.6559	1.1497	27.75
CO_2 hydrogenation (PEM el.)	0.4277	-	0.1349	0.5626	0.4938	-	0.6396	1.1334	50.36

Table 4.5: Utilities cost summary accounted for non-simulated process units (M$/yr)

	MSR to methanol	BR to methanol	Biomass to methanol	CO_2 hydrogenation	
				AW el.	PEM el.
Electricity	-	-	-	54.527	57.080
Steam for turbines	12.490	7.6366	12.534	-	-
Boiler feed water	0.0584	0.0590	0.0652	0.0386	0.0386

4.1.2 Utility cost savings by further heat recovery

In this section the possibility of recovering more heat than that obtained following heat integration, is investigated from an economic point of view. Results are reported in table 4.6, in terms of natural gas or steam cost savings, depending on the process considered: in the case of utility cost resulting in a negative number, the negative part may be considered as a credit for other potential revenues, coming from the possibility of generating electricity to sustain the plant requirements, and, possibly, to be fed into the grid. However, in this analysis it is considered as zero-cost.

Boiler feed water

As already mentioned in chapter 2, a Lurgi-type nearly isothermal reactor is considered for methanol synthesis. Considering that, overall, methanol synthesis is an exothermic process, heat is needed to be removed in order to keep isothermic conditions: the cooling media commonly used is represented by boiler feed water, that exits as steam. This steam can be recovered for the utilization in the process and, following the procedure reported in Seider *et al.* (2017), its value is calculated.

Methanol synthesis is carried out at 252 °C and 75 bar, and heat that must be transferred out of the reactor varies depending on the process considered.

To ensure nucleate boiling of the boiler feed water, an overall driving force of 25 °C is assumed (ΔT)). Thus, boiler feed water will be converted to steam at (252-25)=227 °C: this corresponds to a saturation pressure of 26.49 bar; assuming that the boiler feed water enters the heat exchanger as a liquid at 30 °C, and exits as saturated vapor 227 °C, the change in enthalpy (vaporization enthalpy variation, ΔH_{vap}) is calculated as:

$$\Delta H_{vap} = \Delta H_v^{sat}(227°\text{C}) - \Delta H_l^{sat}(30°\text{C}) = 2802.4 - 125.74 = 2676.66 \text{ kJ/kg} \tag{4.17}$$

where ΔH_v^{sat} and ΔH_v^{sat} are the specific enthalpies of the saturated vapor and saturated liquid, respectively.

From an energy balance, steam produced from the boiler feed water ($\dot{m}_{s,bfw}$) can be obtained from methanol synthesis reactor duty ($\dot{Q}_r$) as:

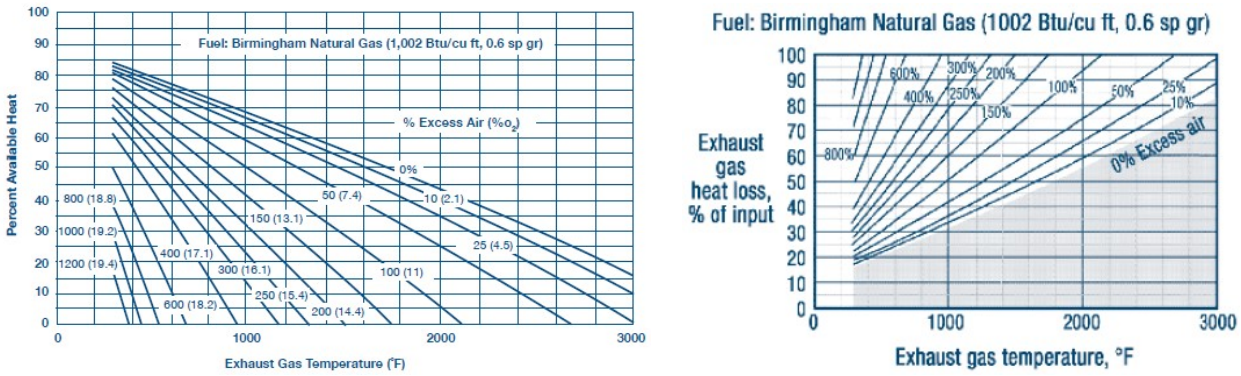

(a) *Percent of available heat (% of input)* **(b)** *Percent of heat loss (% of input)*

Figure 4.4: Typical values of heat recoverable from furnace exhaust gases, considering the exit temperature (from U.S. Department of Energy)

$$\dot{m}_{s,bfw} = \frac{\dot{Q}_r}{\Delta H_{vap}} \tag{4.18}$$

Steam cost credit guaranteed by employing elsewhere in the process the steam generated from boiler feed water, can be calculated on an time basis, assuming a value of 16.331 \$/t, as found in section for a medium-pressure steam. Since steam is not needed to drive turbines for compression in CO_2 hydrogenation (electric drives are employed), steam cost savings are reported as generic steam cost credits.

Furnace waste heat recovery

The thermal efficiency of a heating system can be improved significantly by recovering the heat contained in furnace flue gases. In this work, furnaces are employed in MSR to methanol and BR to methanol processes, and the fired heat is provided by burning NG. In the first process, the exhaust gas is considered to leave the furnace at 960 °C, as reported in Felder and Rousseau (2005); in BR to methanol process, since the furnace temperature needed is lower, an exit temperature of 760 °C is estimated. From tables reported in figure 4.4, considering the exhaust gas exit temperatures for the 2 processes, 55% e 64% of available heat can be obtained for MSR and BR to methanol processes, respectively.

The amount of energy savings obtained by recovering furnace waste heat is higher than the amount of actual heat that can be transferred to a process stream, for example. The net heat delivered has to take into account the efficiency of the furnace, that is typically ranged between 80% and 90%, in this work assumed to be 85% ($\eta_{furnace}$).

The energy savings are translated into natural gas cost credits, calculated from the available heat in the flue gas ($\dot{Q}_{waste}$), obtained as percent of the reformer duty (55% for MSR to methanol, and 64% for BR to methanol):

$$\text{NG cost credit} = C_{ng}\frac{\dot{Q}_{waste}}{LHV \cdot \eta_{furnace}} \tag{4.19}$$

where C_{NG} and LHV_{NG} are the cost and the lower heating value of natural gas, respectively.

Natural gas price is expressed on a mass basis (164.83 \$/t), and LHV of natural gas is reported as 47.7 MJ/kg in Modesti (2021).

Purge fuel valorization

Purge streams are present in three of the five processes presented in this work: MSR to methanol, BR to methanol, and biomass steam gasification to methanol. As reported in table 3.16, purge gases have quite high heating values, so that the use in the process, in substitution to natural gas, is feasible.

Heat recovered from the combustion of purge fuel is considered, as well as furnace waste heat, a credit for total natural gas cost calculation. In this case the NG cost credit is calculated from the LHV of the purge stream, and a furnace efficiency of 85% ($\eta_{furnace}$) is considered, accordingly to previous assumptions:

$$\text{NG cost credit} = C_{NG}\frac{\dot{Q}_{purge}}{LHV_{NG} \cdot \eta_{furnace}} = C_{NG}\frac{\dot{m}_{purge} \cdot LHV_{purge}}{LHV_{NG} \cdot \eta_{furnace}} \tag{4.20}$$

where C_{NG} and LHV_{NG} are the cost and the lower heating value of natural gas, respectively.

Results summary

Considering the results reported in table 4.6, a huge reduction in the cost of utilities can be noticed for MSR and BR to methanol processes, with the latter that is almost energetically auto-sufficient: this is mainly due to the heat recovered by the furnace waste heat, that can be employed in the so-called "waste heat boilers" for steam generation. In the biomass to methanol process the main contribution to cost savings can be attributed to valorization of purge: its LHV is comparable to that of BR to methanol process but the mass flowrate is significantly larger, considering that the R/F ratio is quite high (4.79).

Instead, for CO_2 hydrogenation processes just steam produced by boiler feed water contributes to the further cost reduction, and considering that there is no need to drive turbines with steam, a generic steam credit is considered.

4.1.3 Economic results assessment and discussion

Starting from the assumptions provided in the initial part of this section about capital costs and manufacturing costs, considering the Aspen Plus flowsheet, the need of integrating some other capital costs emerged from the definition of the problem boundaries. The non-simulated

Table 4.6: Utility cost savings by the further heat recovery provided by steam generation from boiler feed water, furnace waste heat, and purge valorization (M$/yr). fwhr: furnace waste heat recovery, pv: purge valorization.

	MSR to methanol	BR to methanol	Biomass to methanol	CO_2 hydrogenation	
				AW el.	PEM el.
Costs before further heat recovery					
Steam for turbines	12.490	7.6366	12.534	0	0
Natural gas	4.6819	4.801	7.9823	3.1525	3.1525
Total cost of utilities	21.001	13.260	28.165	59.357	63.172
Cost savings					
Steam for turbines	10.445	7.6203	2.0106	0.4546	0.4548
Natural gas (fwhr)	1.9282	1.6880	0.0000	0.0000	0.0000
Natural gas (pv)	6.9281	3.8625	20.870	0.0000	0.0000
Final costs/credits					
Steam for turbines cost	2.0454	0.0163	10.523	0.0000	0.0000
Steam credit	-	-	-	0.4546	0.4548
Natural gas cost	0.0000	0.0000	0.0000	0.0000	0.0000
Natural gas credit	5.3505	2.9129	2000.3	-	-
Final cost of utilities after the overall heat recovery					
Total cost of utilities	1.6889	0.0895	5.2849	58.903	62.718
Cost savings	19.301	13.171	22.880	0.4546	0.4548
Cost savings (%)	91.90	99.33	81.42	0.77	0.72

part is clear in BFDs of the processes (figure 2.7 and 2.10). In particular, the following capital investments are needed to be integrated for the following processes:

- biomass to methanol: the gasification reactor cost, assumed as a pyrolysis furnace, contributes to ISBL. Starting from its duty, roughly estimated considering the heat of reaction, a contribution of M$ 7.911 to capital costs is obtained. Gasifier duty is estimated starting from the following considerations: heat of reaction represents the heat lost or gained during the chemical reactions occurring in the gasifier, that are typically endothermic in the case of steam gasification. Considering an overall gasification reaction, where 1 mol of biomass (with a generic atomic composition $C_aH_bO_c$) is gasified with α moles of steam and β moles of oxygen:

$$\begin{aligned} C_aH_bO_c + \alpha\, H_2O + \beta\, O_2 = & A' \cdot H_2 + B' \cdot CO + C' \cdot CO_2 + \\ & D' \cdot CH_4 + E' \cdot C_2H_4 + F' \cdot C_2H_6 + G' \cdot C_3H_8 + Q \end{aligned} \quad (4.21)$$

  Oxygen contribution is neglected in this work, because it was not considered as a gasification agent in the reactor. The heat of reaction, indicated as Q, for the overall gasification reaction (4.21) may be found as the difference between the heat of formation of products and reactants.

  Heat of formation of any product is calculated from the standard heat of formation (defined at 25 °C, or 298 K), by accounting for a temperature increase or decrease through the use of specific heats, as:

$$\Delta H_T^0 = \Delta H_{298\ \mathrm{K}}^0 + \sum \left(\int_{298\ \mathrm{K}}^{T} A' C_{p,i} dT \right)_{product} - \sum \left(\int_{298\ \mathrm{K}}^{T} \alpha C_{p,i} dT \right)_{reactant} \quad (4.22)$$

  where the superscript 0 indicates that the heat of formation is computed at the standard temperature of 25 °C and T stands for a generic temperature (850 °C in the case of the gasifier considered for this work). $C_{p,i}$ is the specific heat of substance i at temperature T and A', ... , β are the stoichiometric coefficients of the products and the reactants, respectively.

  Heat of reaction is finally estimated as 66.938 MW, confirming the endothermic behavior of the overall gasification reaction.

- CO_2 hydrogenation (AW electrolysis): Buttler and Spliethoff (2018) reported an investment cost of AW electrolizer that is ranged between 800 and 1500 €/kW; Keith *et al.* (2018) indicated for DAC process an investment cost per unit capacity of M$ 697.7 per Mt of CO_2 captured. Considering that in this work DAC plant is considered to capture

0.1526 Mt of CO_2 per year, the authors suggest, for the cost scaling, to account for extra $\sim 80\%$ capital costs per unit of capacity. In this work 142.101 MW of power are needed for AW electrolysis, thus a capital investment of M$ 113.7 is required, assuming a specific cost of 800 €/kW, translated into 913.76 $/kW considering the average change between $ and € for year 2020 (from European Central Bank, 1.142 $/€);

- CO_2 hydrogenation (PEM electrolysis): Buttler and Spliethoff (2018) reported an investment cost of PEM electrolizer that is ranged between 1400 and 2100 €/kW. Same considerations as before, can be made for DAC process. In this work 149.925 MW of power are needed for PEM electrolysis operation, thus a capital investment of M$ 239.7 is required, assuming a specific cost of 1500 €/kW, translated into 1599.1 $/kW.

The cost of land and buildings is considered as a capital cost, and estimated as 2% of ISBL+OSBL.

To conclude the economic analysis of a process, it is essential to evaluate the possible incomes deriving from the selling of products: in this work, a selling value of 337.25 $/t has been assumed for methanol, as the non-discounted average price for 2020 provided by Methanex Corporation, the world's largest methanol producer and supplier. Furthermore, in the production of hydrogen through water electrolysis, also oxygen leaving the electrolizer must be accounted and valorized: some of it is considered to be employed in DAC process, the remaining is assumed to be sold, considering a value of 54 $/t, as reported in Pérez-Fortes and Tzimas (2016). Oxygen needed for DAC process is 2106.55 kg/h, while about 18610 kg/h are obtained via electrolysis, both from AW and PEM technologies. Thus, revenues for the CO_2 hydrogenation processes include also the selling of oxygen, while for the other three processes revenues derive entirely by the value of methanol, and its productivity.

The overall economic analysis results for the five processes are reported in table 4.7, where the cost of electrolysis and DAC process units are reported under the "Reactors" voice in the equiment purchase costs.

From the results analysis it can be noticed that the CO_2 hydrogenation processes are characterized by the highest capital costs, related to electrolizers and DAC process, as well as the highest manufacturing costs due to electricity expenses, needed to operate electrolysis units; however, revenues are slightly higher compared to the other processes, because of incomes derived by selling oxygen.

MSR, BR and biomass to methanol processes are comparable from the capital investment point of view, but very important differences are related to manufacturing costs: in particular, cost of raw materials for biomass steam gasification to methanol process is very high; this fact is due to the very high amount needed to generate the syngas necessary for the desired methanol productivity. Furthermore, biomass to methanol process is affected also by a higher cost of utilities, compared to the other two processes, considered the worse performances in terms of energy savings, after the heat integration.

[1]FCI minus the cost of land

Table 4.7: Economic analysis results for the five processes

	MSR to methanol	BR to methanol	Biomass to methanol	CO_2 hydrogenation	
				AW el.	PEM el.
Equipment purchase costs (M$)					
Reactors	5.0934	4.0362	7.9838	305.44	431.50
Compressor	3.9456	1.6548	3.3870	3.6439	3.2058
Pumps	0.0153	0.1613	0.0000	0.0000	0.0000
Flash vessels	0.0630	0.0797	0.1446	0.0320	0.0321
Heat exchangers	5.9079	7.3179	3.1593	2.0563	1.6592
Columns	0.5642	0.3575	0.3842	0.3514	0.3517
Capital investment (M$)					
ISBL	15.589	13.607	15.059	311.52	436.75
OSBL	3.1189	2.7215	3.0117	62.304	87.349
Indirect costs	3.2658	3.6141	4.0026	74.764	104.82
FCI	22.449	19.595	21.686	448.59	628.91
WC	1.8707	1.6329	1.8071	37.382	52.410
StC	1.7959	1.5676	1.7348	35.887	50.313
TCI	26.115	22.795	25.227	521.86	731.64
Cost of manufacturing (M$/yr)					
Cost of operating labour	0.8100	0.9546	0.8720	0.8815	0.8815
Cost of raw materials	11.861	0.1626	23.395	0.0338	0.0384
Cost of utilities	1.6889	0.0895	5.2849	58.903	62.718
COM_d	22.919	6.4444	41.560	155.64	192.80
COM	32.738	12.975	48.788	305.16	402.42
DMC	18.834	3.2640	32.800	95.731	113.11
FMC	5.0446	3.9677	4.2604	75.987	106.28
GE	5.5835	1.3764	6.9991	29.096	36.664
Revenues (M$/yr)	33.800	33.773	33.771	41.015	41.033
Cost of Land (M$)	0.1871	0.3266	0.3614	7.4764	10.482
FCI_L (M$)[1]	22.262	19.268	21.323	441.11	618.43

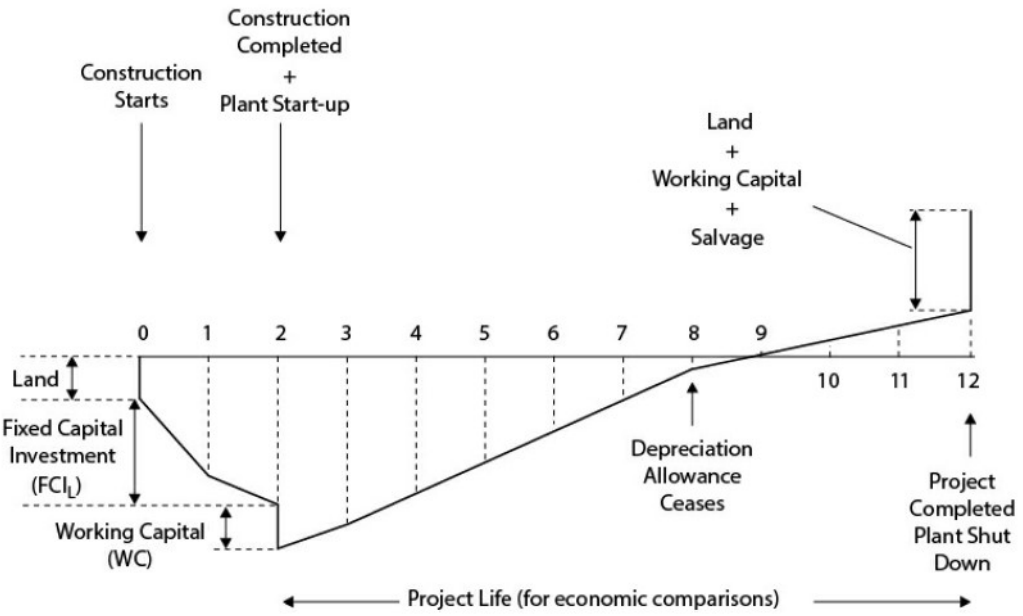

Figure 4.5: A typical cumulative cash flow diagram for the evaluation of a new project (Turton *et al.*, 2018)

4.2 Profitability analysis

The economic analysis carried out in the previous section is used to assess the profitability of the projects, involving both capital costs and yearly manufacturing costs. A project for each one of the five processes is evaluated, all based on the same assumptions reported in the previous section.

Typically, results of profitability analysis for a new project are presented through a cumulative, after-tax, cash flow diagram (CFD); an example of CFD is illustrated in figure 4.5. Different phases can be individuated in a diagram like that:

- time of construction: after the decision to build a new chemical plant is taken, the construction phase starts. It may take from 6 months to 3 years to complete. In the example 2 years are considered, as well as in this work;
- at the end of the previous phase, the capital outlay reaches a maximum that represents the fixed capital expenditures needed to purchase and install the equipment;
- at the end of the second year, when the construction has completed and the plant is started, the working capital expenditure is needed for the first few months of operation. This represents a one-time expense at the startup of the plant and will be recovered at the end of the project;
- after start-up, finished products for sale starts to be obtained, and the yearly cash flows should become positive, as well as the slope of the cumulative CFD curve;
- the cash flow is larger in the first 6 years where depreciation allowances have effect. In the example such a time is considered, but it may vary depending on regulations, and on

the method of depreciation used;

- a plant life of 10 years is considered in the example, while in this work it is established as 15 years. The same plant life is chosen among all the processes, in order to make a comparative assessment of the results;
- at the end of life, the plant is closed down and the cost of land, the working capital, and the possible salvage are recovered.

Some assumptions are needed to build the CFDs for the five processes considered:

- the capital investment for the first year of the construction phase is assumed to be the 60% of FCI;
- the capital investment for the second year of the construction phase is assumed to be the 40% of FCI;
- an interest rate of 10% is assumed for the annualised cash flow calculation;
- a taxation rate of 30% is assumed to calculate the after tax profit;
- a straight-line 6-years depreciation method is considered;
- a discount rate of 5% is considered.

Once CFD curves are obtained, profitability is evaluated through three indices, build-up on different bases: time, cash and interest rate. These indices are defined as follows (Turton *et al.*, 2018):

- Discounted Payback Period (DPBP): time required, after the start-up to recover the FCI and the StC, with all the cash flows discounted back to time zero. The project with the shortest DPBP is the most desirable;
- discounted cumulative cash position or Net Present Value (NPV): cumulative cash position at the end of the project life, with all the cash flows discounted back to time zero. The NPV is largely influenced by the level of FCI, thus a better criterion for the comparison of different projects, with very different investment costs, as in this work, may be the Present Value Ratio (PVR):

$$PVR = \frac{\text{Present value of all positive cash flows}}{\text{Present value of all negative cash flows}} \tag{4.23}$$

  A PVR of unity represents a break-even situation for a project: values greater than one indicate a process as profitable, while values lower represents unprofitable projects.

- discounted cash flow rate of return or Internal Rate of Return (IRR): interest rate at which all the cash flows must be discounted in order for the net present value of the project to be equal to zero. It is the measure of the maximum interest rate that the project could pay and still break even by the end of the project life.

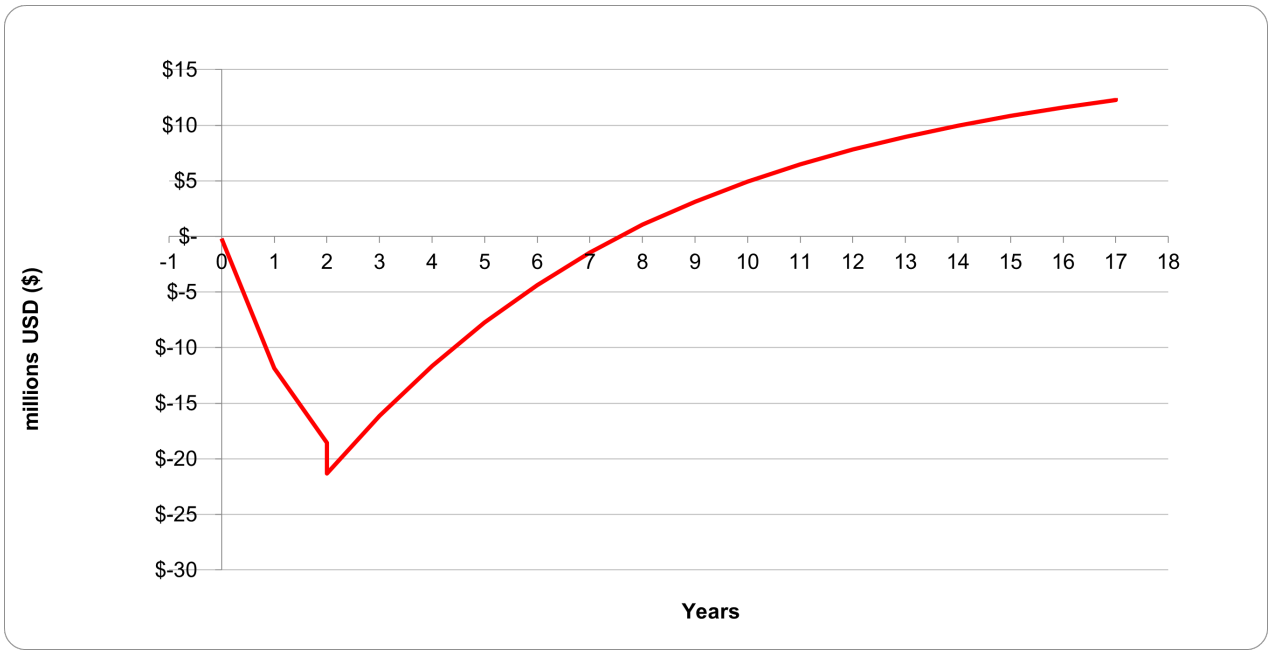

Figure 4.6: CFD for the MSR to methanol process

4.2.1 Profitability analysis assessment and discussion

Profitability analysis results for the MSR to methanol process, represented in figure 4.6, show the expected trend of the cumulative cash flow curve, considering that this is the process currently used in industry for methanol production. Furthermore, the calculation of the indices confirm the process as profitable: DPBP is 6.79 years, the NPV is M$ 12.431, and the IRR has been estimated as 19.66%.

As regards BR to methanol process, which CFD is depicted in figure 4.7 in comparison to the one of MSR to methanol, results of profitability show a better performance with respect to the standard methanol production route; DPBP is calculated as 3.34 years, NPV is M$ 66.415, and the IRR has been estimated as 56.21%. The main reason is the large difference between the price of raw materials, as previously presented in table 4.1.

Confirming the profitability of MSR and BR to methanol processes, a PVR larger than one has been calculated for both of them, with values of 1.58 and 4.54, respectively.

Biomass to methanol cumulative cash flow curve (figure 4.8) is stopped at the beginning of year 3, considering that total manufacturing costs are larger than revenues (M$ 48.788 vs 33.770, see table 4.7). At this point the initial investment of M$ 20.783 is no more recoverable, and the process is not profitable at the common methanol selling price: a reduction in the operating costs should be needed, otherwise methanol value needs to be increased. A negative PVR is obtained as -1.30.

For the two CO_2 hydrogenation processes the same considerations can be made, by looking at figures 4.9 and 4.10. The non-profitability is evident by comparing the total manufacturing costs and the revenues for each one of the two processes, and then by calculating the PVR ratio. Results obtained are as follows:

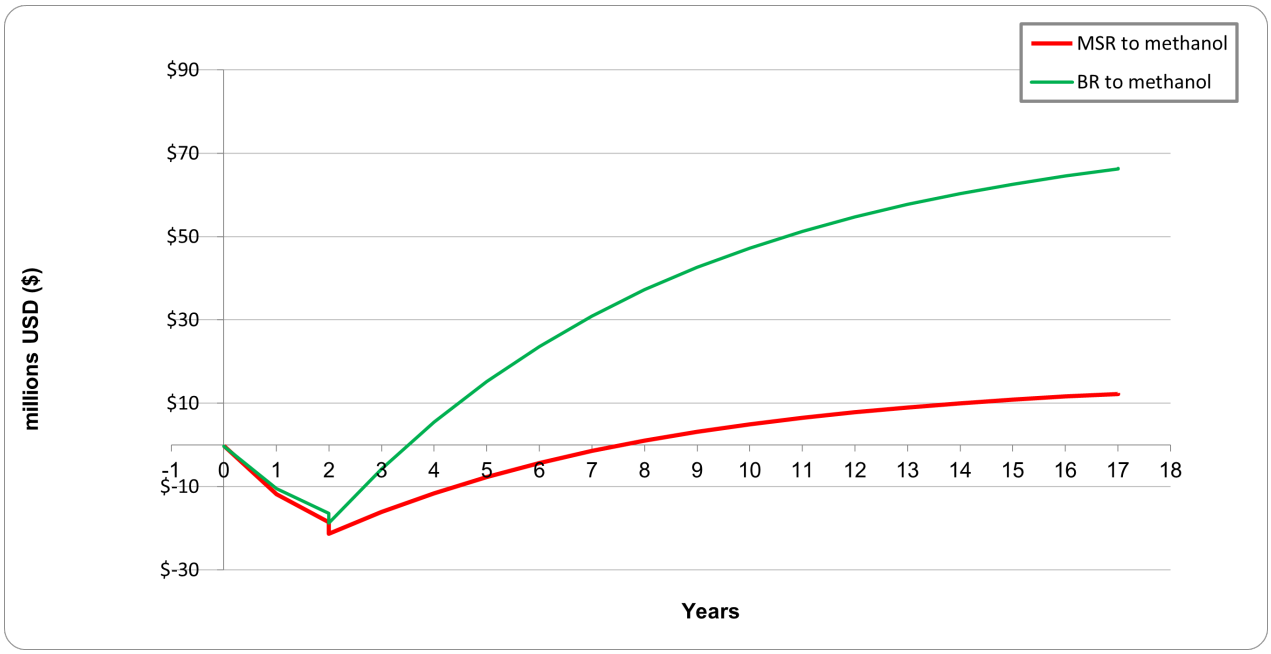

Figure 4.7: CFD for the BR to methanol process, compared to CFD of MSR to methanol process

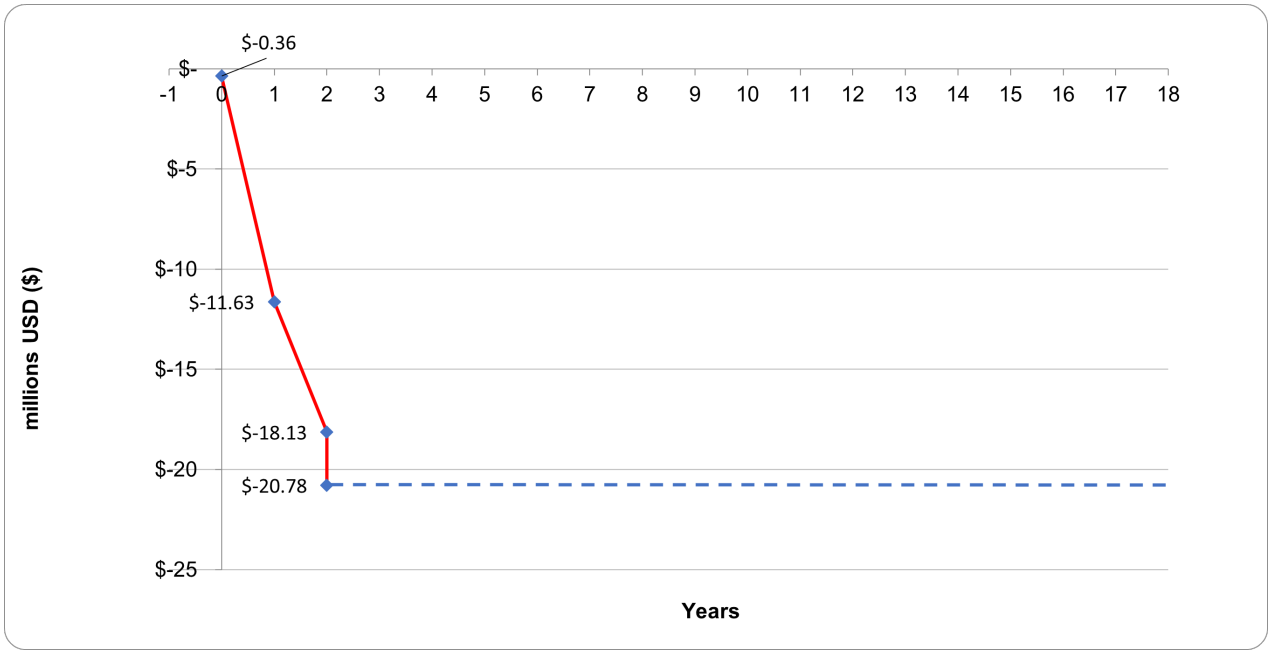

Figure 4.8: Cumulative CFD for the biomass to methanol process

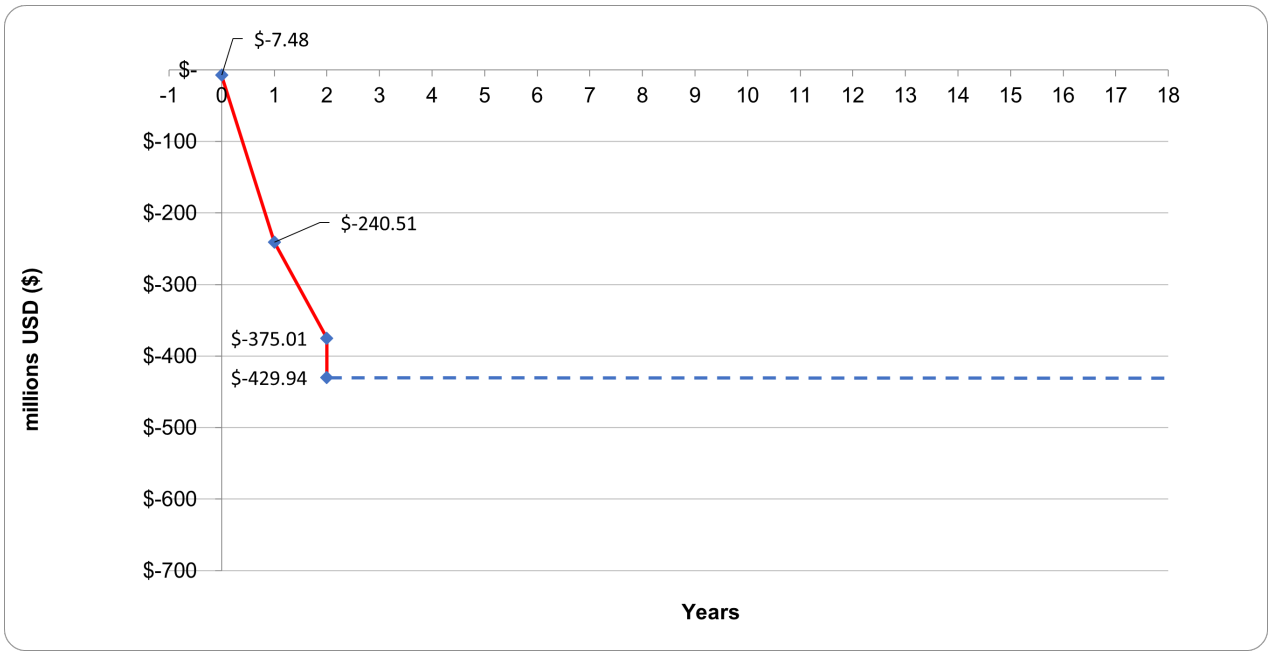

Figure 4.9: Cumulative CFD for the CO_2 hydrogenation process (AW electrolysis)

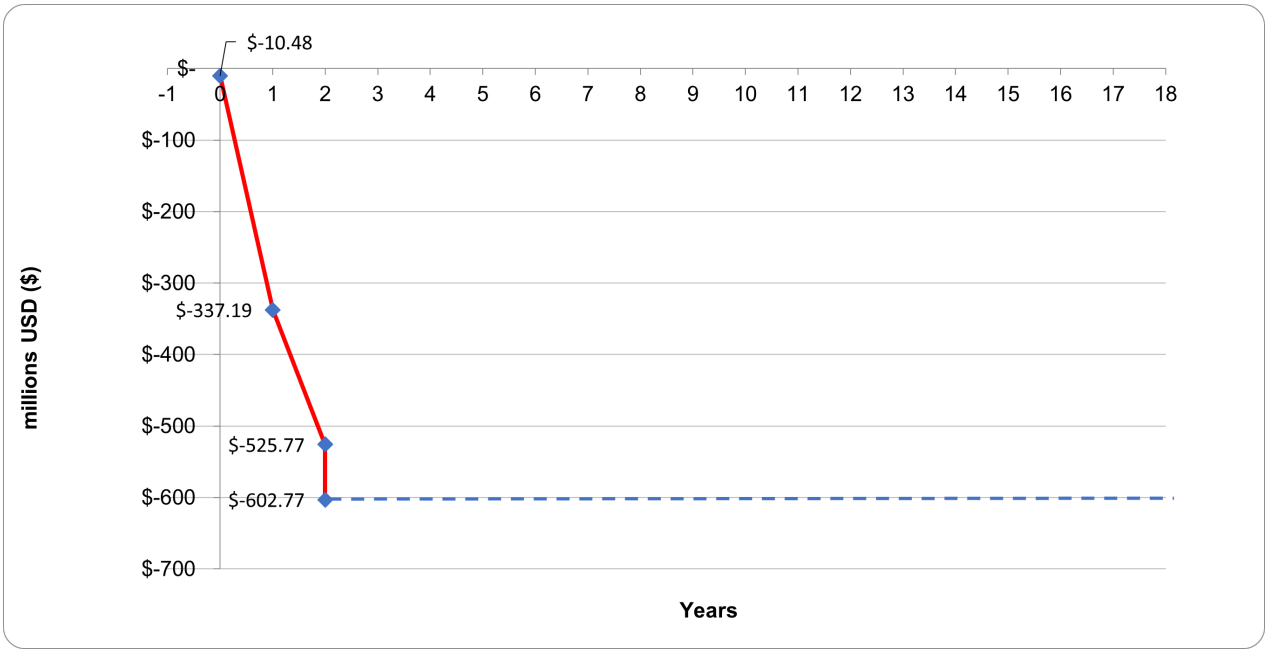

Figure 4.10: Cumulative CFD for the CO_2 hydrogenation process (PEM electrolysis)

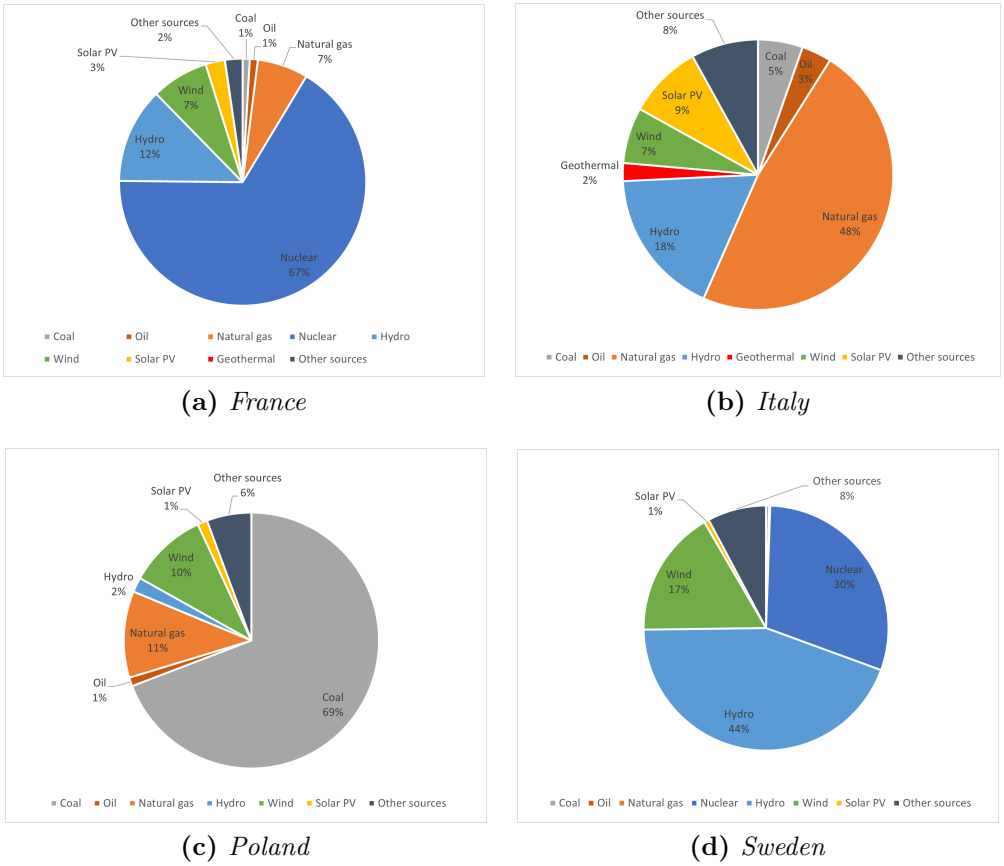

(a) *France* **(b)** *Italy*

(c) *Poland* **(d)** *Sweden*

Figure 4.11: Electricity generation by source for year 2020 (readapted from IEA)

- CO_2 hydrogenation process (AW electrolysis): M$ 305.16 vs 41.015, with a PVR of -0.59. The initial investment of M$ 429.938 can not be recovered under these conditions.
- CO_2 hydrogenation process (PEM electrolysis): M$ 402.42 vs 41.033, with a PVR of -0.54. The initial investment of M$ 602.769 can not be recovered, as well.

4.3 Carbon impact assessment

In this section the "environmental impact" of the five processes is assessed and compared between them, by considering the net GHGs emissions within the considered boundaries; both the direct (process-related) and the indirect (i.e., energy-related) emissions are taken into consideration, and results are expressed in CO_2-equivalents (CO_2e), normalized on a unitary amount of methanol produced. Four case studies are considered, looking at Europe and at the different energetic mix of member countries: based on these criteria, the choice fell on France, Italy, Poland, and Sweden.

4.3.1 Energy mix of the four case studies

Among the four countries chosen for this study, it is noticeable the different quote of renewable electricity generation that characterizes each of them: in figure 4.11 the electricity generation

Table 4.8: Share of renewables, low-carbon sources and fossil fuels in power generation for year 2020 (readapted from IEA)

				Low-carbon sources	
	Gas (%)	Oil (%)	Coal (%)	Renewables (%)	Others (%)
France	6.642	1.055	0.930	89.08	2.295
Italy	47.65	3.580	5.362	35.40	8.034
Poland	10.94	1.107	69.20	13.10	5.657
Sweden	0.059	0.086	0.402	91.69	7.765

share by source is depicted. Data are retrieved from IEA, and are summarized in table 4.8.

Obviously, considering such different mixes, electricity generation-related GHG emissions are estimated to be very different. Following data are reported by the European Environment Agency (EEA) for each country, France generates 60 g of CO_2e/kW h, Italy 216 gCO_2e/kWh, Poland 710 gCO_2e/kWh, and Sweden 8 gCO_2e/kWh.

4.3.2 Process-related carbon emissions

In the five processes considered, two chemical species can be identified as GHGs: methane and carbon dioxide. Since the necessity of presenting data under an unique index, the CO_2e unit is commonly used: it is based on the Global Warming Potential (GWP) that is associated to species that are labeled as GHGs: a GWP of 25 is estimated for CH_4 for a 100-year time horizon as indicated in IPCC (2007), so that a 1 kg of methane emitted to the atmosphere is equivalent to 25 kg of CO_2.

Process-related carbon emissions are distinguished between direct and indirect in this work, considering the following rationale:

- direct emissions are related to streams entering and exiting the process. In general GHGs present in the feed of the process are considered to be subtracted to the environment, thus its contribution in the calculation of direct emissions is negative. However, for MSR to methanol process, the contribution of methane entering the process is not accounted as negative, considering that it is fossil-based; with regard to BR and biomass to methanol processes, CH_4 is not accounted as well, since methane is generated through anaerobic digestion, thus it is not subtracted to atmosphere directly. Direct emissions are thus calculated as net values, considering the following general formulation:

$$\begin{aligned} \text{net direct } CO_2e \text{ emissions} &= (CO_2e)^{out} - (CO_2e)^{in} \\ &= (CO_2e)^{products} + (CO_2e)^{purge} - (CO_2e)^{feed} \end{aligned} \tag{4.24}$$

  Calculation results are reported in table 4.9.

Table 4.9: Net direct carbon emissions related to the streams entering and exiting the processes, normalized to the unit of methanol produced (tCO_2e/tCH_3OH). Feed is represented as a single voice even if there are 2 feeds in four of five processes: only methane, biogas, gasification products, and CO_2 contributes to carbon impact reduction.

	MSR to methanol	BR to methanol	Biomass to methanol	CO_2 hydrogenation	
				AW el.	PEM el.
Feed	0.0000[2]	-0.9974[3]	-2.2389[3]	-1.5263	-1.5263
Light ends	0.0482	0.3317	0.4814	0.1349	0.1341
Methanol	0.0007	0.0012	0.0004	0.0003	0.0010
Wastewater	0.0000	0.0000	0.0000	0.0000	0.0000
Purge	2.3237	2.6671	12.277	-	-
Net direct emissions	**2.3726**	**2.0027**	**10.520**	**-1.3910**	**-1.3911**

Table 4.10: Electricity and NG needed for process utilities generation, with related indirect carbon emissions. Electricity is used for the generation of all the utilities, but the high-pressure steam. Indirect emissions are normalized to the mass of utility generated.

	Utility load	Utilities gen. emissions ($kgCO_2e/t_{util.}$)			
	(kWh/t)	France	Italy	Poland	Sweden
Ammonia	1.2440	0.0746	0.2687	0.8832	0.0100
R-152a	0.4364	0.0262	0.0943	0.3099	0.0035
Cooling water	0.1666	0.0100	0.0360	0.1183	0.0013
Low-pressure steam	102.11	6126.5	22055	72497	816.87
Steam for turbines	77.681	4660.8	16779	55153	621.44
High-pressure steam	1441.3	2743.7	2743.7	2743.7	2743.7

- indirect emissions are related to the utilities usage of the process. In particular, electricity- and NG-related emissions are taken into consideration, along with their use for the generation of the other process utilities: electricity is needed for refrigerants, cooling water, low-pressure steam, and steam for turbine drives; NG is needed for the generation of high-pressure steam. In general indirect emissions can be identified as the sum of four contributions:

$$\text{indirect } CO_2e \text{ emissions} = (CO_2e)^{electr.} + (CO_2e)^{NG} + (CO_2e)^{electr.}_{util.} + (CO_2e)^{NG}_{util.} \quad (4.25)$$

  where the last two are the contributions related to utilities (util.) generation, by the employment of electricity (electr.) and NG. These indirect emission voices are defined for each type of utility, and are reported in table 4.10.

The indirect NG-related carbon emissions are assumed to be the same for all the four countries

[2]Negative contribution not considered
[3]CH_4 fraction not accounted for subtraction

Table 4.11: Total indirect carbon emissions (tCO_2e/tCH_3OH)

	MSR to methanol	BR to methanol	Biomass to methanol	CO_2 hydrogenation	
				AW el.	PEM el.
France	1.912	0.113	4.793	2.419	2.720
Italy	2.195	0.293	5.077	4.264	4.759
Poland	3.092	0.865	5.974	10.11	1.804
Sweden	1.818	0.052	4.699	1.804	2.041

Table 4.12: Total indirect carbon emissions with on-site renewable electricity generation for CO_2 hydrogenation processes (tCO_2e/tCH_3OH)

	MSR to methanol	BR to methanol	Biomass to methanol	CO_2 hydrogenation	
				AW el.	PEM el.
France	1.912	0.113	4.793	1.647	1.873
Italy	2.195	0.293	5.077	1.647	1.873
Poland	3.092	0.865	5.974	1.647	1.873
Sweden	1.818	0.052	4.699	1.647	1.873

considered in this study. Indeed, in a chemical plant NG is bought and burnt in gas turbines, for which an efficiency of 90% is assumed; the carbon emissions are calculated from the stoichiometry of the methane combustion reaction (4.26), thus they do not depend on the location of plant:

$$CH_4 + 2\,O_2 \longrightarrow CO_2 + 2\,H_2O \tag{4.26}$$

from which, theoretically, 2.7347 kg of CO_2 are emitted per kg of CH_4 burnt. Considering the gas turbine efficiency, the actual CO_2 emissions are equal to 3.0486 kg CO_2/kg CH_4.

The overall electricity- and NG-related indirect emissions are summarized in table 4.11. Anyway, a consideration should be made for the CO_2 hydrogenation processes. They are very high-energy demanding for the part related to the green generation of raw materials (CO_2 captured from the atmosphere, and H_2 produced via water electrolysis). However, a production system that is presented not to impact the environment directly, but does so indirectly by consuming a huge amount of electricity that, at least in the majority of countries, is produced for the large part from non-renewable sources, makes no sense. Thus, starting from this consideration, an on-site renewable power generation plant is assumed to assess results in terms of carbon impact, as presented in table 4.12.

4.3.3 Carbon impact results assessment and discussion

As expected, by looking at the plot reported in figure 4.12, MSR and BR to methanol processes are comparable from the point of view of the net direct carbon emissions. Biomass to methanol is characterized by large carbon emissions from the purge stream, thus resulting the more im-

pacting process. Differently, the two CO_2 hydrogenation processes "subtract" carbon from the environment. However, by considering also the indirect emissions (figure 4.13a), the situation becomes favorable to BR to methanol processes, with the overall emissions being very low compared to the other processes; furthermore, the higher utilities demand that characterizes biomass to methanol process reflects into indirect emissions that largely overcome the benefit presented in terms of direct emissions by the process.

As regards the CO_2 hydrogenation processes, in the case of Poland the overall carbon emissions overcome also those of the conventional MSR to methanol process, and in the case of Italy, the total emissions overcome those of the BR to methanol process. For the reasons explained before, the on-site renewable electricity generation case is considered for such processes (figure 4.13b), in comparison with the "base case" previously considered. The result for that processes is that the total emissions are very low, since they are only related to NG consumed for DAC processes. Indeed, the bars are flattened over the four case studies, considering that the same emissions are accounted for NG in the different countries.

By on-site renewable energy generation, applying it to the Poland case, a reduction of between the 95% and 97% of the total carbon emissions is obtained for the CO_2 hydrogenation processes. Following this consideration, such processes become surely the best route to methanol production from an environmental point of view, considered that electricity is entirely provided by renewable sources, while a case-dependent variability is clear in the previous case, as represented in figure 4.13a.

The results obtained for BR and biomas to methanol processes are largely influenced by the assumptions made on methane entering the process as a feed. A prudential approach is adopted in this work for the carbon impact assessment, provided that methane is subtracted to the atmosphere "indirectly": photosynthetic organisms fix CO_2 from the atmosphere and then, only when biogas or syngas are generated through fermentation and gasification of the biomass, respectively, CH_4 is obtained.

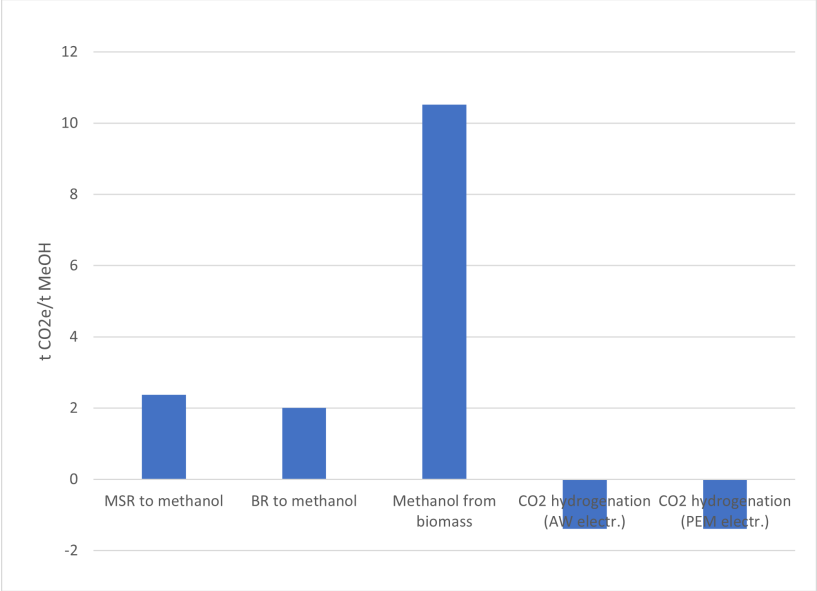

Figure 4.12: Total net direct carbon emissions for the five processes (tCO_2e/tCH_3OH)

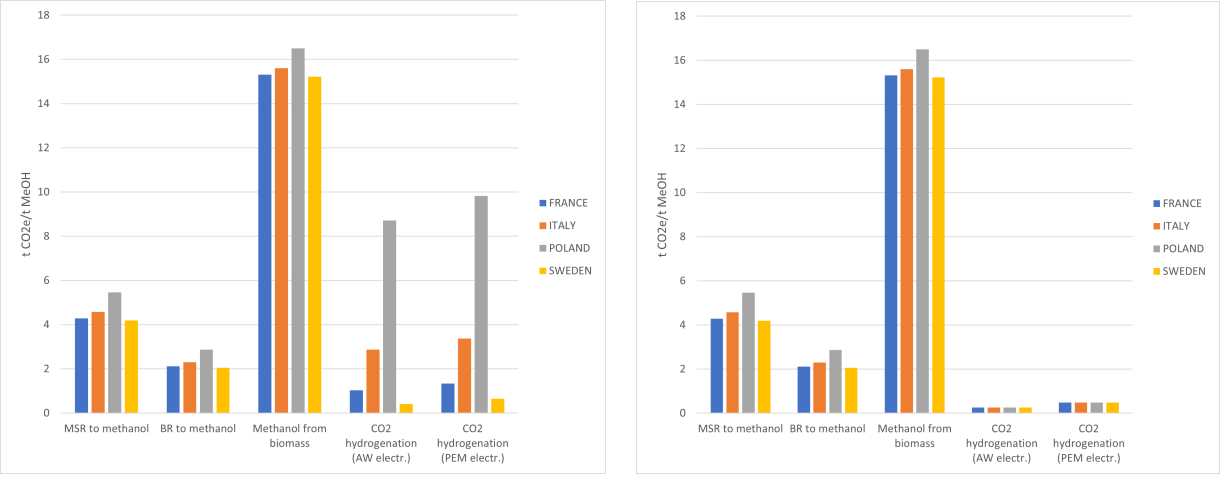

(a) *Base case* **(b)** *On-site renewable electricity generation*

Figure 4.13: Total direct and indirect carbon emissions. The carbon impact related to the employment of an on-site renewable electricity generation for the CO_2 hydrogenation processes is evaluated

Conclusions

In this thesis different methanol synthesis routes were analyzed and compared in terms of technological, economic, and carbon emission aspects, by means of process simulation. Specifically, four alternative routes (biogas reforming BR, biomass gasification, and CO_2 hydrogenation with two different water electrolysis technologies) were considered alongside the conventional synthesis via methane steam reforming (MSR).

The results obtained in this work make clear the potential of the alternative routes, in comparison to the reference process. In particular, BR to methanol showed the best economic performance, that appears to perform even better than the one obtained for the MSR to methanol; this result is mainly related to reduced operating expenses, considering the availability of low-cost feedstocks, to a minor utility usage and energy consumption, and to the capability of the process to operate in an energetically auto-sufficient way. However, considering that the experimental data used to perform the simulations were affected by an error (a 10% difference emerged from carbon mass balance, by neglecting by-products formation) and the experimental campaign was carried out through a micro-reactor, some limitations may be present in the simulation results obtained in this work: further studies should be led to investigate the effects of by-products formation on the process, in particular on the methanol synthesis and purification section, and to evaluate performance data when scaling up the micro-reactor experiments to at least a pilot plant.

With regard to the biomass to methanol process, the main limitations are related to the quality of the syngas produced via steam gasification, in relation to the subsequent methanol synthesis: carbon conversion is very low, and this results in a very high amount of syngas needed to reach the desired methanol productivity. Considering also the quite high energy expense, coupled to the high cost of raw materials needed to keep the desired productivity, the manufacturing costs are too high with respect to the potential revenues coming from the methanol sale: the process is non-profitable mainly as a consequence of technological limitations. In this way, further studies would be suggested in order to investigate the techno-economic sustainability of upgrading syngas via the employment of a WGS reactor, or to find the optimal syngas composition needed for the methanol synthesis (e.g. by studying different types of biomass feedstocks). The process is not yet advisable also from an environmental point of view, due to the high energy duties, that cancel out the contribution given by the renewable feedstock employed.

Among the two CO_2 hydrogenation processes, the one that employs hydrogen produced via alkaline water (AW) electrolysis is currently preferable, from both a techno-economic and environmental point of view. AW technology is more mature than the polymer electrolyte membrane (PEM) electrolysis, that is characterized by higher capital and operating costs: PEM is characterized by higher investment costs, by a slightly higher water consumption and by a higher electricity requirement. In fact, as commonly reported in literature, hydrogen produced via AW electrolysis is less costly than the one produced via PEM technology. Anyway, considering the very high cost of raw materials, and the quite low carbon conversions obtained in methanol reactor, these processes are the less sustainable alternatives from an economic point of view. Green hydrogen production costs via water electrolysis are currently more than 4 times higher with respect to the traditional grey hydrogen coming from MSR reaction; same considerations can be made for CO_2 captured via DAC process, for which the costs are more than 5 times higher with the traditional carbon capture systems currently employed in industry. However, from the environmental point of view, they represent surely the best solution, among all the processes considered in this study. Net direct carbon emissions are in fact negative, considering the removal of CO_2 from the atmosphere, but indirect electricity-related carbon emissions are quite high, considering the electricity demands of DAC and water electrolysis processes: the result is an overall value of carbon emissions that is almost comparable to that of BR to methanol. Nonetheless, by considering the employment of renewable energy to carry out hydrogen and carbon dioxide production processes, e.g. by an on-site wind energy or solar photo-voltaic plant, the overall carbon emissions are almost nullified: only in this way these processes represent a real sustainable alternative route to methanol production.

At the present time, in order to guarantee an economical sustainability to the biomass to methanol route, and to the two CO_2 hydrogenation processes, methanol selling values should be increased with respect to the current value. To achieve the same Net Present Value of the traditional MSR process, methanol should be sold at the following values for the three processes:

- Biomass to methanol: 1.60 times higher than the reference price of 337.3 \$/t, i.e., 539.6 \$/t;
- CO_2 hydrogenation (AW electrolysis): 7.42 times higher, i.e., 2502 \$/t;
- CO_2 hydrogenation (PEM electrolysis): 9.62 times higher, i.e., 3244 \$/t.

In the future, green hydrogen generation production costs are forecast to become 4 times lower towards 2050, while DAC captured CO_2 cost future previsions are not so certain due to the early stage of the technology development, but certainly the process is forecast to improve a lot its efficiency. Thus, considering the concrete possibilities of a technological improvement of the overall CO_2 hydrogenation processes, in particular with regard to the raw materials generation processes, this production route has the potential to become the optimal solution in terms of cost effectiveness, other than the best in environmental sustainability.

Appendices

A - MATLAB codes

MSR reaction equilibrium conversions calculation

```
%% equilibrium constant calculation for MSR reaction
% CH4 + H2O(g) = CO + 3 H2

t=850; % REFORMER operating temperature (C)
T=t+273.15; % converting C to K
p=17; % REFORMER operating pressure (bar)
P=p/1.01325; % converting bar to atm
Kp1=10^((-11769/T)+13.1927); % equilibrium constant

% solving Kp equation to determine maximum equilibrium CH4
    conversion
syms x
eqn=(P^2*27*x^4)/(4*x^4-36*x^2-16*x+48)==Kp1;
assume(x,'real')
X=vpasolve(eqn,x,[0 1]); % equilibrium CH4 conversion

%% equilibrium constant calculation for WGS reaction assumed
    subsequent
% to methane steam reforming reaction
% CO + H2O = CO2 + H2

Kp2=10^((1197.8/T)-1.6485); % equilibrium constant

% solving Kp equation to determine maximum equilibrium CH4
    conversion
syms csi
eqn=(csi^2+3*csi*X)/(csi^2-3*csi+(3*X-X^2))==Kp2;
assume(csi,'real')
Csi=vpasolve(eqn,csi,[0 X]); % extent of WGS subsequent to MSR
Xco=Csi/X; % CO maximum equilibrium conversion WGS reaction
```

Least-squares optimization function

```
% varying both XCH4_1 (and thus XCO2_2) and XCO, fixed XCH4_tot
StoC=1.28;  % steam to carbon ratio
MR=0.65; % molar ratio CO2:CH4
XCH4_tot=0.838; % global CH4 conversion
XCH4_1=linspace(0,1,200); % CH4 conversion of MSR reaction
XCH4_2=XCH4_tot-XCH4_1; % CH4 conversion of MDR reaction
XCO=linspace(0,1,200)'; % XCO varying from 0 to 1, with 200
    intermediate points

% experimental product yield
Y_H2=2.28;
Y_CO2=0.637;
Y_CO=0.7;
Y_CH4=0.162;

% product yield error: calculated value - experimental value
H2=3.*XCH4_1+2.*XCH4_2+XCO.*(XCH4_1+2.*XCH4_2)-Y_H2;
CO2=MR-XCH4_2+XCO.*(XCH4_1+2.*XCH4_2)-Y_CO2;
CO=XCH4_1+2.*XCH4_2-XCO.*(XCH4_1+2.*XCH4_2)-Y_CO;
CH4=1-XCH4_1-XCH4_2-Y_CH4;

% relative error
Er_H2=H2./Y_H2;
Er_CO2=CO2./Y_CO2;
Er_CO=CO./Y_CO;
%Er_CH4=CH4/Y_CH4; % equalized to zero

SSRE=Er_H2.^2+Er_CO2.^2+Er_CO.^2; % sum of square relative errors of
    H2, CO2 and CO
% least square optimization function
[MINSSRE,i]=min(SSRE);
[minSSRE,j]=min(MINSSRE);
xch4_1=XCH4_1(j); % optimal CH4 conversion of MSR reaction
xch4_2=XCH4_2(j); % optimal CH4 conversion of MDR reaction
[MINSSRET,k]=min(SSRE');
[minSSRET,l]=min(MINSSRET);
xCO=XCO(l); % optimal CO conversion of WGS reaction
xCO2_2=xch4_2/MR; % optimal CO2 conversion of MDR reaction
```

B - Distillation columns specifications and results

Light ends column

	MSR to methanol	BR to methanol	Biomass to methanol	CO_2 hydrogenation	
				AW el.	PEM el.
Number of stages	3	6	6	5	5
Feed stage position	2	5	5	4	4
Diameter (m)	0.521	0.796	0.834	0.857	0.856
Tray distance (m)	0.610	0.610	0.610	0.610	0.610
Height (m)	5.676	7.962	9.486	7.200	7.200
Capacity factor (m^3)	1.209	3.961	5.176	4.156	4.147
Condenser					
Temperature (°C)	-14.208	11.905	-27.330	9.022	10.062
Heat duty (kW)	-539.270	-615.689	-574.066	-1159.126	-1156.052
Surface (m^2)	5.8610	24.940	9.437	29.630	29.090
Distillate rate (kmol/h)	4.95248	76.629	101.000	41.324	41.279
Reflux rate (kmol/h)	45.868	54.704	45.869	103.428	103.295
Reboiler					
Temperature (°C)	66.660	66.660	65.193	73.168	73.003
Heat duty (kW)	410.069	410.069	540.523	1264.491	1222.997
Surface (m^2)	2.4320	5.421	98.890	41.860	34.720
Bottoms rate (kmol/h)	455.973	455.973	427.361	772.108	772.166
Boilup rate (kmol/h)	39.505	75.308	52.305	118.200	115.015

Methanol column

	MSR to methanol	BR to methanol	Biomass to methanol	CO_2 hydrogenation	
				AW el.	PEM el.
Number of stages	29	29	29	21	21
Feed stage position	18	18	18	16	16
Diameter (m)	0.521	1.848	1.908	2.165	2.166
Tray distance (m)	0.610	0.610	0.610	0.610	0.610
Height (m)	25.003	24.240	27.290	18.903	18.903
Capacity factor (m^3)	66.792	72.310	78.023	69.568	69.668
Condenser					
Temperature (°C)	64.159	63.480	63.911	64.233	63.634
Heat duty (kW)	-6943.685	-7728.821	-7352.591	-9466.736	-9485.702
Surface (m^2)	57.040	91.330	67.590	95.510	101.900
Distillate rate (kmol/h)	383.338	383.030	383.004	382.689	382.899
Reflux rate (kmol/h)	324.283	403.658	366.374	582.705	583.022
Reboiler					
Temperature (°C)	94.582	94.582	80.420	99.013	99.078
Heat duty (kW)	6984.074	6984.074	7346.777	9608.392	9624.248
Surface (m^2)	229.200	405.200	210.200	384.600	346.600
Bottoms rate (kmol/h)	72.635	72.635	44.357	389.419	389.266
Boilup rate (kmol/h)	613.139	686.471	695.770	844.857	846.478

C - Stream Tables

Units of measure:

- Temperature in °C
- Pressure in bar
- Mass Density in kg/m^3
- Enthalpy Flow in MW
- Average MW in kg/kmol
- Mass Flows in kg/h
- Volume Flow in m^3/h
- Mole flows in kg/h

Abbreviations used are: MW for molecular weight, FRAC for fraction.

Methane steam reforming to methanol

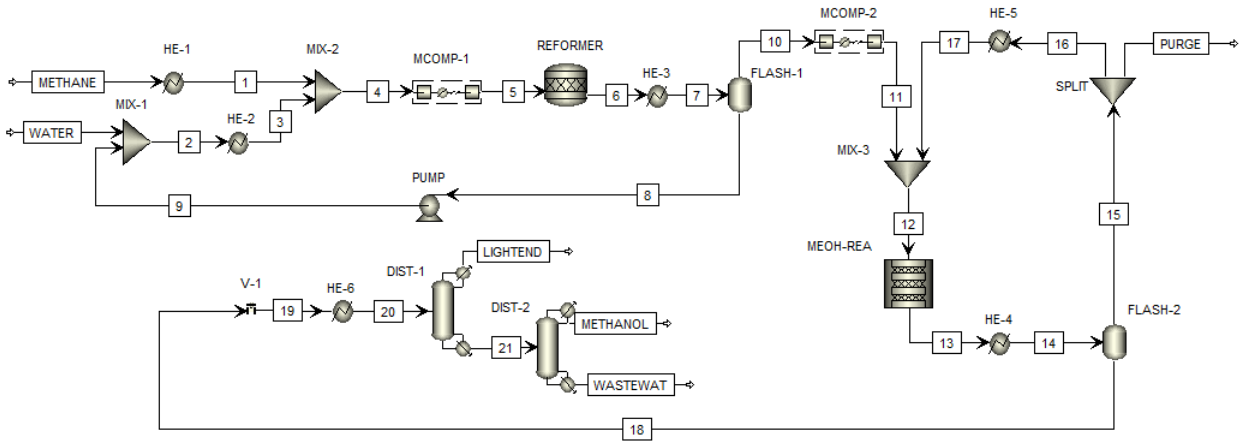

	METHANE	WATER	1	2	3	4	5	6	7	8
Temperature	25.000	25.000	600.000	35.011	600.000	599.972	850.000	850.000	40.000	40.000
Pressure	1.013	1.013	1.013	1.013	1.013	1.013	17.000	17.000	17.000	17.000
Molar Vapor Frac	1.000	0.000	1.000	0.000	1.000	1.000	1.000	1.000	0.655	0.000
Molar Liquid Frac	0.000	1.000	0.000	1.000	0.000	0.000	0.000	0.000	0.345	1.000
Mass Density	0.657	961.076	0.224	943.373	0.252	0.245	3.187	2.217	12.010	948.301
Enthalpy Flow	-11369	-44874	-6855	-131803	-101128	-107984	-100545	-71188	-109143	-86924
Average MW	16.043	18.015	16.043	18.016	18.016	17.523	17.523	12.211	12.211	18.016
Mass Flows	8809.410	10075.145	8809.410	29682.450	29682.450	38491.861	38491.868	38491.868	38491.868	19607.305
Volume Flow	13411.194	10.483	39356.167	31.464	117989.136	157350.287	12077.247	17364.022	3205.049	20.676
Mole Flows	549.121	559.256	549.121	1647.568	1647.568	2196.689	2196.689	3152.160	3152.160	1088.313
H_2O	0.000	559.256	0.000	1647.516	1647.516	1647.516	1647.517	1095.732	1095.732	1088.261
CH_4	549.121	0.000	549.121	0.001	0.001	549.121	549.121	71.386	71.386	0.001
CO	0.000	0.000	0.000	0.000	0.000	0.000	0.000	403.687	403.687	0.000
CO_2	0.000	0.000	0.000	0.044	0.044	0.044	0.044	74.093	74.093	0.044
H_2	0.000	0.000	0.000	0.006	0.006	0.006	0.006	1507.262	1507.262	0.006
CH_3OH	0.000	0.000	0.000	0.000	0.000	0.000	0.000	0.000	0.000	0.000
Mole frac H_2O	0.000	1.000	0.000	1.000	1.000	0.750	0.750	0.348	0.348	1.000
Mole frac CH_4	1.000	0.000	1.000	0.000	0.000	0.250	0.250	0.023	0.023	0.000
Mole frac CO	0.000	0.000	0.000	0.000	0.000	0.000	0.000	0.128	0.128	0.000
Mole frac CO_2	0.000	0.000	0.000	0.000	0.000	0.000	0.000	0.024	0.024	0.000
Mole frac H_2	0.000	0.000	0.000	0.000	0.000	0.000	0.000	0.478	0.478	0.000
Mole frac CH_3OH	0.000	0.000	0.000	0.000	0.000	0.000	0.000	0.000	0.000	0.000
Mass frac H_2O	0.000	1.000	0.000	1.000	1.000	0.771	0.771	0.513	0.513	1.000
Mass frac CH_4	1.000	0.000	1.000	0.000	0.000	0.229	0.229	0.030	0.030	0.000
Mass frac CO	0.000	0.000	0.000	0.000	0.000	0.000	0.000	0.294	0.294	0.000
Mass frac CO_2	0.000	0.000	0.000	0.000	0.000	0.000	0.000	0.085	0.085	0.000
Mass frac H_2	0.000	0.000	0.000	0.000	0.000	0.000	0.000	0.079	0.079	0.000
Mass frac CH_3OH	0.000	0.000	0.000	0.000	0.000	0.000	0.000	0.000	0.000	0.000

	9	10	11	12	13	14	15	16	17	18
Temperature	40.158	40.000	252.000	251.996	251.996	40.000	40.000	40.000	252.000	40.000
Pressure	1.013	17.000	75.000	75.000	75.000	75.000	75.000	75.000	75.000	75.000
Molar Vapor Frac	0.000	1.000	1.000	1.000	1.000	0.947	1.000	1.000	1.000	0.000
Molar Liquid Frac	1.000	0.000	0.000	0.000	0.000	0.053	0.000	0.000	0.000	1.000
Mass Density	947.827	5.930	15.284	11.502	12.544	21.881	17.382	17.382	10.449	777.522
Enthalpy Flow	-86929	-22219	-18499	-49159	-59208	-80631	-49106	-44195	-30660	-31525
Average MW	18.016	9.150	9.150	6.881	7.496	7.496	6.250	6.250	6.250	29.788
Mass Flows	19607.305	18884.563	18884.563	65275.477	65275.477	65275.477	51545.499	46390.949	46390.913	13729.977
Volume Flow	20.687	3184.372	1235.580	5675.225	5203.873	2983.139	2965.480	2668.932	4439.680	17.659
Mole Flows	1088.313	2063.848	2063.848	9486.042	8707.857	8707.857	8246.931	7422.238	7422.194	460.926
H_2O	1088.261	7.471	7.471	11.692	75.601	75.601	4.689	4.220	4.220	70.912
CH_4	0.001	71.385	71.385	702.256	702.256	702.256	700.968	630.871	630.871	1.288
CO	0.000	403.686	403.686	1107.356	782.173	782.173	781.848	703.663	703.669	0.325
CO_2	0.044	74.049	74.049	148.326	84.417	84.417	82.532	74.279	74.277	1.885
H_2	0.006	1507.256	1507.256	7479.736	6637.642	6637.642	6636.142	5972.528	5972.480	1.500
CH_3OH	0.000	0.000	0.000	36.676	425.769	425.769	40.753	36.677	36.676	385.016
Mole frac H_2O	1.000	0.004	0.004	0.001	0.009	0.009	0.001	0.001	0.001	0.154
Mole frac CH_4	0.000	0.035	0.035	0.074	0.081	0.081	0.085	0.085	0.085	0.003
Mole frac CO	0.000	0.196	0.196	0.117	0.090	0.090	0.095	0.095	0.095	0.001
Mole frac CO_2	0.000	0.036	0.036	0.016	0.010	0.010	0.010	0.010	0.010	0.004
Mole frac H_2	0.000	0.730	0.730	0.788	0.762	0.762	0.805	0.805	0.805	0.003
Mole frac CH_3OH	0.000	0.000	0.000	0.004	0.049	0.049	0.005	0.005	0.005	0.835
Mass frac H_2O	1.000	0.007	0.007	0.003	0.021	0.021	0.002	0.002	0.002	0.093
Mass frac CH_4	0.000	0.061	0.061	0.173	0.173	0.173	0.218	0.218	0.218	0.002
Mass frac CO	0.000	0.599	0.599	0.475	0.336	0.336	0.425	0.425	0.425	0.001
Mass frac CO_2	0.000	0.173	0.173	0.100	0.057	0.057	0.070	0.070	0.070	0.006
Mass frac H_2	0.000	0.161	0.161	0.231	0.205	0.205	0.260	0.260	0.260	0.000
Mass frac CH_3OH	0.000	0.000	0.000	0.018	0.209	0.209	0.025	0.025	0.025	0.899

	19	20	21	PURGE	LIGHTEND	METHANOL	WASTEWAT
Temperature	14.593	62.000	66.660	40.000	-14.203	64.159	94.582
Pressure	1.013	1.013	1.013	75.000	1.013	1.013	1.013
Molar Vapor Frac	0.005	0.050	0.000	1.000	1.000	0.000	0.000
Molar Liquid Frac	0.995	0.950	1.000	0.000	0.000	1.000	1.000
Mass Density	183.973	21.223	754.931	17.382	1.078	744.680	907.060
Enthalpy Flow	-31525	-30767	-30659	-4911	-237	-24992	-5627
Average MW	29.788	29.788	29.863	6.250	22.858	32.017	18.495
Mass Flows	13729.977	13729.977	13616.772	5154.550	113.205	12273.383	1343.389
Volume Flow	74.630	646.935	18.037	296.548	104.976	16.481	1.481
Mole Flows	460.926	460.926	455.973	824.693	4.952	383.338	72.635
H_2O	70.912	70.912	70.912	0.469	0.001	0.760	70.151
CH_4	1.288	1.288	0.010	70.097	1.278	0.010	0.000
CO	0.325	0.325	0.000	78.185	0.325	0.000	0.000
CO_2	1.885	1.885	0.103	8.253	1.781	0.103	0.000
H_2	1.500	1.500	0.000	663.614	1.500	0.000	0.000
CH_3OH	385.016	385.016	384.948	4.075	0.068	382.464	2.484
Mole frac H_2O	0.154	0.154	0.156	0.001	0.000	0.002	0.966
Mole frac CH_4	0.003	0.003	0.000	0.085	0.258	0.000	0.000
Mole frac CO	0.001	0.001	0.000	0.095	0.066	0.000	0.000
Mole frac CO_2	0.004	0.004	0.000	0.010	0.360	0.000	0.000
Mole frac H_2	0.003	0.003	0.000	0.805	0.303	0.000	0.000
Mole frac CH_3OH	0.835	0.835	0.844	0.005	0.014	0.998	0.034
Mass frac H_2O	0.093	0.093	0.094	0.002	0.000	0.001	0.941
Mass frac CH_4	0.002	0.002	0.000	0.218	0.181	0.000	0.000
Mass frac CO	0.001	0.001	0.000	0.425	0.080	0.000	0.000
Mass frac CO_2	0.006	0.006	0.000	0.070	0.692	0.000	0.000
Mass frac H_2	0.000	0.000	0.000	0.260	0.027	0.000	0.000
Mass frac CH_3OH	0.899	0.899	0.906	0.025	0.019	0.999	0.059

Biogas reforming to methanol

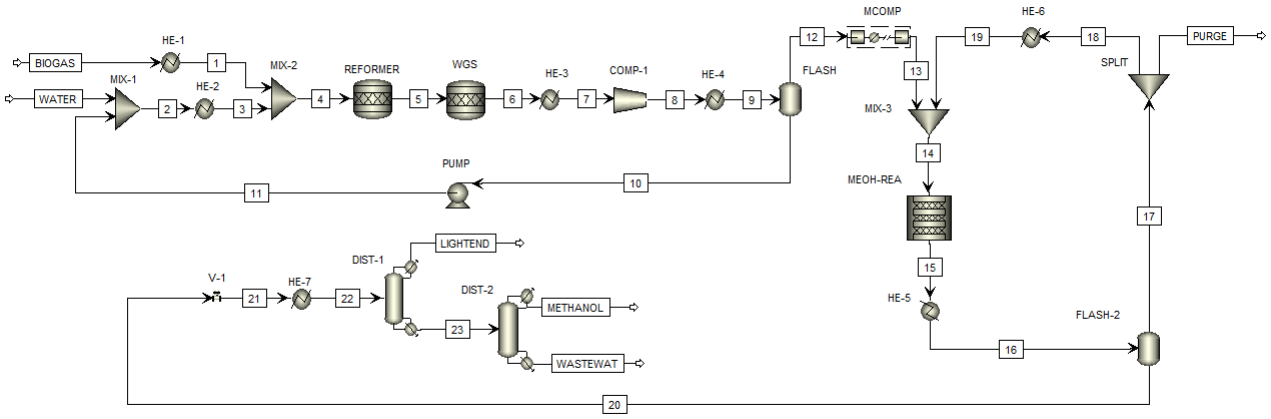

	BIOGAS	WATER	1	2	3	4	5	6	7	8
Temperature	37.000	25.000	650.000	33.405	650.000	649.974	650.000	650.000	250.000	588.684
Pressure	1.013	1.013	1.013	1.013	1.013	1.013	1.013	1.013	1.013	5.000
Molar Vapor Frac	1.000	0.000	1.000	0.000	1.000	1.000	1.000	1.000	1.000	1.000
Molar Liquid Frac	0.000	1.000	0.000	1.000	0.000	0.000	0.000	0.000	0.000	0.000
Mass Density	1.066	961.076	0.357	951.903	0.238	0.290	0.201	0.201	0.354	1.060
Enthalpy Flow	-39121.101	-31958.549	-33031.822	-72231.198	-54892.839	-87923.842	-65139.242	-65806.185	-74868.798	-67253.314
Average MW	27.060	18.015	27.060	18.016	18.016	21.983	15.208	15.208	15.208	15.208
Mass Flows	19077.351	7175.312	19077.351	16258.892	16258.892	35335.934	35335.934	35335.934	35335.934	35335.934
Volume Flow	17897.376	7.466	53420.773	17.080	68338.153	121762.456	176046.136	176047.113	99746.592	33333.960
Mole Flows	705.000	398.290	705.000	902.466	902.466	1607.454	2323.564	2323.564	2323.564	2323.564
H_2O	0.000	398.290	0.000	902.437	902.437	902.430	593.255	525.785	525.785	525.785
CH_4	427.273	0.000	427.273	0.000	0.000	427.273	69.218	69.218	69.218	69.218
CO	0.000	0.000	0.000	0.000	0.000	0.000	406.935	339.465	339.465	339.465
CO_2	277.727	0.000	277.727	0.028	0.028	277.751	228.871	296.341	296.341	296.341
H_2	0.000	0.000	0.000	0.001	0.001	0.000	1025.284	1092.754	1092.754	1092.754
CH_3OH	0.000	0.000	0.000	0.000	0.000	0.000	0.000	0.000	0.000	0.000
Mole frac H_2O	0.000	1.000	0.000	1.000	1.000	0.561	0.255	0.226	0.226	0.226
Mole frac CH_4	0.606	0.000	0.606	0.000	0.000	0.266	0.030	0.030	0.030	0.030
Mole frac CO	0.000	0.000	0.000	0.000	0.000	0.000	0.175	0.146	0.146	0.146
Mole frac CO_2	0.394	0.000	0.394	0.000	0.000	0.173	0.099	0.128	0.128	0.128
Mole frac H_2	0.000	0.000	0.000	0.000	0.000	0.000	0.441	0.470	0.470	0.470
Mole frac CH_3OH	0.000	0.000	0.000	0.000	0.000	0.000	0.000	0.000	0.000	0.000
Mass frac H_2O	0.000	1.000	0.000	1.000	1.000	0.460	0.302	0.268	0.268	0.268
Mass frac CH_4	0.359	0.000	0.359	0.000	0.000	0.194	0.031	0.031	0.031	0.031
Mass frac CO	0.000	0.000	0.000	0.000	0.000	0.000	0.323	0.269	0.269	0.269
Mass frac CO_2	0.641	0.000	0.641	0.000	0.000	0.346	0.285	0.369	0.369	0.369
Mass frac H_2	0.000	0.000	0.000	0.000	0.000	0.000	0.058	0.062	0.062	0.062
Mass frac CH_3OH	0.000	0.000	0.000	0.000	0.000	0.000	0.000	0.000	0.000	0.000

	9	10	11	12	13	14	15	16	17
Temperature	40.000	40.000	40.049	40.000	252.000	251.835	251.835	40.000	40.000
Pressure	5.000	5.000	1.013	5.000	75.000	75.000	75.000	75.000	75.000
Molar Vapor Frac	0.783	0.000	0.000	1.000	1.000	1.000	1.000	0.886	1.000
Molar Liquid Frac	0.217	1.000	1.000	0.000	0.000	0.000	0.000	0.114	0.000
Mass Density	3.724	948.065	947.938	2.769	24.138	29.760	34.846	67.461	56.802
Enthalpy Flow	-85746.458	-40272.208	-40272.648	-45474.250	-42039.570	-192761.503	-202914.318	-219999.797	-177355.770
Average MW	15.208	18.017	18.017	14.429	14.429	17.730	20.505	20.505	19.216
Mass Flows	35335.934	9083.580	9083.580	26252.354	26252.354	103865.978	103865.978	103865.978	86235.804
Volume Flow	9489.466	9.581	9.582	9479.885	1087.591	3490.153	2980.733	1539.649	1518.191
Mole Flows	2323.564	504.176	504.176	1819.388	1819.388	5858.346	5065.330	5065.330	4487.778
H_2O	525.785	504.147	504.147	21.639	21.639	25.926	117.688	117.688	4.764
CH_4	69.218	0.000	0.000	69.218	69.218	666.155	666.155	666.155	663.263
CO	339.465	0.000	0.000	339.465	339.465	648.592	343.845	343.845	343.479
CO_2	296.341	0.028	0.028	296.313	296.313	1540.573	1448.811	1448.811	1382.468
H_2	1092.754	0.001	0.001	1092.753	1092.753	2952.360	2067.583	2067.583	2066.314
CH_3OH	0.000	0.000	0.000	0.000	0.000	24.741	421.248	421.248	27.490
Mole frac H_2O	0.226	1.000	1.000	0.012	0.012	0.004	0.023	0.023	0.001
Mole frac CH_4	0.030	0.000	0.000	0.038	0.038	0.114	0.132	0.132	0.148
Mole frac CO	0.146	0.000	0.000	0.187	0.187	0.111	0.068	0.068	0.077
Mole frac CO_2	0.128	0.000	0.000	0.163	0.163	0.263	0.286	0.286	0.308
Mole frac H_2	0.470	0.000	0.000	0.601	0.601	0.504	0.408	0.408	0.460
Mole frac CH_3OH	0.000	0.000	0.000	0.000	0.000	0.004	0.083	0.083	0.006
Mass frac H_2O	0.268	1.000	1.000	0.015	0.015	0.004	0.020	0.020	0.001
Mass frac CH_4	0.031	0.000	0.000	0.042	0.042	0.103	0.103	0.103	0.123
Mass frac CO	0.269	0.000	0.000	0.362	0.362	0.175	0.093	0.093	0.112
Mass frac CO_2	0.369	0.000	0.000	0.497	0.497	0.653	0.614	0.614	0.706
Mass frac H_2	0.062	0.000	0.000	0.084	0.084	0.057	0.040	0.040	0.048
Mass frac CH_3OH	0.000	0.000	0.000	0.000	0.000	0.008	0.130	0.130	0.010

	18	19	20	21	22	23	PURGE	LIGHTEND	METHANOL	WASTEWAT
Temperature	40.000	252.000	40.000	10.520	63.000	67.408	40.000	11.897	63.480	93.522
Pressure	75.000	75.000	75.000	1.013	75.000	1.013	75.000	1.013	1.013	1.013
Molar Vapor Frac	1.000	1.000	0.000	0.101	0.003	0.000	1.000	1.000	0.000	0.000
Molar Liquid Frac	0.000	0.000	1.000	0.899	0.997	1.000	0.000	0.000	1.000	1.000
Mass Density	56.802	32.308	821.605	12.904	767.181	761.443	56.802	1.774	745.565	903.442
Enthalpy Flow	-159620.19	-150721.93	-42644.03	-42644.03	-41958.25	-34116.95	-17735.58	-7638.90	-24982.40	-9119.04
Average MW	19.216	19.216	30.526	30.526	30.526	28.888	19.216	41.233	32.043	18.637
Mass Flows	77612.22	77613.62	17630.17	17630.17	17630.17	14470.57	8623.58	3159.61	12273.38	2197.18
Volume Flow	1366.372	2402.284	21.458	1366.300	22.980	19.004	151.819	1781.297	16.462	2.432
Mole Flows	4039.000	4038.958	577.553	577.553	577.553	500.924	448.778	76.629	383.030	117.894
H_2O	4.287	4.287	112.924	112.924	112.924	112.915	0.476	0.008	0.247	112.668
CH_4	596.937	596.937	2.892	2.892	2.892	0.003	66.326	2.889	0.003	0.000
CO	309.132	309.127	0.366	0.366	0.366	0.000	34.348	0.366	0.000	0.000
CO_2	1244.221	1244.260	66.343	66.343	66.343	0.316	138.247	66.027	0.316	0.000
H_2	1859.682	1859.607	1.269	1.269	1.269	0.000	206.631	1.269	0.000	0.000
CH_3OH	24.741	24.741	393.759	393.759	393.759	387.689	2.749	6.069	382.464	5.225
Mole frac H_2O	0.001	0.001	0.196	0.196	0.196	0.225	0.001	0.000	0.001	0.956
Mole frac CH_4	0.148	0.148	0.005	0.005	0.005	0.000	0.148	0.038	0.000	0.000
Mole frac CO	0.077	0.077	0.001	0.001	0.001	0.000	0.077	0.005	0.000	0.000
Mole frac CO_2	0.308	0.308	0.115	0.115	0.115	0.001	0.308	0.862	0.001	0.000
Mole frac H_2	0.460	0.460	0.002	0.002	0.002	0.000	0.460	0.017	0.000	0.000
Mole frac CH_3OH	0.006	0.006	0.682	0.682	0.682	0.774	0.006	0.079	0.999	0.044
Mass frac H_2O	0.001	0.001	0.115	0.115	0.115	0.141	0.001	0.000	0.000	0.924
Mass frac CH_4	0.123	0.123	0.003	0.003	0.003	0.000	0.123	0.015	0.000	0.000
Mass frac CO	0.112	0.112	0.001	0.001	0.001	0.000	0.112	0.003	0.000	0.000
Mass frac CO_2	0.706	0.706	0.166	0.166	0.166	0.001	0.706	0.920	0.001	0.000
Mass frac H_2	0.048	0.048	0.000	0.000	0.000	0.000	0.048	0.001	0.000	0.000
Mass frac CH_3OH	0.010	0.010	0.716	0.716	0.716	0.858	0.010	0.062	0.998	0.076

Biomass steam gasification to methanol

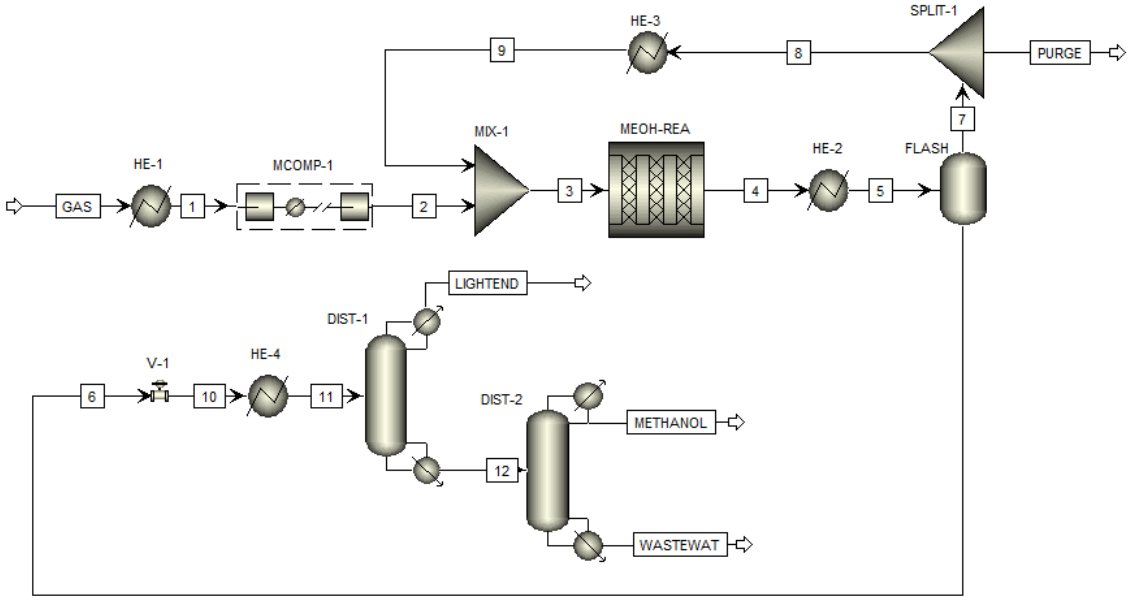

	GAS	1	2	3	4	5
Temperature	850.000	252.000	252.000	247.597	251.815	40.000
Pressure	1.013	1.013	75.000	75.000	74.997	75.000
Molar Vapor Fraction	1.000	1.000	1.000	1.000	1.000	0.967
Molar Liquid Fraction	0.000	0.000	0.000	0.000	0.000	0.033
Mass Density	0.223	0.477	34.477	18.043	46.862	91.723
Enthalpy Flow	-70423.0	-90790.2	-90868.1	-721754.6	-732970.9	-779087.6
Average MW	20.569	20.569	20.569	26.169	27.520	27.520
Mass Flows	59095.4	59095.4	59095.4	435169.6	435169.6	435169.6
Volume Flow	264847.8	123841.0	1714.1	24118.4	9286.3	4744.4
Mole Flows	2873.00	2873.00	2873.00	16629.00	15812.96	15812.96
H_2	1074.502	1074.502	1074.502	3083.038	2232.495	2232.495
CO	701.012	701.012	701.012	3632.979	3259.452	3259.452
CO_2	623.441	623.441	623.441	5204.858	5170.362	5170.362
CH_4	325.224	325.224	325.224	3198.656	3198.656	3198.656
C_2H_4	74.698	74.698	74.698	703.860	703.860	703.860
C_2H_6	51.714	51.714	51.714	478.625	478.625	478.625
CH_3OH	0.000	0.000	0.000	126.790	534.813	534.813
H_2O	0.000	0.000	0.000	8.256	42.752	42.752
C_3H_8	22.409	22.409	22.409	191.943	191.943	191.943
Mole frac H_2	0.374	0.374	0.374	0.185	0.141	0.141
Mole frac CO	0.244	0.244	0.244	0.218	0.206	0.206
Mole frac CO_2	0.217	0.217	0.217	0.313	0.327	0.327
Mole frac CH_4	0.113	0.113	0.113	0.192	0.202	0.202
Mole frac C_2H_4	0.026	0.026	0.026	0.042	0.045	0.045
Mole frac C_2H_6	0.018	0.018	0.018	0.029	0.030	0.030
Mole frac CH_3OH	0.000	0.000	0.000	0.008	0.034	0.034
Mole frac H_2O	0.000	0.000	0.000	0.000	0.003	0.003
Mole frac C_3H_8	0.008	0.008	0.008	0.012	0.012	0.012
Mass frac H_2	0.037	0.037	0.037	0.014	0.010	0.010
Mass frac CO	0.332	0.332	0.332	0.234	0.210	0.210
Mass frac CO_2	0.464	0.464	0.464	0.526	0.523	0.523
Mass frac CH_4	0.088	0.088	0.088	0.118	0.118	0.118
Mass frac C_2H_4	0.035	0.035	0.035	0.045	0.045	0.045
Mass frac C_2H_6	0.026	0.026	0.026	0.033	0.033	0.033
Mass frac CH_3OH	0.000	0.000	0.000	0.009	0.039	0.039
Mass frac H_2O	0.000	0.000	0.000	0.000	0.002	0.002
Mass frac C_3H_8	0.017	0.017	0.017	0.019	0.019	0.019

	6	7	8	9	10	11
Temperature	40.000	40.000	40.000	252.000	0.313	36.000
Pressure	75.000	75.000	75.000	75.000	1.013	1.013
Molar Vapor Fraction	0.000	1.000	1.000	1.000	0.149	0.239
Molar Liquid Fraction	1.000	0.000	0.000	0.000	0.851	0.761
Mass Density	802.015	88.477	88.477	46.376	9.799	5.419
Enthalpy Flow	-38208.4	-740879.2	-666791.3	-630886.5	-38208.4	-37349.8
Average MW	32.759	27.339	27.339	27.339	32.759	32.759
Mass Flows	17308.75	417860.86	376074.77	376074.16	17308.75	17308.75
Volume Flow	21.58	4722.81	4250.53	8109.25	1766.41	3194.27
Mole Flows	528.36	15284.60	13756.14	13756.00	528.36	528.36
H_2	0.651	2231.844	2008.659	2008.536	0.651	0.651
CO	1.707	3257.745	2931.971	2931.967	1.707	1.707
CO_2	79.891	5090.471	4581.424	4581.417	79.891	79.891
CH_4	5.953	3192.703	2873.432	2873.432	5.953	5.953
C_2H_4	4.792	699.068	629.162	629.162	4.792	4.792
C_2H_6	4.280	474.345	426.910	426.911	4.280	4.280
CH_3OH	393.935	140.878	126.790	126.790	393.935	393.935
H_2O	33.579	9.173	8.255	8.256	33.579	33.579
C_3H_8	3.573	188.370	169.533	169.533	3.573	3.573
Mole frac H_2	0.001	0.146	0.146	0.146	0.001	0.001
Mole frac CO	0.003	0.213	0.213	0.213	0.003	0.003
Mole frac CO_2	0.151	0.333	0.333	0.333	0.151	0.151
Mole frac CH_4	0.011	0.209	0.209	0.209	0.011	0.011
Mole frac C_2H_4	0.009	0.046	0.046	0.046	0.009	0.009
Mole frac C_2H_6	0.008	0.031	0.031	0.031	0.008	0.008
Mole frac CH_3OH	0.746	0.009	0.009	0.009	0.746	0.746
Mole frac H_2O	0.064	0.001	0.001	0.001	0.064	0.064
Mole frac C_3H_8	0.007	0.012	0.012	0.012	0.007	0.007
Mass frac H_2	0.000	0.011	0.011	0.011	0.000	0.000
Mass frac CO	0.003	0.218	0.218	0.218	0.003	0.003
Mass frac CO_2	0.203	0.536	0.536	0.536	0.203	0.203
Mass frac CH_4	0.006	0.123	0.123	0.123	0.006	0.006
Mass frac C_2H_4	0.008	0.047	0.047	0.047	0.008	0.008
Mass frac C_2H_6	0.007	0.034	0.034	0.034	0.007	0.007
Mass frac CH_3OH	0.729	0.011	0.011	0.011	0.729	0.729
Mass frac H_2O	0.035	0.000	0.000	0.000	0.035	0.035
Mass frac C_3H_8	0.009	0.020	0.020	0.020	0.009	0.009

	12	PURGE	LIGHTEND	METHANOL	WASTEWAT
Temperature	65.193	40.000	-27.330	63.911	80.422
Pressure	1.013	75.000	1.013	1.013	1.013
Molar Vapor Fraction	0.000	1.000	1.000	0.000	0.000
Molar Liquid Fraction	1.000	0.000	0.000	1.000	1.000
Mass Density	749.358	88.477	2.021	744.583	842.933
Enthalpy Flow	-28273.7	-74087.9	-9109.7	-24955.6	-3323.8
Average MW	30.949	27.339	40.421	32.045	21.482
Mass Flows	13226.26	41786.09	4082.49	12273.38	952.88
Volume Flow	17.65	472.28	2019.58	16.48	1.13
Mole Flows	427.36	1528.46	101.00	383.00	44.36
H_2	0.000	223.184	0.651	0.000	0.000
CO	0.000	325.775	1.707	0.000	0.000
CO_2	0.095	509.047	79.796	0.095	0.000
CH_4	0.001	319.270	5.952	0.001	0.000
C_2H_4	0.012	69.907	4.780	0.012	0.000
C_2H_6	0.024	47.434	4.256	0.024	0.000
CH_3OH	393.427	14.088	0.508	382.464	10.963
H_2O	33.579	0.917	0.000	0.186	33.393
C_3H_8	0.223	18.837	3.350	0.223	0.000
Mole frac H_2	0.000	0.146	0.006	0.000	0.000
Mole frac CO	0.000	0.213	0.017	0.000	0.000
Mole frac CO_2	0.000	0.333	0.790	0.000	0.000
Mole frac CH_4	0.000	0.209	0.059	0.000	0.000
Mole frac C_2H_4	0.000	0.046	0.047	0.000	0.000
Mole frac C_2H_6	0.000	0.031	0.042	0.000	0.000
Mole frac CH_3OH	0.921	0.009	0.005	0.999	0.247
Mole frac H_2O	0.079	0.001	0.000	0.000	0.753
Mole frac C_3H_8	0.001	0.012	0.033	0.001	0.000
Mass frac H_2	0.000	0.011	0.000	0.000	0.000
Mass frac CO	0.000	0.218	0.012	0.000	0.000
Mass frac CO_2	0.000	0.536	0.860	0.000	0.000
Mass frac CH_4	0.000	0.123	0.023	0.000	0.000
Mass frac C_2H_4	0.000	0.047	0.033	0.000	0.000
Mass frac C_2H_6	0.000	0.034	0.031	0.000	0.000
Mass frac CH_3OH	0.953	0.011	0.004	0.999	0.369
Mass frac H_2O	0.046	0.000	0.000	0.000	0.631
Mass frac C_3H_8	0.001	0.020	0.036	0.001	0.000

CO_2 hydrogenation (AW electrolysis)

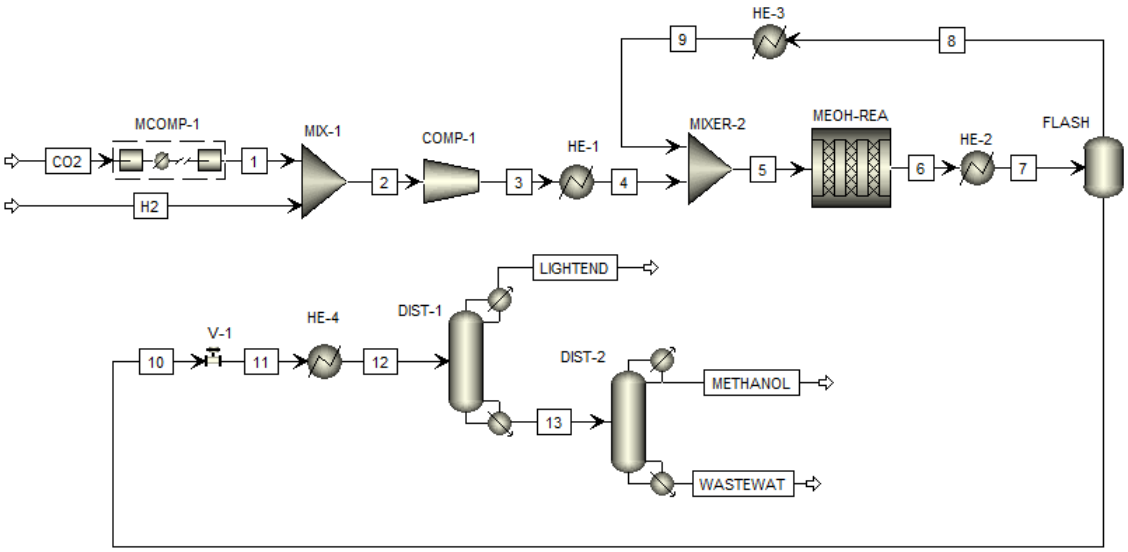

	CO2	H2	1	2	3	4	5	6	7
Temperature	25.000	90.000	90.000	85.053	215.999	252.000	252.085	251.630	40.000
Pressure	1.013	30.000	30.000	30.000	75.000	75.000	75.000	75.000	75.000
Molar Vapor Frac	1.000	1.000	1.000	1.000	1.000	1.000	1.000	1.000	0.855
Molar Liquid Frac	0.000	0.000	0.000	0.000	0.000	0.000	0.000	0.000	0.145
Mass Density	1.808	1.976	47.330	13.252	23.848	22.218	8.762	24.852	47.954
Enthalpy Flow	-46460.811	618.889	-46263.404	-45644.515	-43729.075	-43188.198	-162352.450	-168996.418	-189100.921
Average MW	44.010	2.016	44.010	13.253	13.253	13.253	12.880	14.662	14.662
Mass Flows	18704.165	2345.013	18704.165	21049.178	21049.178	21049.178	82117.200	82117.200	82117.200
Volume Flow	10345.520	1186.598	395.186	1588.371	882.645	947.375	9371.798	3304.257	1712.406
Mole Flows	425.000	1163.270	425.000	1588.270	1588.270	1588.270	6375.524	5600.840	5600.840
CO_2	425.000	0.000	425.000	425.000	425.000	425.000	1555.261	1167.883	1167.883
CO	0.000	0.000	0.000	0.000	0.000	0.000	124.833	124.870	124.870
H_2	0.000	1163.270	0.000	1163.270	1163.270	1163.270	4669.112	3507.050	3507.050
CH_3OH	0.000	0.000	0.000	0.000	0.000	0.000	20.487	407.828	407.828
H_2O	0.000	0.000	0.000	0.000	0.000	0.000	5.831	393.209	393.209
Mole frac CO_2	1.000	0.000	1.000	0.268	0.268	0.268	0.244	0.209	0.209
Mole frac CO	0.000	0.000	0.000	0.000	0.000	0.000	0.020	0.022	0.022
Mole frac H_2	0.000	1.000	0.000	0.732	0.732	0.732	0.732	0.626	0.626
Mole frac CH_3OH	0.000	0.000	0.000	0.000	0.000	0.000	0.003	0.073	0.073
Mole frac H_2O	0.000	0.000	0.000	0.000	0.000	0.000	0.001	0.070	0.070
Mass frac CO_2	1.000	0.000	1.000	0.889	0.889	0.889	0.834	0.626	0.626
Mass frac CO	0.000	0.000	0.000	0.000	0.000	0.000	0.043	0.043	0.043
Mass frac H_2	0.000	1.000	0.000	0.111	0.111	0.111	0.115	0.086	0.086
Mass frac CH_3OH	0.000	0.000	0.000	0.000	0.000	0.000	0.008	0.159	0.159
Mass frac H_2O	0.000	0.000	0.000	0.000	0.000	0.000	0.001	0.086	0.086

	8	9	10	11	12	13	LIGHTEND	METHANOL	WASTEWAT
Temperature	40.000	252.000	40.000	39.621	57.000	73.168	9.011	64.234	99.013
Pressure	75.000	75.000	75.000	1.013	1.013	1.013	1.013	1.013	1.013
Molar Vapor Frac	1.000	1.000	0.000	0.024	0.078	0.000	1.000	0.000	0.000
Molar Liquid Frac	0.000	0.000	1.000	0.976	0.922	1.000	0.000	1.000	1.000
Mass Density	36.190	8.678	841.101	39.870	12.179	793.563	1.834	744.471	916.437
Enthalpy Flow	-128542.070	-119164.252	-60558.851	-60558.851	-59726.011	-55353.487	-4267.154	-24939.927	-30271.901
Average MW	12.756	12.756	25.879	25.879	25.879	25.006	42.189	32.040	18.094
Mass Flows	61066.100	61068.023	21051.101	21051.101	21051.101	19307.673	1743.427	12261.446	7046.227
Volume Flow	1687.378	7036.731	25.028	527.995	1728.485	24.330	950.777	16.470	7.689
Mole Flows	4787.408	4787.254	813.432	813.432	813.432	772.108	41.324	382.689	389.419
CO_2	1130.215	1130.261	37.667	37.667	37.667	0.093	37.574	0.093	0.000
CO	124.822	124.833	0.048	0.048	0.048	0.000	0.048	0.000	0.000
H_2	3506.054	3505.842	0.997	0.997	0.997	0.000	0.997	0.000	0.000
CH_3OH	20.486	20.487	387.342	387.342	387.342	384.655	2.687	382.464	2.191
H_2O	5.831	5.831	387.378	387.378	387.378	387.360	0.018	0.132	387.228
Mole frac CO_2	0.236	0.236	0.046	0.046	0.046	0.000	0.909	0.000	0.000
Mole frac CO	0.026	0.026	0.000	0.000	0.000	0.000	0.001	0.000	0.000
Mole frac H_2	0.732	0.732	0.001	0.001	0.001	0.000	0.024	0.000	0.000
Mole frac CH_3OH	0.004	0.004	0.476	0.476	0.476	0.498	0.065	0.999	0.006
Mole frac H_2O	0.001	0.001	0.476	0.476	0.476	0.502	0.000	0.000	0.994
Mass frac CO_2	0.815	0.815	0.079	0.079	0.079	0.000	0.949	0.000	0.000
Mass frac CO	0.057	0.057	0.000	0.000	0.000	0.000	0.001	0.000	0.000
Mass frac H_2	0.116	0.116	0.000	0.000	0.000	0.000	0.001	0.000	0.000
Mass frac CH_3OH	0.011	0.011	0.590	0.590	0.590	0.638	0.049	0.999	0.010
Mass frac H_2O	0.002	0.002	0.332	0.332	0.332	0.361	0.000	0.000	0.990

CO_2 hydrogenation (PEM electrolysis)

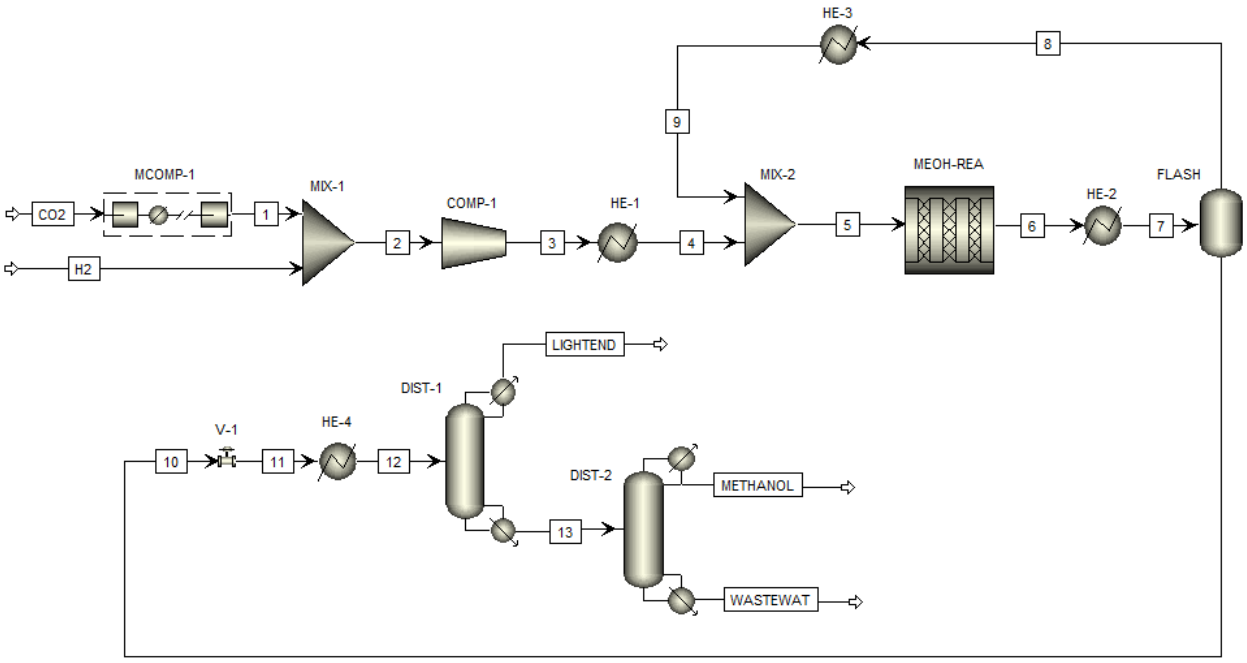

	CO2	H2	1	2	3	4	5	6	7
Temperature	25.000	80.000	80.000	70.661	123.589	252.000	252.087	251.630	40.000
Pressure	1.013	50.000	50.000	50.000	75.000	75.000	75.000	75.000	75.000
Molar Vapor Frac	1.000	1.000	1.000	1.000	1.000	1.000	1.000	1.000	0.855
Molar Liquid Frac	0.000	0.000	0.000	0.000	0.000	0.000	0.000	0.000	0.145
Mass Density	1.808	3.355	87.663	22.915	29.451	22.218	8.756	24.836	47.922
Enthalpy Flow	-46460.811	531.764	-46400.361	-45868.597	-45106.644	-43188.160	-162224.764	-168868.953	-188973.184
Average MW	44.010	2.016	44.010	13.253	13.253	13.253	12.872	14.652	14.652
Mass Flows	18704.165	2345.053	18704.165	21049.218	21049.218	21049.218	82067.177	82067.177	82067.177
Volume Flow	10345.520	698.900	213.365	918.573	714.715	947.387	9372.156	3304.386	1712.530
Mole Flows	425.000	1163.290	425.000	1588.290	1588.290	1588.290	6375.736	5601.004	5601.004
CO_2	425.000	0.000	425.000	425.000	425.000	425.000	1554.117	1166.712	1166.712
CO	0.000	0.000	0.000	0.000	0.000	0.000	124.745	124.785	124.785
H_2	0.000	1163.290	0.000	1163.290	1163.290	1163.290	4670.561	3508.424	3508.424
CH_3OH	0.000	0.000	0.000	0.000	0.000	0.000	20.483	407.849	407.849
H_2O	0.000	0.000	0.000	0.000	0.000	0.000	5.829	393.235	393.235
Mole frac CO_2	1.000	0.000	1.000	0.268	0.268	0.268	0.244	0.208	0.208
Mole frac CO	0.000	0.000	0.000	0.000	0.000	0.000	0.020	0.022	0.022
Mole frac H_2	0.000	1.000	0.000	0.732	0.732	0.732	0.733	0.626	0.626
Mole frac CH_3OH	0.000	0.000	0.000	0.000	0.000	0.000	0.003	0.073	0.073
Mole frac H_2O	0.000	0.000	0.000	0.000	0.000	0.000	0.001	0.070	0.070
Mass frac CO_2	1.000	0.000	1.000	0.889	0.889	0.889	0.833	0.626	0.626
Mass frac CO	0.000	0.000	0.000	0.000	0.000	0.000	0.043	0.043	0.043
Mass frac H_2	0.000	1.000	0.000	0.111	0.111	0.111	0.115	0.086	0.086
Mass frac CH_3OH	0.000	0.000	0.000	0.000	0.000	0.000	0.008	0.159	0.159
Mass frac H_2O	0.000	0.000	0.000	0.000	0.000	0.000	0.001	0.086	0.086

	8	9	10	11	12	13	LIGHTEND	METHANOL	WASTEWAT
Temperature	40.000	252.000	40.000	29.723	57.000	73.003	10.064	63.634	99.078
Pressure	75.000	75.000	75.000	1.013	1.013	1.013	1.013	1.013	1.013
Molar Vapor Frac	1.000	1.000	0.000	0.029	0.075	0.000	1.000	0.000	0.000
Molar Liquid Frac	0.000	0.000	1.000	0.971	0.925	1.000	0.000	1.000	1.000
Mass Density	36.158	8.671	841.082	35.231	12.734	793.845	1.824	745.335	916.560
Enthalpy Flow	-128414.975	-119036.604	-60558.208	-60558.208	-59688.471	-55369.070	-4252.446	-24969.157	-30261.353
Average MW	12.745	12.745	25.878	25.878	25.878	25.009	42.134	32.045	18.089
Mass Flows	61016.549	61017.959	21050.628	21050.628	21050.628	19311.349	1739.278	12269.939	7041.410
Volume Flow	1687.502	7036.907	25.028	597.505	1653.087	24.326	953.304	16.462	7.682
Mole Flows	4787.560	4787.446	813.444	813.444	813.444	772.165	41.279	382.899	389.266
CO_2	1129.084	1129.117	37.628	37.628	37.628	0.274	37.354	0.274	0.000
CO	124.737	124.745	0.048	0.048	0.048	0.000	0.048	0.000	0.000
H_2	3507.428	3507.271	0.997	0.997	0.997	0.000	0.997	0.000	0.000
CH_3OH	20.483	20.483	387.367	387.367	387.367	384.508	2.858	382.464	2.044
H_2O	5.829	5.829	387.405	387.405	387.405	387.382	0.023	0.161	387.222
Mole frac CO_2	0.236	0.236	0.046	0.046	0.046	0.000	0.905	0.001	0.000
Mole frac CO	0.026	0.026	0.000	0.000	0.000	0.000	0.001	0.000	0.000
Mole frac H_2	0.733	0.733	0.001	0.001	0.001	0.000	0.024	0.000	0.000
Mole frac CH_3OH	0.004	0.004	0.476	0.476	0.476	0.498	0.069	0.999	0.005
Mole frac H_2O	0.001	0.001	0.476	0.476	0.476	0.502	0.001	0.000	0.995
Mass frac CO_2	0.814	0.814	0.079	0.079	0.079	0.001	0.945	0.001	0.000
Mass frac CO	0.057	0.057	0.000	0.000	0.000	0.000	0.001	0.000	0.000
Mass frac H_2	0.116	0.116	0.000	0.000	0.000	0.000	0.001	0.000	0.000
Mass frac CH_3OH	0.011	0.011	0.590	0.590	0.590	0.638	0.053	0.999	0.009
Mass frac H_2O	0.002	0.002	0.332	0.332	0.332	0.361	0.000	0.000	0.991

D - AEA Composite Curves and Grand Composite Curves

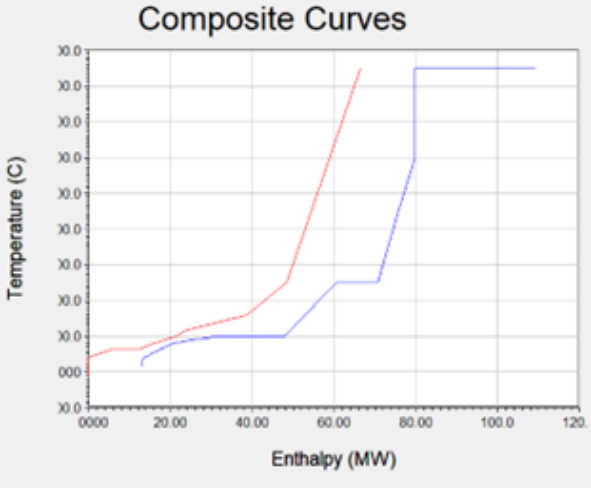

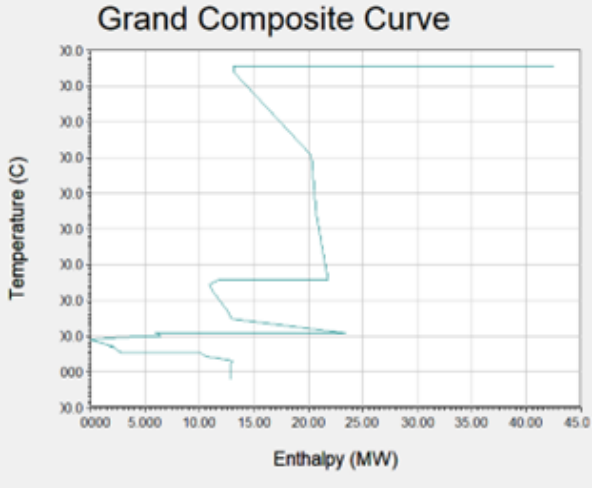

Methane steam reforming to methanol process

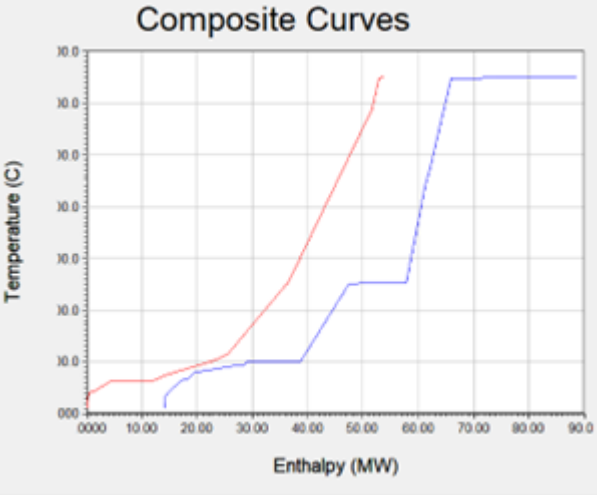

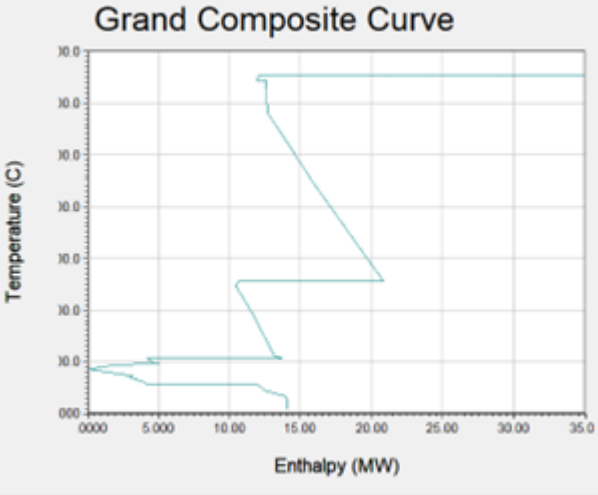

Biogas reforming to methanol process

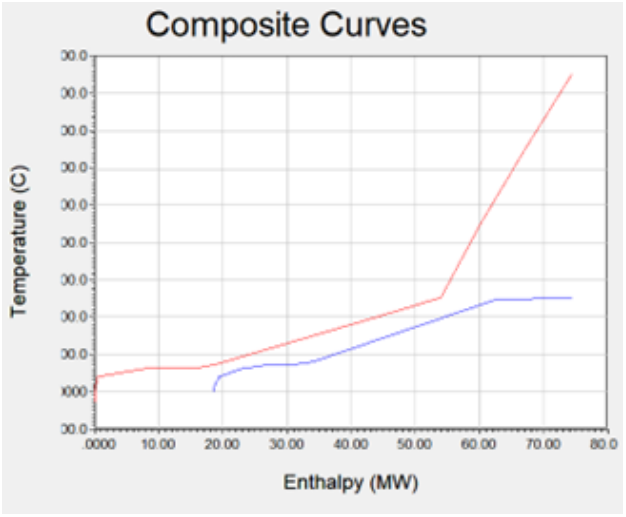

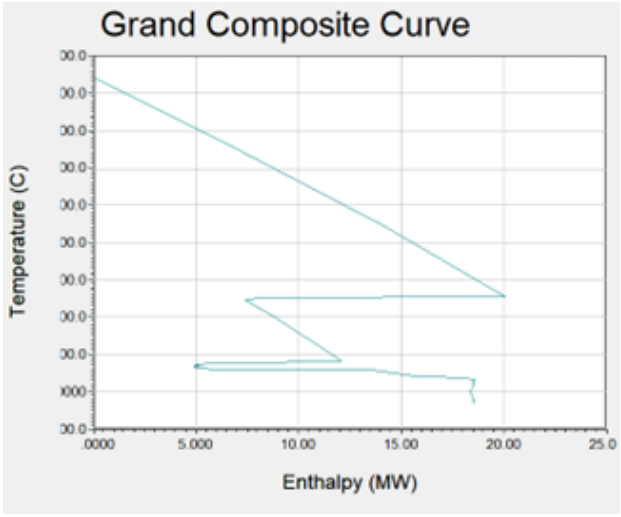

Biomass steam gasification to methanol process

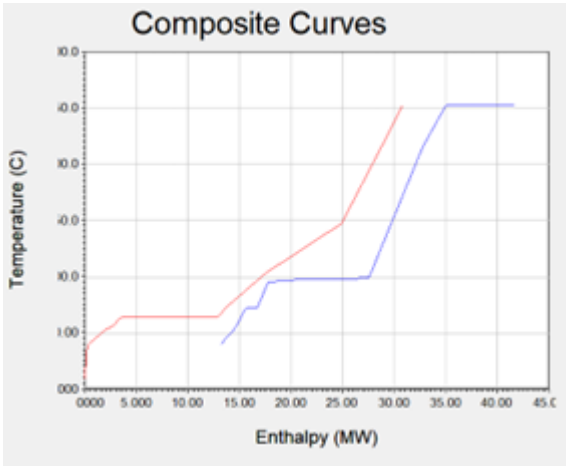

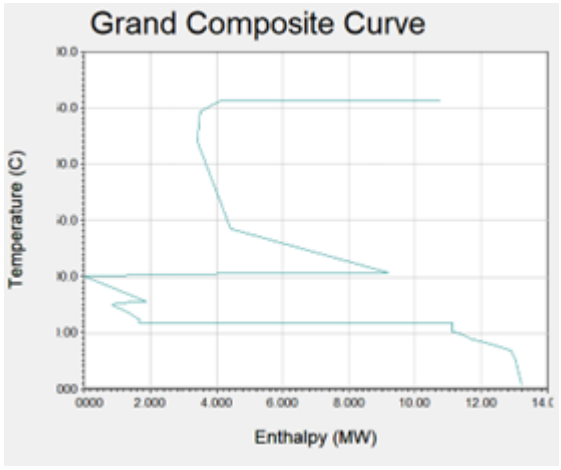

CO_2 hydrogenation (AW electrolysis)

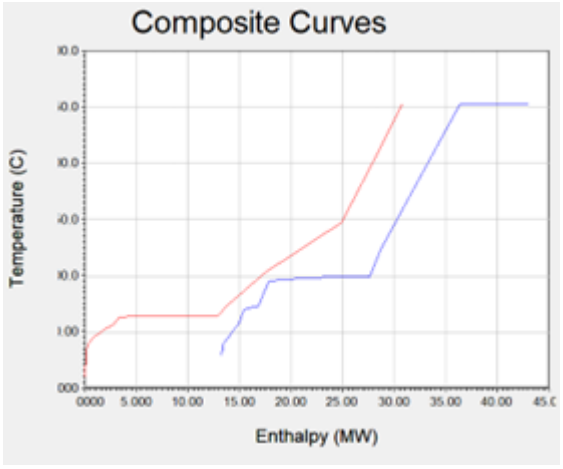

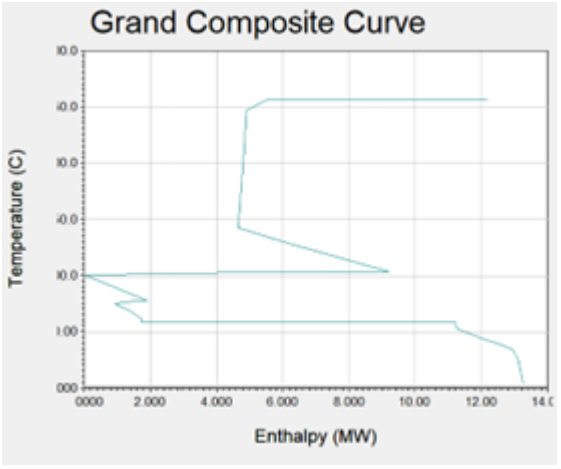

CO_2 hydrogenation (PEM electrolysis)

Nomenclature

AEA	Aspen Energy Analyzer
ASTM	American Society for Testing and Materials
AW	Alkaline Water
BECCS	Bioenergy with Carbon Capture and Storage
BFD	Block Flow Diagram
BR	Biogas Reforming
CCS	Carbon Capture and Storage
CCU	Carbon Capture and Utilization
CCUS	Carbon Capture Storage and Utilization
CDR	Carbon Dioxide Removal
CEPCI	Chemical Engineering Plant Cost Index
CFD	Cash Flow Diagram
COM	Cost of Manufacturing
COP	Conference of Parties
COR	Carbon Oxide Ratio
DAC	Direct Air Capture
DACCS	Direct Air Carbon Capture and Storage
db	dry biomass
DEA	Diethanolamine
DFBG	Dual Fluidized-Bed Gasifier
DPBP	Discounted Payback Period
DMC	Direct Manufacturing Costs
DME	Dimethyl Ether
DS	Design Specification
EAP	Environmental Action Programme
EEA	European Environment Agency
EoS	Equation of State
EU	European Union
EUROSTAT	European Statistical Office
FCI	Fixed Capital Investment
FMC	Fixed Manufacturing Costs
GCC	Grand Composite Curve

GE	General Expenses
GHG	Greenhouse Gas
GWP	Global Warming Potential
HEN	Heat Exchanger Network
MDR	Methane Dry Reforming
HEN	Heat Exchanger Network
IPCC	Intergovernmental Panel on Climate Change
IRENA	International Renewable Energy Agency
IRR	Internal Rate of Return
ISBL	Inside Battery Limits
ISO	International Organization for Standardization
LHHW	Langmuir-Hinshelwood-Hougen-Watson
LPG	Liquefied Petroleum Gas
MDEA	Methyl-diethanolamine
MEA	Monoethanolamine
MEK	Methyl Ethyl Ketone
MER	Maximum Energy Recovery
MON	Motor Octane Number
MSR	Methane Steam Reforming
MTBE	Methyl *Tert*-Butyl Ether
MTO	Methanol To Olefine
NET	Net Present Value
NG	Natural Gas
NRTL	Non-Random Two-Liquid
OSBL	Outside Battery Limits
PEM	Polymer Electrolyte Membrane
PFD	Process Flow Diagram
PFR	Plug Flow Reactor
PO	Partial Oxidation
PS	Process Simulator
PSA	Pressure Swing Adsorption
PVR	Present Value Ratio
R/F	Recycle-to-feed
RK	Redlich-Kwong
RON	Research Octane Number
rWGS	reverse Water Gas Shift
S/C	Steam to Carbon
SA	Sensitivity Analysis
SDS	Sustainable Development Strategy
SEA	Single European Act
SN	Stoichiometric Number

SRK	Soave-Redlich-Kwong
SSRE	Sum of Square Relative Errors
StC	Start-up Costs (Capital)
STP	Standard Temperature and Pressure
TCI	Total Capital Investment
UN	United Nations
UNEP	United Nations Environment Programme
UNFCCC	United Nations Framework Convention on Climate Change
VdW	Van der Waals
VLE	Vapor-Liquid Equilibrium
WC	Working Capital
WGS	Water Gas Shift
WMO	World Meteorological Organization

References

Adil, A., A. M. Shivapuji, L. Rao (2022). Thermodynamic analysis for methanol synthesis using biomass-derived syngas. *Biomass Conversion and Biorefinery*, **12**, 1819-1834

Ahmed, S., S. H. D. Lee, M. S. Ferrandon (2015). Catalytic steam reforming of biogas – Effects of feed composition and operating conditions. *Int. J. of Hydrogen Energy*, **40**, 1005-1015

Al-Kalbani, H., J. Xuan, S. García, H. Wang (2016). Comparative energetic assessment of methanol production from CO2: Chemical versus electrochemical process. *Applied Energy*, **165**, 1-13

An, X., Y. Zuo, Q. Zhang, J. Wang (2009). Methanol synthesis from CO_2 hydrogenation with a Cu/Zn/Al/Zr fibrous catalyst. *Chinese Journal of Chemical Engineering*, **17(1)**, 88-94

Asif, M., X. Gao, H. Lu, X. Xi, P. Dong (2018). Catalytic hydrogenation of CO2 from 600 MW supercritical coal power plant to produce methanol: a techno-economic analysis. *International Journal of Hydrogen energy*, **43**, 2726-2741

Basu, P. (2010). *Biomass Gasification and Pyrolysis, Practical Design and Theory.* Elsevier, Burlington (U.S.A.)

Bertucco, A. and E. Barbera (2021). *Separation Unit Operations and Process Simulation*, Lecture notes

Bezzo F. (2020). *Process Design*, Lecture slides

Butera, G., R. O. Gadsboll, G. Ravenni, J. Ahrenfeldt, U. B. Henriksen, L. R. Clausen (2020). Thermodynamic analysis of methanol synthesis combining straw gasification and electrolysis via the low temperature circulating fluid bed gasifier and a char bed gas cleaning unit. *Energy*, **199**, 117405

Buttler, A. and H. Spliethoff (2018). Current status of water electrolysis for energy storage, grid balancing and sector coupling via power-to-gas and power-to-liquids: A review. *Renewable and Sustainable Energy Reviews*, **82**, 2440-2454

Di Marcoberardino, G., D. Vitali. F. Spinelli, M. Binotti, G. Manzolini (2018). Green hydrogen production from raw biogas: a techno-economic investigation of conventional processes using pressure swing adsorption unit. *Processes*, **6**, 19

Dybkjær, I., T. Nørgaard, J. Perregaard, F. Joensen, H. Topsøe (2006). Methanol, Dimethyl Ether, Ammonia, Urea. In: *Encyclopaedia of Hydrocarbons*, Volume II (C. Amadei, Ed.), Istituto della Enciclopedia Italiana fondata da Giovanni Treccani, Rome (Italy)

Effendi, A., K. Hellgardt, Z.-G. Zhang, T. Yoshida (2005). Optimising H_2 production from model biogas via combined steam reforming and CO shift reactions. *Fuel*, **84**, 869-874

Evans, S. E., J. Z. Staniforth, R. J. Darton, R. M. Ormerod (2014). A nickel doped perovskite catalyst for reforming methane rich biogas with minimal carbon deposition. *Green Chem.*, **16**, 4587-4594

Felder, R. and R. Rousseau (2005). *Elementary Principles of Chemical Processes* (3rd edition). Wiley, U.S.A

Fogler, H. S. (2016). *Elements of Chemical Reaction Engineering* (5th edition). Pearson Education, U.S.A.

Freund, P. (2006). Cattura e stoccaggio di CO_2 prodotto dai combustibili fossili. In: *Enciclopedia degli Idrocarburi*, Volume III (C. Amadei, Ed.), Istituto della Enciclopedia Italiana fondata da Giovanni Treccani, Rome (Italy)

Galvagno, A., V. Chiodo, F. Urbani, F. Freni (2013). Biogas as hydrogen source for fuel cell applications. *Int. J. of Hydrogen Energy*, **38**, 3913-3920

Ghosh, S., J. Sebastian, L. Olsson, D. Creaser (2021). Experimental and kinetic modeling studies of methanol synthesis from CO_2 hydrogenation using In_2O_3 catalyst. *Chemical Engineering Journal*, **416**, 129120

Graaf, G. H., E. J. Stamhuis, A. A. C. M. Beenackers (1988). Kinetics of low-pressure methanol synthesis. *Chemical Engineering Science*, **43**, 3185-3195

Green, D. W., M. Z. Southard (2019). *Perry's Chemical Engineers' Handbook* (9th edition). McGraw-Hill, U.S.A.

Häussinger, P., R. Lohmüler, A. M. Watson (2002). Hydrogen. In: *Ullmann's Encyclopedia of Chemical Industry*, Volume 8 (F. Ullmann, Ed.), Wiley, Weinheim (Germany)

Henkel, T. (2011). Modellierung von Reaktion und Stofftransport in geformten Katalysatoren am Beispiel der Methanolsynthese. *Ph.D. Thesis*, Technical University of Munich (Germany)

IEA (2019). *The Future of Hydrogen*, IEA, Paris

IEA (2020a). *Clean Energy Innovation*, IEA, Paris

IEA (2020b). *Outlook for biogas and biomethane: Prospects for organic growth*, IEA, Paris

IEA (2022). *Carbon Capture, Utilisation and Storage*, IEA, Paris

IPCC (2007). *Climate Change 2007: Synthesis Report. Contribution of Working Groups I, II and III to the Fourth Assessment Report of the Intergovernmental Panel on Climate Change* [Core Writing Team, Pachauri, R.K and Reisinger, A. (eds.)]. IPCC, Geneva, Switzerland

IPCC (2021, August 9). Climate Change widespread, rapid, and intensifying - IPCC [Press release]

IPCC (2022). Summary for Policymakers. In: *Climate Change 2022: Mitigation of Climate Change. Contribution of Working Group III to the Sixth Assessment Report of the Intergovernmental Panel on Climate Change* (P.R. Shukla, J. Skea, R. Slade, A. Al Khourdajie, R. van Diemen, D. McCollum, M. Pathak, S. Some, P. Vyas, R. Fradera, M. Belkacemi, A. Hasija, G. Lisboa, S. Luz, J. Malley, Eds.), Cambridge University Press, Cambridge, UK and New York, NY (USA)

IRENA and Methanol Institute (2021). *Innovation Outlook: Renewable Methanol*, International Renewable Energy Agency, Abu Dhabi

Izquierdo, U., V. L. Barrio, N. Lago, J. Requies, J. F. Cambra, M. B. Güemez, P. L. Arias (2012). Biogas steam and oxidative reforming processes for synthesis gas and hydrogen production in conventional and microreactor reaction systems. *Int. J. of Hydrogen Energy*, **37**, 13829-13842

Jang, D., J. Kim, D. Kim, W. Han, S. Kang (2022). Techno-economic analysis and Monte Carlo simulation of green hydrogen production technology through various water electrolysis technologies. *Energy Conversion and Management*, **258**, 115499

Kanuri, S., S. Roy, C. Chakraborty, S. P. Datta, S. A. Singh, S. Dinda (2022). An insight of CO_2 hydrogenation to methanol synthesis: Thermodynamics, catalysts, operating parameters, and reaction mechanism. *Int. J. Energy Res.*, **46**, 5503-5522

Keith, D. W., G. Holmes, D. St. Angelo, K. Heidel (2018). A Process for Capturing CO_2 from the Atmosphere. *Joule*, **2 (10)**, 1573-1594

Kiss, A. A., J. J. Pragt, H. J. Vos, G. Bargeman, M. T. de Groot (2016). Novel efficient process for methanol synthesis by CO_2 hydrogenation. *Chemical Engineering Journal*, **284**, 260-269

Klier, K., V. Chatikavanij, R. G. Herman, G. W. Simmons (1982). Catalytic synthesis of methanol from CO/H_2. IV. The effect of carbon dioxide. *J. Catal.*, **74**, 343-360

Leonzio, G., E. Zondervan, P. U. Foscolo (2019). Methanol production by CO_2 hydrogenation: analysis and simulation of reactor performance. *Int. J. of Hydrogen Energy*, **44**, 7915-7933

Luyben, W. L. (2013). *Distillation Design and Control Using Aspen Simulation* (2nd edition). Wiley, U.S.A.

Meunier, N., R. Chauvy, S. Mouhoubi, D. Thomas, G. De Weireld (2020). Alternative production of methanol from industrial CO_2. *Renewable Energy*, **146**, 1192-1203

Meyer, J. J., P. Tan, A. Apfelbacher, R. Daschner, A. Hornung (2016). Modeling of a methanol synthesis reactor for storage of renewable energy and conversion of CO_2 – Comparison of two kinetic models. *Chem. Eng. Technol.*, **39**, 233-245

Mignard, D. and C. Pritchard (2008). On the use of electrolytic hydrogen from variable renewable energies for the enhanced conversion of biomass to fuels. *Chemical Engineering Research and Design*, **86**, 473-487

Modesti, M. (2021). *Processi Industriali Chimici 2*, Lecture slides

Morandin, M. and S. Harvey (2015). Methanol via biomass gasification. Thermodynamic performances and process integration aspects in Swedish chemical cluster and pulp and paper sites. *Technical Report*, Chalmers University of Technology, Göteborg, Sweden

Moulijn, J. A., M. Makkee, A. Van Diepen (2013). *Chemical Process Technology* (2nd edition). Wiley, Delft (The Netherlands)

Nestler, F., A. R. Schütze, M. Ouda, M. J. Hadrich, A. Schaadt, S. Bajohr, T. Kolb (2020). Kinetic modelling of methanol synthesis over commercial catalysts: a critical assessment. *Chem. Eng. J.*, **394**, 124881

Ng, K. L., D. Chadwick, B. A. Toseland (1999). Kinetics and modelling of dimethyl ether synthesis from synthesis gas. *Chemical Engineering Science*, **54**, 3587-3592

Ott, J., V. Gronemann, F. Pontzen, E. Fiedler, G. Grossmann, D. B. Kersebohm, G. Weiss, C. Witte (2002). Methanol. In: *Ullmann's Encyclopedia of Chemical Industry*, Volume 12 (F. Ullmann, Ed.), Wiley, Weinheim (Germany)

Pala, L. P. R., Q. Wang, G. Kolb, V. Hessel (2017). Steam gasification of biomass with subsequent syngas adjustement using shift reaction for syngas production: An Aspen Plus model. *Renewable Energy*, **101**, 484-492

Park, N., M. J. Park, Y. J. Lee, K. S. Ha, K. W. Jun (2014). Kinetic modeling of methanol synthesis over commercial catalysts based on three-site adsorption. *Fuel Processing Technology*, **125**, 139-147

Pérez-Fortes, M. and E. Tzimas (2016). Techno-economic and Environmental Evaluation of CO_2 Utilisation for Fuel Production, EU, Luxembourg

Pérez-Fortes, M., J. C. Schöneberger, A. Boulamanti, E. Tzimas (2016). Methanol synthesis using captured CO_2 as raw material: techno-economic and environmental assessment. *Applied Energy*, **161**, 718-732

Peter, M., M. B. Fichtl, H. Ruland, S. Kaluza, M. Muhler, O. Hinrichsen (2012). Detailed kinetic modeling of methanol synthesis over a ternary copper catalyst. *Chemical Engineering Journal*, **203**, 480-491

Pfeifer, C., S. Koppatz, H. Hofbauer (2011). Steam gasification of various feedstocks at a dual fluidized bed gasifier: Impacts of operation conditions and bed materials. *Biomass Conv. Bioref.*, **1**, 39-53

Poling, B. E., J. M. Prausnitz, J. P. O'Connell (2001). *The Properties of Gases and Liquids* (5th edition). McGraw-Hill, U.S.A.

Roy, P. S., J. Song, K. Kim, C. S. Park, A. S. K. Raju (2018). CO_2 conversion to syngas through the steam-biogas reforming process. *Journal of CO_2 utilization*, **25**, 275-282

Sandler, S. I. (2015). *Using Aspen Plus in Thermodynamics Instruction.* Wiley, U.S.A.

Santos, R. O., L. de Sousa Santos, D. M. Prata (2018). Simulation and optimization of a methanol synthesis process from different biogas sources. *Journal of Cleaner Production*, **186**, 821-830

Schiaroli, N., M. Volanti, A. Crimaldi, F. Passarini, A. Vaccari, G. Fornasari, S. Copelli, F. Florit, C. Lucarelli (2021). Biogas to syngas thourgh the combined steam/dry reforming process: an environmental impact assessment. *Energy Fuels*, **35**, 4224-4236

Seidel, C., A. Jörke, B. Vollbrecht, A. Seidel-Morgenstern, A. Kienle (2018). Kinetic modeling of methanol synthesis from renewable sources. *Chemical Engineering Science*, **175**, 130-138

Seider, W. D., D. R. Lewin, J. D. Seader, S. Widagdo, R. Gani, K. M. Ng (2017). *Product and Process Design Principles: Synthesis, Analysis and Evaluation* (4th edition). Wiley, U.S.A.

Subramani, V., A. Basile, T. N. Veziroglu (2015). *Compendium of Hydrogen Energy*, Volume 1: Hydrogen Production and Purification. Elsevier, Cambridge (UK)

Topham, S., A. Bazzanella, S. Schiebahn, S. Luhr, L. Zhao, A. Otto, D. Stolten (2014). Carbon dioxide. In: *Ullmann's Encyclopedia of Chemical Industry*, Volume 3 (F. Ullmann, Ed.), Wiley, Weinheim (Germany)

Towler, G. and R. Sinnott (2008). *Chemical Engineering Design: Principles, Practice and Economics of Plant and Process Design.* Butterworth-Heinemann, U.S.A.

Tuna, C. E., J. L. Silveira, M. E. da Silva, R. M. Boloy, L. B. Braga, N. P. Pérez (2018). Biogas steam reformer for hydrogen production: evaluation of the reformer prototype and catalysts. *Int. J. of Hydrogen Energy*, **43**, 2108-2120

Turton, R., J. A. Shaeiwitz, D. Bhattacharyya, W. B. Whiting (2018). *Analysis, Synthesis, and Design of Chemical Processes* (5th edition). Pearson Education, U.S.A.

UNEP (2020, December 2). World's governments must wind down fossil fuel production by 6% per year to limit catastrophic warming [Press release]

Van-Dal, E. S. and C. Bouallou (2013). Design and simulation of a methanol production plant from CO_2 hydrogenation. *Journal of Cleaner Production*, **57**, 38-45

Vanden Bussche, K. M. and G. F. Froment (1996). A steady-state kinetic model for methanol synthesis and the water gas shift reaction on a commercial $Cu/ZnO/Al_2O_3$ catalyst. *Journal of Catalysis*, **161**, 1-10

Vita, A., C. Italiano, D. Previtali, C. Fabiano, A. Palella, F. Freni, G. Bozzano, L. Pino, F. Manenti (2018). Methanol synthesis from biogas: a thermodynamic analysis. *Renewable Energy*, **118**, 673-684

Vollbrecht, B. (2007). Zur Kinetik der Methanolsynthese an einem technischen Cu/ZnO/Al2O3-Katalysator. *Ph.D. thesis*, Otto-von-Guericke-Universität Magdeburg (Germany)

WMO (2021, January 15). 2020 was one of three warmest year on record [Press release]

Yang, Q., Z. Zhang, Y. Fan, G. Chu, D. Zhang, J. Yu (2022). Advanced exergy analysis and optimization of a CO2 to methanol process based on rigorous modeling and simulation. *Fuel*, **325**, 124944

Yao, J., M. Kraussler, F. Benedikt, H. Hofbauer (2017). Techno-economic assessment of hydrogen production based on dual fluidized bed biomass steam gasification, biogas steam reforming, and alkaline water electrolysis processes. *Energy Conversion and Management*, **145**, 278-292

Zhao, X., B. Joseph, J. Kuhn, S. Ozcan (2020). Biogas reforming to syngas: A review. *iScience*, **23**, 1-35

Websites

European Central Bank: *www.ecb.europa.eu* (last access: 18/09/2022)

European Commission: *www.ec.europa.eu* (last access: 11/11/2022)

ENI: *www.eni.com* (last access: 10/11/2022)

European Parliament: *www.europarl.europa.eu* (last access: 10/11/2022)

Intergovernmental Panel on Climate Change: *www.ipcc.ch* (last access: 16/11/2022)

International Energy Agency: *www.iea.org* (last access: 10/11/2022)

Market Research: *www.marketresearch.com* (last access: 08/11/2022)

Statista: *www.statista.com* (last access: 08/11/2022)

United Nations: *www.un.org* (last access: 12/11/2022)

United Nations Environment Programme: *www.unep.org* (last access: 16/11/2022)

World Meteorological Organization: *www.public.wmo.int* (last access: 11/11/2022)